

QUASIGEOSTROPHIC DIAGNOSIS OF AN EXPLOSIVELY DEVELOPING
CYCLONE ALONG THE NORTHERN CALIFORNIA COAST

AS
36
2014
GEOL
-R64

A Thesis submitted to the faculty of
San Francisco State University
In partial fulfillment of
the requirements for
the Degree

Master of Science

In

Geosciences

by

Geoffrey Scott Roest

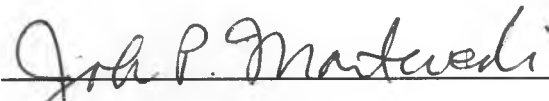
San Francisco, California

May 2014

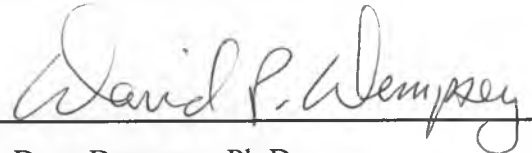
Copyright by
Geoffrey Scott Roest
2014

CERTIFICATION OF APPROVAL

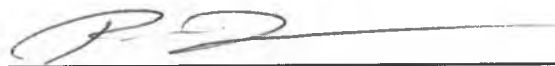
I certify that I have read *Quasigeostrophic Diagnosis of an Explosively Developing Cyclone Along The Northern California Coast* by Geoffrey Scott Roest, and that in my opinion this work meets the criteria for approving a thesis submitted in partial fulfillment of the requirement for the degree Master of Science in Geoscience at San Francisco State University.



John Monteverdi, Ph.D.
Professor of Meteorology



Dave Dempsey, Ph.D.
Professor of Meteorology



Petra Dekens, Ph.D.
Associate Professor of Oceanography

QUASIGEOSTROPHIC DIAGNOSIS OF AN EXPLOSIVELY DEVELOPING CYCLONE ALONG THE NORTHERN CALIFORNIA COAST

Geoffrey Scott Roest
San Francisco, California
2014

A strong extratropical cyclone made landfall in Northern California on 19 February 1993, bringing wind gusts in excess of 90 mph to the Mendocino County coastline and rainfall amounts greater than four inches in mountainous areas. NOAA buoy data showed a 13 mb pressure fall in 14 hours, a rate that exceeds the criterion for 'meteorological bombs'. The eye-like feature at the center of circulation that developed prior to landfall was reminiscent of hurricane-like cyclones that develop at high latitudes termed "polar lows". A qualitative assessment of the quasigeostrophic forcing showed that the storm developed in an area in which synoptic scale forcing both from cyclonic differential vorticity advection and warm air advection were favorable for mid-tropospheric upward vertical motion and surface cyclone development. A quantitative assessment of the terms in the quasigeostrophic Sutcliffe-Petterssen Development Equation (SPDE) showed that the dominant factor in the development of this cyclone was the large change in the 1000-500 mb thickness field. A quantitative assessment of the three contributing terms to thickness changes returned mixed results. The largest contribution to that term was adiabatic heating due to vertical motion in an environment with weak static stability. The author hypothesizes that diabatic heating occurring in the cooler boundary layer air overrunning the warm ocean surface decreased stability in the lower troposphere. The calculations produced an inconsistent result, as the contribution to thickness change due to sensible heating, calculated as a residual, was negative. This is impossible since meteorological data showed that this term should have been positive. Nevertheless, the results were conclusive that the thickness changes consistent with the warming core of the disturbance made the largest contribution to surface development as the explosive growth occurred just off the coast. This conclusion, along with other

diagnostic aspects of the storm, including the clear eye, suggests that the disturbance can be classified as a polar low, the first to be identified in California.

I certify that the Abstract is a correct representation of the content of this thesis.

John P. Martwed
Chair, Thesis Committee

May 14, 2014
Date

ACKNOWLEDGEMENTS

I would not have had such success during my graduate studies at San Francisco State University without the support of my academic mentors and colleagues and the love of my friends and family. Firstly, my professor, advisor, and thesis committee chair John Monteverdi has been immensely helpful during the last two years. My thesis would not exist without the help of my committee members Dave Dempsey and Petra Dekens. I'd also like to thank my former professors – Oz Garcia, Jason Gurdak, Leonard Sklar – and the rest of the faculty and staff in the Department of Geosciences for being so helpful during my studies. Thanks to my fellow meteorology/geoscience students for being so cool, too.

Where would I be without the support of my family - especially my mom. I would not have been able to obtain this degree without her help. I also have a wonderfully supportive group of friends, all the way from New York, New Hampshire, California, and beyond.

Lastly, I would like to thank Sonoma Technology Inc. for providing me with a wonderful summer internship that has only strengthened my interest in meteorology and inspired me to pursue a Ph.D. in Atmospheric Science. I am very lucky to have been given that opportunity, and I am looking forward to continuing my education.

TABLE OF CONTENTS

| | |
|--|-----|
| List of Tables | ix |
| List of Figures | xi |
| List of Appendices | xvi |
| 1. Introduction..... | 1 |
| 2. Overview of Storm..... | 4 |
| a. Impacts | 6 |
| 3. Synoptic Analysis of Storm | 10 |
| a. Pre-storm Environment | 11 |
| b. Initial Low Development | 12 |
| c. Rapid Deepening and Landfall..... | 15 |
| 4. Explosive Cyclogenesis in Cold Air Masses | 20 |
| a. Explosive Cyclogenesis | 21 |
| b. Conditional Instability of the Second Kind and Destabilization Due to Air-sea Diabatic Heating | 23 |
| c. Polar Lows | 25 |
| d. Explosive Cyclogenesis, Polar Lows, and the 19 February 1993 Storm | 28 |
| 5. Methodology | 29 |
| a. Review of Quasigeostrophic Theory..... | 31 |
| b. Qualitative Assessment of QG-Forcing on the Basis of the QG-Omega Equation | 34 |
| c. Quantitative Assessment of QG-Forcing on the Basis of the Sutcliffe-Petterssen Development Equation..... | 36 |

| | |
|--|-----|
| d. Quantitative Assessment of the Expanded Thickness Tendency Term of the SPDE | 39 |
| 6. Quasigeostrophic Diagnosis and Polar Low Assessment | 43 |
| a. Qualitative Assessment of QG-Forcing on the Basis of the QG-omega Equation | 44 |
| b. Quantitative Assessment of the QG-forcing on the Basis of the SPDE | 48 |
| c. Quantitative Assessment of the SPDE Expanded Thickness Tendency Term .. | 49 |
| 7. Discussion of Results..... | 52 |
| a. Results of Qualitative Assessment of QG Forcing on the Basis of the QG- omega equation | 53 |
| b. Results of Quantitative Assessment of the QG Forcing on the Basis of the SPDE | 54 |
| c. Results of Quantitative Assessment of the SPDE with Expanded Thickness Tendency Term | 55 |
| d. Discussion of Static Stability and Diabatic Terms | 57 |
| e. Assessment of Explosive Cyclogenesis and Polar Low Development | 61 |
| 8. Summary | 63 |
| References..... | 66 |
| Tables..... | 72 |
| Figures..... | 81 |
| Appendix A..... | 126 |

LIST OF TABLES

| Table | Page |
|---|------|
| 1. Peak sustained winds in mph at selected stations in California during the Feb 19 1993 storm, from AWOS/ASOS stations. | 72 |
| 2. Wind gusts in mph at selected stations in California during the Feb 19 1993 storm, from AWOS/ASOS stations. * denotes report from NWS statement. † denotes report from NCDC (1993). | 73 |
| 3. 1-hr precipitation totals. | 74 |
| 4. 6-hr precipitation totals. | 75 |
| 5. 24-hr precipitation totals | 76 |
| 6. Classification of polar lows from, adapted from table in Rasmussen and Turner (2003, p. 159). | 76 |
| 7. Comparison between 19 February 1993 storm with typical explosively developing cyclones (Sanders and Gyakum 1980, Reed and Albright 1986), ‘cold low’ polar lows (Rasmussen and Turner 2003, p. 172-189, 335-340), and strong polar lows (Rasmussen 1981). | 77 |
| 8. A summary of the qualitative nature of forcing for upward vertical motion as assessed by the QG-omega equation (Eq. (1)). | 78 |

9. Solution to the SPDE without expanded thickness term (Eq. (5)), calculated by hand, compared to actual 6-hr vorticity changes. Terms B and C contribute to the total computed vorticity tendency (Term A). All values are in units of 10^{-5} s^{-1} per 6 hour time step.79
10. Solution to the SPDE with expanded thickness term (Eq. (9)) using IDV, compared to actual 6-hr vorticity changes. Terms B, C, and D contribute to the total computed vorticity tendency (term A). All values are in units of 10^{-5} s^{-1} per 6 hour time step.79
11. Solution to SPDE with expanded thickness terms (Eq. (9)), calculated by hand, compared to actual 6-hr vorticity changes. Terms B, C, D, and E contribute to the total computed vorticity tendency (term A). All values are in units of 10^{-5} s^{-1} per 6 hour time step.80

LIST OF FIGURES

| Figures | Page |
|---|------|
| 1. Track of the main low-pressure center based on the NARR surface analysis, from 00 UTC 17 February 1993 to 00 UTC 20 February 1993. | 81 |
| 2. Visible satellite image for 2315 UTC 19 February 1993, showing cyclone with eye-like feature making landfall on Northern California coast. Thunderstorm anvils can be seen in the eastern Central Valley and Sierra Nevada regions. | 82 |
| 3. a. Transect through the storm along 38°N, from 127°W (left) to 121°W (right), 00 UTC 20 February 1993. The lines show temperature deviations (K) from the transect mean at various pressure levels. | 83 |
| b. Transect through the storm along 124°W, from 36.5°N (right) to 40.5°N (left), 00 UTC 20 February 1993. The lines show temperature deviations (K) from the transect mean at various pressure levels. | 84 |
| 4. Sea surface temperature anomalies (°C) in coastal waters of Northern California and Oregon for 19 February 1993. | 85 |
| 5. Sea surface temperatures (solid, °C) and sea surface – air temperature difference (dashed, °C) for 12 UTC 19 February 1993. Positive sea surface – air temperature differences indicate sea surface temperature is warmer than air temperature. | 86 |

| | |
|---|----|
| 6. AVHRR infrared satellite image for Northern California for 2315 UTC 19 February 1993. | 87 |
| 7. ASOS/AWOS in Northern California (A) and Southern California (b) used for wind and rainfall data in Tables 2 through 5..... | 88 |
| 8. a. Pressure at mean sea level (top left), 1000-500 mb thickness (bottom left), 250 mb geopotential heights (top right), and 500 mb geopotential heights (bottom right) for 00 UTC 10 February 1993. From Reanalysis-2 (NOAA/NCEP 2014) | 89 |
| b. As in Fig. 8a, but for 00 UTC 12 February 1993. | 90 |
| c. As in Fig. 8a, but for 00 UTC 14 February 1993. | 91 |
| d. As in Fig. 8a, but for 00 UTC 15 February 1993. | 92 |
| e. As in Fig. 8a, but for 00 UTC 16 February 1993. | 93 |
| f. As in Fig. 8a, but for 12 UTC 16 February 1993. | 94 |
| g. As in Fig. 8a, but for 00 UTC 17 February 1993. | 95 |
| h. As in Fig. 8a, but for 12 UTC 17 February 1993. | 96 |
| i. As in Fig. 8a, but for 00 UTC 18 February 1993. | 97 |
| j. As in Fig. 8a, but for 12 UTC 18 February 1993. | 98 |

| | |
|---|-----|
| k. As in Fig. 8a, but for 00 UTC 19 February 1993. | 99 |
| l. As in Fig. 8a, but for 12 UTC 19 February 1993. | 100 |
| m. As in Fig. 8a, but for 00 UTC 20 February 1993. | 101 |
| n. As in Fig. 8a, but for 12 UTC 20 February 1993. | 102 |
| 9. a. GOES west imagery for 12 UTC 16 February 1993 (NOAA/NESDIS, 2014)..... | 103 |
| b. As in Fig. 9a, but for 00 UTC 17 February 1993. | 104 |
| c. As in Fig. 9a, but for 12 UTC 17 February 1993. | 105 |
| d. As in Fig. 9a, but for 00 UTC 18 February 1993. | 106 |
| e. As in Fig. 9a, but for 12 UTC 18 February 1993. | 107 |
| f. As in Fig. 9a, but for 00 UTC 19 February 1993..... | 108 |
| g. As in Fig. 9a, but for 12 UTC 19 February 1993. | 109 |
| h. As in Fig. 9a, but for 18 UTC 19 February 1993. | 110 |
| i. As in Fig. 9a, but for 00 UTC 20 February 1993. | 111 |
| j. As in Fig. 9a, but for 06 UTC 20 February 1993. | 112 |

| | |
|---|-----|
| 10. An infrared satellite image of the eastern Pacific and western North America for 10 UTC 19 February 1993. | 113 |
| 11. An infrared satellite image of the eastern Pacific and western North America for 18 UTC 19 February 1993. | 114 |
| 12. a. Analyzed surface analysis for Northern California for 18 UTC 19 February 1993. | 115 |
| b. Analyzed surface analysis for Northern California for 21 UTC 19 February 1993. Due to time constraints, the exact nature of the surface boundary was not analyzed. However, this boundary (represented by a dashed purple line) formed from the remnants of the occlusion of the main cyclone. This pertains to subsequent surface analyses as well. | 116 |
| c. Analyzed surface analysis for Northern California for 23 UTC 19 February 1993. | 117 |
| d. Analyzed surface analysis for Northern California for 01 UTC 20 February 1993. | 118 |
| e. Analyzed surface analysis for Northern California for 06 UTC 20 February 1993. | 119 |
| 13. Climatology of 'bombs' in the eastern Pacific and western North America developed by Sanders and Gyakum (1980). Numbers represent number of bombs observed in 2.5° latitude by 2.5° grid during three cold seasons. Note the maxima in frequency in the north-central Pacific and the Gulf of Alaska, as well as the lack of bomb observations along the California Coast. | 120 |

| | |
|--|-----|
| 14. Comparison of terms in the Sutcliffe-Petterssen Development Equation during the period of surface pressure falls. | 121 |
| 15. 500 mb vorticity ($\times 10^{-5} \text{ s}^{-1}$), as analyzed by the NARR and displayed with IDV, for 00 UTC February 1993. Note the strong small-scale gradients, which are not representative of synoptic scale gradients | 122 |
| 16. Sea surface pressure (mb, black) and 700 mb vertical velocity (Pa s^{-1} , blue) from the NARR for 00 UTC 19 February 1993. X's mark maxima in upward vertical motion while N's represent minima in upward vertical motion (or maxima in downward vertical motion). | 123 |
| 17. NARR analyzed surface based CAPE (J/kg) over the eastern Pacific and western North America for 00Z February 18 1993 (top) and 00Z February 19 1993 (bottom). | 124 |
| 18. Sounding for KVBG for 00Z Feb 19 1993. | 125 |

LIST OF APPENDICES

| Appendix | Page |
|--|------|
| A. Derivation of the Sutcliffe-Petterssen Development Equation | 126 |

1. Introduction

On 19 February 1993, a disturbance off the coast of Northern California rapidly developed into a strong cyclone, deepening 13 mb in 14 hours (Monteverdi et. al. 1993). As the storm made landfall in Mendocino County, it brought several inches of rain and near-hurricane force winds to coastal California. Gusts in excess of 90 mph were reported in Northern California by the National Weather Service, along with property damage and one death (National Weather Service 1993b). The disturbance was also associated with several strong to severe thunderstorms, with multiple funnel cloud reports and one tornado touchdown in the San Joaquin Valley. Further south, numerous roads in Southern California was damaged by flooding rains (NCDC 1993).

The initial surface low developed in the eastern Pacific Ocean and reached a mature stage as the associated frontal system moved across California late on the 18 February through the day on 19 February 1993 (see Fig. 1 for a map of the storm track), while a new area of low pressure explosively developed over the eastern Pacific along the occluded boundary. Just prior to landfall, visible satellite imagery (Fig. 2) shows a clear eye-like feature at the center of the low that was surrounded by cumulonimbus clouds. This type of structure is typically associated with intense tropical cyclones such as hurricanes and typhoons. Preliminary analyses of the storm (e.g. Monteverdi et. al. 1993) suggested that the storm featured a warm core, another feature associated with tropical cyclones.

California generally experiences numerous landfalling extratropical cyclones each winter, and damage from rain and winds is not uncommon. However, to the author's knowledge, no hurricane-like cyclones are reported to have affected California in recent times. The only previous account of a tropical cyclone-like storm affecting California was the "Columbus Day windstorm", which evolved into a wave cyclone from the remnants of Typhoon Freda and made landfall in the Pacific Northwest in October of 1962 (Lynott and Cramer 1966).

Sanders and Gyakum (1980) developed a climatology of rapidly developing cyclones in the Northern Hemisphere. Their findings show that explosive deepening is uncommon over the coastal waters of California. Subsequently, the literature on explosive cyclogenesis has become quite robust (e.g., Reed and Albright 1986). This literature will partially serve as a basis for the quantitative assessments that form bases for some of the conclusions of this thesis.

As early as the 1980s (e.g., Businger 1987), relatively small, intense cyclones over the Northern oceans in polar latitudes called "polar lows" have been observed and studied. These lows share several characteristics with tropical cyclones, including cloud-free eyes and warm cores, and can develop explosively themselves, producing hurricane-like wind conditions. The literature on polar lows in subsequent years has also become robust (e.g., Condrón et al. 2006, Yanase et al. 2007). An interesting research area that has opened up in recent years (e.g., Rasmussen and Zick 1987) centers on similar disturbances developing in the midlatitudes, for example, over the Mediterranean Sea.

The present study will explore the development of the 19 February 1993 storm. Previous studies have shown that meteorological factors responsible for both explosively developing cyclones and polar lows can be assessed or diagnosed quasigeostrophically. Therefore, an analysis of the mechanisms associated with the unusual development of this storm will be guided by the author utilizing rubrics outlined in the referred literature for both rapidly developing cyclones and polar lows.

The explicit purpose of this thesis is to conduct a thorough investigation into the planetary, synoptic, and mesoscale aspects of the atmosphere that led to the development of this unusual storm. A complete synoptic history of the disturbance will be constructed on the basis of a combination of subjective analyses and objective reanalyses. The features and processes that are now understood to be of importance to explosive cyclogenesis and polar low development will be assessed quasigeostrophically both qualitatively and quantitatively on the basis of methodologies that have successfully been used in the study of similar disturbances. The important questions to be answered center on whether the development of the low was dominated by terms in the pertinent equations associated with the pattern itself (as assessed by vorticity advection) or changes in that pattern due to heating or cooling (as assessed by thickness changes).

The thesis is organized in the following manner. An overview of the characteristics of the disturbance that made it remarkable and the effects of the storm across California are provided in Chapter 2. The synoptic scale evolution of the storm as it developed over the eastern Pacific Ocean and made landfall along the California

coastline is provided in Chapter 3. An overview of what is known about explosive cyclogenesis and polar low development and evolution is provided in Chapter 4. The methodology used by the author in assessing the development factors of the storm is discussed in Chapter 5. Chapter 6 contains both the qualitative quasigeostrophic diagnosis of the development of the disturbance and the quantitative assessment of the contributing terms. A discussion of the results and comparison to those found in the literature for similar disturbances comprises the bulk of Chapter 7. The author's summary of why the analyses performed in the thesis justify the conclusions about the contributing factors to this storm's development are found in Chapter 8, along with suggestions for future research.

2. Overview of Storm

While extratropical cyclones are a common occurrence along the West Coast of the United States during the cold season, the 19 February 1993 storm had numerous characteristics that make it a particularly noteworthy case. As mentioned in Chapter 1, the storm developed an eye-like feature prior to landfall. Fig. 2 shows the eye as it approached the coast of Mendocino County in Northern California. It appears as though the eye was nearly cloud-free at its center and was surrounded by clusters of cumulonimbi. The eye and the surrounding convective wall serve as visual evidence of a warm core, as latent heating from the surrounding cumulus convection would raise temperatures at the center of the storm. Again, eyes and warm cores are often associated

with tropical cyclones and polar lows, two classifications of cyclones that are generally not found along the coast of California.

Numerical evidence of the storm's warm core comes in the form of temperature data from TIROS Operational Vertical Sounder (TOVS) from 00 UTC 20 February 1993, the approximate time of landfall. Fig. 3a and Fig. 3b show zonal and meridional transects of temperature through the storm, respectively. Along the 38th parallel, temperatures at lower levels (850 to 700 mb) reached a maximum within 1 degree longitude to the east of the eye. Low level temperatures decreased to the west and east of the storm center. On the contrary, temperatures at upper levels (200 mb) reached their minimum directly over the eye of the storm. The meridional transect shows a similar temperature trend, with warm low level temperatures near the center of the low and cooler temperatures to the north and south. Again, upper level temperatures directly above the cyclone center were cold relative to the air to the north and south.

Sea surface temperature data reveals another interesting feature within the storm. Fig. 4 shows that sea surface temperatures in the coastal waters of California were warmer than the climatological mean, with anomalies reaching +2°C. An advisory issued by the NOAA Coastal Ocean Program (1993) suggests that residual warmth from the 1991-1992 El Niño, an apparent resurgence of El Niño, and the advection of warm subtropical waters into the North Pacific were responsible for the anomalously warm sea surface temperatures in the region. At the same time, the cyclone appears to have developed in an area where temperatures in the lower troposphere were significantly

colder than the ocean surface. Fig. 5 shows sea surface temperatures were as much as 7°C warmer than the overlying air off the coast of California. The temperature difference between the sea surface and overlying air within the vicinity of the developing cyclone suggest that mechanisms associated with a class of cyclones called “polar lows” (Rasmussen and Turner 2003, p. 2) may have contributed to this case. Clearly, an investigation into the possibility that the 19 February 1993 storm was a polar low is warranted.

Additionally, the strength of the convection associated with the cyclone was remarkable. An infrared AVHRR satellite image for 2315 UTC 19 February 1993 (Fig. 6) shows cold anvils surrounding the eye of the storm. While shallow convection is common in the coastal waters of California (Monteverdi 1976), the vertical extent of the convection surrounding this storm is noteworthy. The impacts of the strong convection in California were far reaching, and are discussed in detail in the next section.

a. Impacts

As the cyclone deepened and approached the western United States, clouds and precipitation along and ahead of the main fronts associated with the low began passing over the state of California around 06 UTC 18 February 1993. Over the next 48 hours, heavy rain, high elevation snow, thunderstorms, and strong winds were observed across the state. The unsettled weather moved eastward and finally exited California around 06 UTC 20 February 1993. Data from Automated Surface Observing System (ASOS)

stations and Automated Weather Observing System (AWOS) stations in California were obtained from 00 UTC 18 February to 12 UTC 20 February 1993 (NCDC 2014). All automated reports of heavy rain and high winds associated with the storm should fall within this 60 hour dataset. Fig. 7 shows the locations of the stations where significant rain and wind reports were observed.

Strong sustained winds were reported in Southern California with the passage of the main frontal boundaries associated with the low on 18 February 1993. Table 1 shows observations of sustained winds of 35 mph or greater at ASOS/AWOS stations in California during the passage of the cyclone, along with the date and time of the report. Winds of 63 mph were recorded at San Clemente Island on the afternoon of 18 February, with other stations in Southern California reporting strong winds within several hours of that time. Table 2 shows peak gusts that were recorded at ASOS/AWOS stations. A gust of 87 mph was observed at Mount Wilson, although this was one of the only strong gusts observed by ASOS/AWOS stations in Southern California during the passage of the cyclone. However, according to storm data from the NCDC (1993, p. 10), a gust of 94 mph was observed at Vandenberg Air Force Base near Lompoc, CA on 18 February 1993. The report also mentions gusts in excess of 60 mph at other coastal locations.

The highest sustained winds and gusts observed during the event occurred as the cyclone with the eye-like feature made landfall in Mendocino County, where Point Arena reported sustained winds of 71 mph at 00 UTC 20 February 1993. A statement issued by the San Francisco National Weather Service Weather Forecast Office (NWS WFO) cited

a gust of 89 mph at Point Arena (National Weather Service 1993a), although this gust was not present in the ASOS/AWOS data. Another statement issued by the Eureka NWS WFO reported gusts of 90-95 mph in Mendocino County (National Weather Service 1993b). Three to four hours later, sustained winds in excess of 45 mph were observed at Chico and Redding. The strongest gusts observed at ASOS/AWOS stations were 61 mph and 60 mph, reported at Chico and Redding, respectively, and were concurrent with the high sustained winds.

Heavy rains were also observed by ASOS/AWOS stations throughout the duration of the storm. Table 3 shows peak 1-hr rainfall totals in California. Nearly all of the observed 1-hr precipitation totals in excess of 0.20 in. occurred in Southern California. Table 4 shows 6-hr precipitation totals. Unlike 1-hr precipitation observations, many 6-hr precipitation totals were observed in Central and Northern California. Most notably, Mount Wilson received nearly 3 inches of rain over two consecutive 6 hour periods. High 24-hr precipitation totals were observed across the state of California during the event, as shown in Table 5. Eureka had the highest observation with 1.78 in. of rain. However, a statement issued by the San Francisco NWS WFO, 24 hour rainfall totals reached 4 in. in the northern Sierra Nevada Mountains and the Coastal Mountains south of Big Sur (National Weather Service 1993a). These reports, along with high rainfall rates recorded at Mount Wilson, suggest that orographic lift enhanced rainfall totals at high elevations.

The strong winds, heavy rains, and severe thunderstorms associated with the storm produced damage across the state of California. According to a statement issued by the Eureka NWS WFO, property damage in Mendocino County was estimated at 1 million dollars, with damage being reported to buildings, businesses, and roofs (National Weather Service 1993b). Storm data from the NCDC (1993, p. 10) reports redwood trees with diameters up to 5 feet were blown over by heavy winds. Further inland, in the Sacramento Valley, high winds produced extensive property damage. In Yuba County, a home was reported to have lost half of its roof and three mobile homes were removed from their foundations. Property damage and closed roads due to falling trees were also reported in Yolo and Napa counties. In the Sierra Nevada Mountains, 3 to 6 feet of snow fell during the passage of the storm. Portions of Interstate 80 were closed periodically on 20 February 1993. Unfortunately, in addition to property damage, there was one death directly attributed to the storm in Northern California, as a man in Tehama County was killed when a tree fell onto his car during the passage of the storm on 19 February 1993.

Heavy rains, strong winds, and thunderstorms also produced damage in Central and Southern California. In coastal areas of Central California, near San Luis Obispo and Santa Barbara, portions of U.S. Highway 101 were closed due to flooding, mudslides, and accumulated hail. Thunderstorms in this area produced frequent lightning, with one observer in Santa Barbara County reportedly counting 135 individual strikes. Multiple funnel clouds were reported in the San Joaquin Valley in inland Central California, along with at least one tornado touchdown (NCDC 1993, p. 11). In Southern California, many

roads were closed due to flooding in Orange County (Los Angeles Times 1993a). In Southern California, portions of the Sierra Highway were damaged by flooding, which was described by local residents as the “worst in decades”. Cars, trucks, and tractors were reported to have been buried in as much as five feet of mud (Los Angeles Times 1993b). The extensive damage across California demonstrates the significance of the 19 February 1993 and provides additional motivation to explore the development of the storm.

3. Synoptic Analysis of Storm

In order to further investigate the development of the storm’s aforementioned notable characteristics, a thorough analysis of the storm will be conducted. In this section, I will explore the planetary and synoptic scale setting in which the initial surface low developed and deepened.

Data for the following analyses will come from several sources. Firstly, data from the NCEP/DOE AMIP-II Reanalysis (NOAA/ESRL PSD 2014), hereafter referred to as the Reanalysis-2, in the form of charts will be used to visualize surface pressure fields, 500 mb and 250 geopotential height fields, and 1000-500 mb thickness patterns, among other data. Infrared satellite imagery (NOAA/NESDIS 2014) will be used to identify cloud features associated with the storm. Additional data, including satellite imagery, surface maps, and sea surface temperature data were obtained from Dr. John Monteverdi, Professor of Meteorology at San Francisco State University.

a. Pre-Storm Environment

On 10 February 1993, approximately 10 days prior to the landfall of the storm, a large upper level low was located east of Kamchatka, near the tail of the Aleutian Islands (see 500 mb height map in lower right of Fig. 8a). A strong zonal jet existed to the south of the low, extending from Japan to the north-central Pacific Ocean. A subtle ridge axis was located at about 155-160°W, while a broad trough was just east of Hawaii. A trough with a markedly negative tilt¹ was associated with the low over the Aleutians was extending over the Gulf of Alaska while a large ridge was in place over western Canada and the northwestern United States.

The surface map for this time (upper left of Fig. 8a) shows a deep low pressure system associated with the low east of Kamchatka. Further east, two areas of low pressure were located in the Gulf of Alaska. To the south, off the coast of Baja California, there was a broad high pressure system with a central pressure exceeding 1020 mb.

In the following days, many of these features shifted to the east. Two days later, at 00 UTC 12 February 1993, the 500 mb low east of Kamchatka had shifted towards the Aleutians (lower right of Fig. 8b). The jet situated just south of the upper level low had developed a broad cyclonic curvature. Over the eastern Pacific, the ridge axis that had been over 155-160°W had amplified and shifted towards the west coast of North

¹ A negatively-tilted trough is an area of low pressures or heights not completely encircled by a contour and whose axis extends from northwest to southeast.

America. Similarly, the trough that had been over Hawaii had moved towards Baja California.

By 00 UTC 14 February 1993, the planetary scale pattern that eventually produced the 19 February 1993 storm becomes apparent. The upper level low that had been over the Aleutians had opened into a trough, evident at 250 mb and 500 mb (upper right and lower right of Fig. 8c, respectively), the axis of which extended from the western Aleutian Islands southeastward towards Hawaii. There were two surface lows downstream from this trough in the Gulf of Alaska. The upper level ridge off the west coast of North America had amplified further, with the axis at approximately 135°W over the ocean and curving towards the west over Alaska. The planetary scale troughs and ridges continued to amplify on 15 February 1993 (see 250 mb map, upper right of Fig. 8d), while the surface lows associated with the trough over the Aleutians began to dissipate. Meanwhile, a strong surface high over Canada became apparent (see surface map, upper left of Fig. 8d). This high was downstream from the ridge near the west coast of North America.

b. Initial Low Development

By 00 UTC 16 February 1993, a few noteworthy changes at both upper and lower levels can be identified. The trough axis associated with the upper level low over the Aleutians extended from the western Aleutians towards the southeast, with the Southern portion of the axis situated roughly halfway between Hawaii and Baja California (see 250

mb map, upper right of Fig. 8e). A surface pressure trough, which opened towards the deep surface low near Kamchatka, began to develop at this time near 35°N , 150°W , just to the southwest of the upper level trough axis. Some warm air advection in the vicinity of the developing surface pressure trough is also evident at this time (see 1000-500 mb thickness map, bottom left of Fig. 8e). The ridge off the west coast of North America encompassed a closed high at 500 mb, situated just south of the Yukon Territory (bottom right Fig. 8e). The ridge had nearly closed at 250 mb (top right Fig. 8e). Additionally, a positively tilted trough over western North America began to amplify. The axis of this trough extended from central Canada towards the southwest, reaching the Pacific Ocean near the Oregon coast.

By 12 UTC 16 February 1993, the surface pressure trough had closed to form a low pressure system with a central pressure below 1004 mb (see top left of Fig. 8f). This is the low that went on to strengthen before making landfall in California. At this time, the newly developed low was located within a planetary scale trough at 500 mb (bottom right Fig. 8f) and downstream from a thermal trough (see the 1000-500 mb thickness map, bottom left Fig. 8f). The infrared satellite image in Fig. 9a showed a comma shaped cloud in the eastern Pacific, with banded cumulus convection to the east of the surface low. Open cell cumulus clouds were visible to the west and north of the comma cloud, suggesting that deep convection was inhibited in this area.

As of 00 UTC 17 February 1993, another notable change occurred at upper levels. The upper level trough that had been over the Aleutians had become largely positively

tilted and was lifting off to the north (see 250 mb map in upper right of Fig. 8g). At the same time, the ridge axis shifted westward, allowing the negatively tilted trough over western North America to dig southward over the eastern Pacific Ocean. Meanwhile, the surface map (top right of Fig. 8g) shows that the surface low, which still had a central pressure below 1004 mb, had moved southeastward, now located at approximately 30°N, 140°W. Infrared satellite imagery (Fig. 9b) shows that the surface low was now under the influence of the latter upper level trough, located just downstream from the 250 mb trough axis. A closed low at 500 mb (see bottom right of Fig. 8g) had developed over the surface low. However, the 1000-500 mb thickness pattern (bottom left of Fig. 8g) shows warm air advection was still occurring to the east of the surface low center. Satellite imagery continued to show banded cumulus convection in a comma shape around the surface low.

The surface low had moved further east by 12 UTC 17 February 1993 (top left of Fig. 8h), although the central pressure had not changed significantly in the previous 24 hours. The low was located just downstream from the 250 mb trough axis (top right of Fig. 8h). The 500 mb closed low had opened into a trough (bottom right of Fig. 8h), and the surface low was located barely downstream from the axis (top left of Fig. 8h). Warm air advection to the east of the surface low had strengthened (see 1000-500 mb thickness map, bottom left of Fig. 8h). However, the infrared satellite image in Fig. 9c showed a leaf cloud containing cold anvils of cumulonimbus clouds had developed further east of the trough axis, due west of the southern tip of Baja California.

c. Rapid Deepening and Landfall

By 00 UTC 18 February 1993, the surface low had moved a few degrees eastward while the trough remained stationary at both 250 and 500 mb (top and bottom right of Fig. 8i, respectively). The trough axis was identifiable on infrared satellite imagery at this time (see Fig. 9d), with distinct areas of open cell and closed cell cumulus clouds to the east and west of the trough axis, respectively. The surface low (see top left of Fig. 8i) had shifted further downstream from the upper level trough axis. This time marks the beginning of a period of significant surface pressure falls at the low center. The infrared satellite image in Fig. 9d showed that the original banded cumulus convection wrapped around the surface low had significantly dissipated. Meanwhile, the leaf cloud had more than doubled in size, with additional anvil clusters to the north and northwest of the original leaf cloud. The western edge of the leaf cloud was beginning to develop a comma shape, indicating that the frontal wave was beginning to mature.

By 12 UTC 18 February 1993, the central pressure of the surface low was below 996 mb (upper left of Fig. 8j). The low was downstream from the 250 mb trough axis (upper right of Fig. 8j), although the closed low had redeveloped at 500 mb (lower right of Fig. 8j). However, it appears as though a few shortwave troughs were rotating around the 500 mb low. An area of enhanced open cell cumulus convection southeast of the surface low is visible in the infrared satellite image in Fig. 9e. Warm air advection was still very strong to the northeast of the surface low (lower left of Fig. 8j), including coastal areas of the southwestern United States. The leaf cloud had continued to develop

into a more mature comma cloud, indicating that the cyclone was reaching a mature stage (Conway 1997, pp. 134). A triple point is evident in the imagery, suggesting that the fronts associated with the cyclone had begun to occlude. The triple point of the comma cloud was located near the Point Conception area, with a warm front positioned east to west across Central California and a cold front extending southward into the tropical eastern Pacific.

As of 00 UTC 19 February 1993, the surface map in Fig. 8k shows that the surface low was located several hundred miles to the west of the San Francisco Bay Area. The central pressure was still below 996 mb. The 250 mb trough had become neutrally tilted (upper right of Fig. 8k), suggesting that it was beginning to move out of the eastern Pacific. The 500 mb low remained closed (lower right of Fig. 8k), although a slightly negatively tilted short wave trough is evident to the south of the closed low. The 1000-500 mb thickness map (lower left of Fig. 8k) shows that the strongest warm air advection was occurring over Washington, Oregon, and southwestern Canada, although weaker warm air advection was still evident over California. Infrared satellite imagery at this time (Fig. 9f) showed that the large comma cloud had moved inland over the western United States, with an occluded front extending from the surface low center over Oregon and Idaho. The enhanced open cell cumulus convection that had been to the southeast of the surface low had developed into a new leaf cloud. The western edge of the leaf cloud had already developed noticeable cyclonic curvature, reminiscent of a small comma cloud. While the Reanalysis-2 does not show a surface low in this area, the shape of the

cloud indicates that a sub-synoptic scale low developed with this localized area of cumulonimbus development.

By 12 UTC 19 February 1993, the Reanalysis-2 shows that the main surface low had deepened to below 992 mb and was located within just offshore from the Mendocino County coast in California (see top left of Fig. 8l). The 250 mb trough was flattening and lifting northeastward (top right of Fig. 8l). At 500 mb (bottom right of Fig. 8l), the closed low west of California had reopened while a new closed low formed further north within the same trough, off the coast of British Columbia.

However, beginning at this time, there is a notable discrepancy between the reanalysis and the satellite imagery. An infrared satellite image (Fig. 10) from two hours prior to this time showed that newly developed leaf cloud had grown in size and moved over Northern California, north of San Francisco. The cyclonic curvature of the leaf cloud had become less identifiable as it moved onshore. At the same time, the western end of what had been the large comma cloud extending over the northwest began to show signs of developing cyclonic curvature, with a distinct s-shape along the occluded frontal boundary. This suggests that a new wave cyclone was developing along the boundary, well to the west of the surface low analyzed by Reanalysis-2 reanalysis. Due to the incongruity between Reanalysis-2 and the satellite observations, the reanalyzed surface analysis is no longer considered an accurate representation of reality at this time. However, planetary scale features in the reanalysis are likely to be close to reality, due to the relatively slow rate at which those features change.

Six hours later, at 18 UTC 19 February 1993, an infrared GOES west satellite image (Fig. 11) showed cumulonimbus anvils over the eastern Central Valley and western Sierra Nevada mountains in Central California. A large area of clouds was also located over the northwest portion of the state. An analyzed surface analysis (Fig. 12a) showed scattered reports of rain and high-elevation snow over Northern California. Additionally, the wave along the frontal boundary further west continued to develop, with a well-defined cyclonic circulation identifiable in satellite imagery (Fig. 11) at the inflection point of the wave. This provides evidence of a newly developed surface low. The eye-like feature at the center of the cyclone provides evidence of abnormally strong circulation within this cyclone, and is reminiscent of a polar low (Emanuel and Rotunno, 1989). Subsequent surface analyses showed falling pressure over Northern California with scattered reports of rain and snow showers continuing for several hours.

The surface analysis for 21 UTC 19 February 1993 (Fig. 12b) showed that winds along the coasts of Humboldt and Del Norte counties in far Northern California had shifted from southeasterly to north-northwesterly, with temperatures and dew points dropping several degrees. This, along with increasing surface pressures, suggests that a surface boundary had passed. This was likely the old occluded boundary on which the secondary cyclone had developed. Also, thunderstorms were observed at two sites in the northern Sacramento River Valley.

An AVHRR infrared satellite image of Northern California from 2315 UTC 19 February 1993 (Fig. 6) provided a detailed view of the newly developed cyclone as it

made landfall on the coast of Mendocino County. The eye-like feature was even more defined than it had been 6 hours prior, with cold cumulonimbus anvils nearly encircling a cloud-free area. Additional anvils can be identified over the eastern San Joaquin River Valley and the central Sacramento River Valley. A broad area of cold cloud tops was located to the northwest of the eye-like feature, over the coastal waters adjacent to northern Mendocino County and southern Humboldt County. The surface analysis for 23 UTC 19 February 1993 (Fig. 12c) showed strong southerly winds over much of Northern California, with scattered rain observations and continued snow observations in higher elevations. There was a report of a thunderstorm on the San Francisco Peninsula.

While 00 UTC 20 February 1993 surface observations were sparse, the surface analysis for 01 UTC (Fig. 12d) showed that the surface low had moved onshore. There was a strong pressure gradient in Mendocino County, indicating strong sustained winds in the vicinity of the low center. Heavy rain was observed in inland Mendocino County, while scattered reports of light to moderate rain were observed across Northern California, especially over the San Francisco Bay Area. During the following hours, surface analyses showed winds shifting from southerly to westerly as cyclone moved eastward across Northern California. By 06 UTC 20 February 1993, infrared satellite imagery (Fig. 9j) shows that remaining cold cloud tops had moved eastward over the Sierra Nevada Mountains and San Joaquin River Valley. Remnant cloud bands over western Northern California were warmer, suggesting that deep cumulus convection had ended in that area. Widespread open cell cumulus convection can be seen over coastal

waters east of the upper level trough axis, with close cell cumulus clouds further west. This marks the end of the storm's impact on Northern California, with only isolated observations of precipitation remaining at this time (Fig. 12e).

In the wake of the storm, damage was reported across California, as was described in Chapter 2. The severity of the storm received media attention (e.g., Los Angeles Times 1993a and 1993b) and the meteorological community in California took note of the unusual characteristics of the storm (e.g., Monteverdi et. al. 1993). The following chapters present an analysis of the storm and characterize the meteorological processes that contributed to its remarkable development and its 'polar low'-like features.

4. Explosive Cyclogenesis in Cold Air Masses

There is a robust literature on the forecast issues associated with rapidly developing cyclones in cold air masses². In the late 1980s, there was a convergence in the research literature on studies of cyclones of any sort that develop quickly and a class of surface low pressure areas that form and intensify rapidly over warmer ocean temperatures (Businger and Reed 1989a). While rapid cyclogenesis can occur with tropical and extratropical cyclones of any sort, it was recognized as early as the late 1960s that formation and development of unusually strong disturbances can occur over

² There is no quantitative definition of a "cold air mass". In the context of this study, and others of rapidly developing cyclones, "cold air mass" means that the temperature of the underlying ocean is much warmer than that of the atmosphere passing over it.

the northern oceans in polar latitudes. These cyclones were termed “polar lows”.

(Anderson et. al. 1969; World Meteorological Organization 1973).

The synoptic history and notable characteristics of the strong cyclone that moved across Northern California on 19 February 1993 were summarized in Sections 2 and 3. In the course of that evaluation, the author noted a number of attributes of the evolution of the storm that matched those found for cyclones that rapidly intensify in general (termed “explosively developing” as discussed below) and those found for certain subclasses of polar lows. Thus, the literature on both of these phenomena yields insights into the factors that might have been in play along the California coast on 18 and 19 February 1993.

a. Explosive Cyclogenesis

The initial studies on rapidly developing extratropical cyclones mostly were concerned with establishing the climatology of those disturbances. For example, Sanders and Gyakum (1980) developed a climatology of rapidly developing cyclones in the Northern Hemisphere. They defined cyclones whose central pressure deepened at an average rate of at least 1 mb per hour for at least 24 hours as “meteorological bombs”, or simply “bombs”. The process was loosely termed “bombogenesis.”

Their study of three years’ worth of data concluded that bombs were cold season, maritime events that generally occurred in areas of strong baroclinicity. In the Pacific Ocean, two areas were climatologically favorable for bombogenesis. In the western

Pacific, there was a maximum in bomb frequency off the coast of Japan, while a secondary maximum was observed in the central Pacific south of the Aleutian Islands (Fig. 13).

It is interesting to note that bombogenesis was not common in the eastern Pacific Ocean near the coast of California during the period of study. While the 19 February 1993 storm did not maintain its deepening rate quite long enough to meet the criteria for a bomb, the climatology developed by Sanders and Gyakum show that the rapid development of the storm off the coast of California was unusual.

Sanders and Gyakum (1980) also calculated the deepening rates of selected bombs. Their calculated rates fell far short of the observed rates, indicating the importance of factors that were not accounted for in equations that were used.

Their analysis suggests that boundary layer processes and bulk effects of cumulus convection must play an important role in cyclogenesis. In essence, Sanders and Gyakum (1980) concluded bombs are largely baroclinic events and their development is strongly related to stability of the lower atmosphere and are aided by diabatic heating at the ocean surface.

Later, Reed and Albright (1986) completed a series of analyses of the controls on an explosively developing cyclone in the eastern Pacific Ocean. The storm deepened at a much faster rate and achieved a lower central pressure than the 19 February 1993 storm, yet their analyses of the processes that controlled the deepening still form the basis of studies of rapidly developing cyclones.

Reed and Albright (1986) performed a quantitative diagnose of the vertical motion fields associated with the storm. The authors' evaluation showed that cyclogenesis occurred in an area of unusually strong baroclinicity and diabatic heating via latent heat release associated with deep cumulus convection contributed largely to the upward vertical motion field. They further found that sensible heating contributed to the destabilization of the lower troposphere, resulting in a lowered static stability parameter. In essence, the lower the static stability, the greater the forcing for vertical motion.

b. Conditional Instability of the Second Kind and Destabilization Due to Air-sea Diabatic Heating

As the 19 February 1993 storm moved into California, multiple areas of cyclonic development can be identified behind the main cold front and along the old occlusion, where sea surface temperatures were significantly warmer than the overlying air. The air-sea temperature difference (see Fig. 5) provides evidence of strong sensible heat fluxes from the ocean to the atmosphere, and strong convection evident in satellite imagery (e.g. Fig 6) indicates further warming of lower levels due to latent heat release. Diabatic heating of the lower troposphere would have contributed to locally positive thickness tendencies (which would have caused upper level divergence and upward mid-tropospheric vertical motion due to isallobaric flow at upper levels) as well as decreased static stability, which would create a more favorable environment for upward vertical motion. Since these terms are of importance to surface cyclogenesis (as upward vertical

motion would be associated with low level convergence), the relationship between diabatic heating and cyclone development must be considered as a contributing factor to the development of the 19 February 1993 storm.

Diabatic heating has been shown to make a large positive contribution to cyclogenesis (Sanders and Gyakum 1980, Reed and Albright 1986). However, during the latter half of the 20th century, the effects of diabatic heating in the development of surface lows (especially tropical cyclones) have been explained using alternative hypotheses. Charney and Eliassen (1964) suggest that Conditional Instability of the Second Kind (CISK) contributes to the development of tropical cyclones. CISK is a synergistic relationship between low-level convergence and latent heat released by cumulus convection.

A positive feedback loop is created in which an increase in low level convergence is associated with an increase in mid-tropospheric vertical motion, thereby enhancing cloud development and cumulus convection. In turn, the cumulus convection releases latent heat, increasing layer thicknesses hypsometrically. These increases are associated with positive isallobaric tendencies at the top of the column, leading to horizontal divergence aloft. The upper tropospheric divergence is linked to low level pressure falls, thereby enhancing low level convergence. The loop only occurs if a conditionally unstable atmosphere is an environment of low level convergence, a phenomenon that does occur in developing tropical cyclones.

Emanuel (1986) challenges the findings of Charney and Eliassen (1964) and proposes his own hypothesis regarding the role of diabatic heating tropical cyclone development. Emanuel suggests that, rather than an organized release of latent heat via CISK, tropical cyclones can develop and become self-sustaining through a process that he refers to as air-sea latent and sensible heat transfer, without any preexisting conditional instability. Sensible and latent heat fluxes from a warm ocean surface to the boundary layer provide the energy needed for a tropical cyclone to strengthen.

Preliminary observations of the 19 February 1993 storm indicate the presence of strong diabatic heating at lower levels. Latent heat release associated with strong convection may have enhanced cyclogenesis via CISK. Additionally, strong sensible heating of the lower troposphere from the relatively warm sea surface suggest that the air-sea latent and sensible heating process outlined by Emanuel (1986) may have contributed to cyclone development. The contributions from CISK and air-sea latent and sensible heat transfer to the development of the 19 February 1993 storm will be considered during the forthcoming analysis.

c. Polar Lows

Satellite imagery (Fig. 2, Fig. 6, Fig. 11) of the 19 February 1993 storm is remarkably reminiscent of a polar low, which is a special type of extratropical cyclone that has been compared to tropical cyclones. Several features typically associated with polar lows (which are discussed in detail below) can be identified within the cyclone as it

made landfall in Mendocino County in Northern California, including a warm core with a cloud free eye and strong convection. To the author's knowledge, no polar lows have ever been documented over the coastal waters of California. This study may be the first documented case of a landfalling polar low in California, as well as the first documented polar low within the vicinity of the west coast of the Continental United States.

Small, relatively strong cyclones have been observed at high latitudes throughout the latter half of the 20th century. However, it was not until the 1980's that the distinguishing characteristics of these polar lows were studied in detail. Polar lows are small, rapidly developing extratropical cyclones that develop over warm sea surfaces in the winter. They can be described as small, intense cyclonic circulations, often with an eye-like structure surrounded by strong convection. Like tropical cyclones, polar lows have warm cores with high equivalent potential temperatures.

During the 1980's and 1990's, the mechanisms responsible for polar low development became a focal point of polar low research. Sardie and Warner (1985) numerically modeled polar lows in order to assess the various mechanisms responsible for their development. Their study found baroclinic instability was largely responsible for polar low development in the Pacific Ocean while a combination of baroclinicity and CISK contributed to polar lows in the Atlantic. They also suggest that the frequency of polar lows in the northern Pacific and northern Atlantic coincides with the climatology of bombs found by Sanders and Gyakum (1980), indicating that polar lows likely develop from residual circulations within the polar air mass behind strong, occluded extratropical

cyclones (e.g. the cyclone that impacted California on 18-19 February 1993). In addition to baroclinic instability and CISK, Emanuel and Rotunno (1989) suggest that the same air-sea latent and sensible heating process that can cause tropical cyclones to deepen can contribute to the development of polar lows as well. However, they clarify that a significant disturbance is necessary to initiate cyclogenesis due to the air-sea latent and sensible heat flux.

Businger and Reed (1989b) identified three general polar low development schemes, each with their own characteristics. 1 – The short wave and jet streak type, which relies heavily on vorticity advection and baroclinicity. 2 – The arctic front type, featuring shallow baroclinicity and strong surface fluxes. And lastly, 3 – cold low type, characterized by strong heat fluxes at the surface and deep convection. Rasmussen and Turner (2003, p. 159) developed a more detailed classification scheme, featuring 7 different polar low types identified in a study by Wilhelmsen (1985) (Table 6). The authors note that Group 4, the ‘cold low’ type of polar low (which similar to the third development scheme described by Busing and Reed (1989)), was the most common frequent polar low type identified in the study (Rasmussen and Turner 2003, p. 172). This type of polar low develops within the core old, occluded lows, without strong vorticity advection at upper levels or low-level baroclinic zones. ‘Cold low’ polar lows have been identified in the Gulf of Alaska and the Bering Sea (Businger 1987) during cold-air outbreaks over the northern Pacific Ocean. Preliminary observations suggest that the 19 February 1993 storm may have developed in an environment similar to the pattern

associated with the 'cold low' type of polar lows. As the 19 February 1993 storm's characteristics are compared to those of polar lows, features associated with 'cold low' polar low development will be specifically referenced.

Lastly, while polar lows are generally thought of as a high latitude phenomenon, there have been observations of polar lows in the mid-latitudes. Notably, the Mediterranean Sea has been known to provide a setting for polar low development. Rasmussen and Zick (1987) discuss a polar low that developed as the result of convection over the Mediterranean. The low developed within a deep, cut-off cold core low, where low-level baroclinicity was relatively weak (i.e. a 'cold low' polar low). Rasmussen and Turner (2003, p. 215) state that polar lows over the Mediterranean provide evidence that convection is an important mechanism for the development of polar lows, as opposed to strong baroclinicity. Since the 19 February 1993 storm also developed in the middle-latitudes, its features will be compared to those of polar lows in the Mediterranean Sea (e.g. strong convection).

d. Explosive Cyclogenesis, Polar Lows, and the 19 February 1993 Storm

The 19 February 1993 storm underwent a period of rapid deepening in an environment that was generally favorable for synoptic-scale upward vertical motion, which would have been associated with surface cyclogenesis. Furthermore, a synoptic and mesoscale analysis of the storm highlighted features commonly associated with explosive cyclogenesis, including baroclinicity, strong diabatic heating at low levels, and

low static stability. The evidence of latent and sensible heat fluxes within the storm also highlight the possibility of CISK and air-sea latent and sensible heat transfers contributing to cyclogenesis.

Observations of the 19 February 1993 storm prior to landfall show an eye-like structure surrounded by strong convection (see Fig. 6) and a warm core (Fig. 3a and 3b). Both of these features are reminiscent of polar lows. While polar lows are generally thought of as high latitude events, they have been observed in the mid-latitudes (Rasmussen and Zick 1987, Rasmussen and Turner 2003, p. 215), and the pattern in which the 19 February 1993 storm developed resembles a development scheme associated with a particular class of polar lows associated with cold lows. The features associated 'cold low' polar low development will receive careful consideration when assessing the possibility of the 19 February 1993 storm as a polar low.

5. Methodology

A qualitative discussion of the mechanisms controlling cyclogenesis is necessary to assess the environment in which the 19 February 1993 storm formed. An analysis of processes associated with forcing for vertical motion will provide evidence of conditions favorable for surface cyclogenesis. Specifically, the evolution of the vertical motion field throughout the life of the storm will allow the author to reconstruct the timeline of the development of the surface low, including the period of explosive cyclogenesis.

While qualitative observations will provide useful insight during the diagnosis of the 19 February 1993 storm, a quantitative assessment of the factors contributing to cyclogenesis is necessary to support the forthcoming conclusions with numerical evidence. An outline of both the qualitative and quantitative analyses is provided in the following sections.

As the contributing factors to the development of the 19 February 1993 storm are analyzed, the literature associated with explosive cyclogenesis and polar low development will need to be referenced systematically so observations and comparisons can be made. Therefore, a table (Table 7) will be used to identify features within the 19 February 1993 storm that are typical of polar low development (including explosive deepening within strong polar lows). Specifically, group 4 of Rasmussen and Turner's (2003, p. 159) table (Table 8), known as 'cold low' polar lows, will be used to provide typical patterns and features associated with polar low development, as preliminary analyses of the 19 February 1993 storm show similar traits to this class of polar lows. The climatology of 'cold low' polar lows, along with literature regarding mid-latitude polar lows (e.g. Rasmussen and Zick 1987, Rasmussen and Turner 2003, p. 215) will provide the criteria for the rubric that I will use to assess the possibility of the 19 February 1993 storm as a polar low.

a. Review of Quasigeostrophic Theory

The development of the initial surface low, along with its subsequent evolution into a mature extratropical cyclone, can be explained by examining processes that are known to contribute to cyclogenesis. At the synoptic scale, these processes include the presence, movement, and development of upper level troughs and ridges, as well changes to the temperature field within the storm via temperature advection, adiabatic heating, and diabatic heating. The relationship between these processes and both vertical motion and cyclone/anticyclone development is commonly understood on the basis of the quasigeostrophic (QG) equations.

QG theory is a conceptual model that allows meteorologists to explain vertical motion and the development of surface pressure fields at the synoptic scale using conventional meteorological charts. Many authors (e.g. Sanders and Gyakum 1980) have used QG theory to add insight to the factors that influence storm development at the synoptic scale. The quasigeostrophic omega equation (hereafter referred to as the QG-omega equation), illustrates the relationship between vertical motion and forcing mechanisms that can diagnose vertical motion at the synoptic scale (Bluestein 1992, p. 329).

$$\underbrace{\left(\nabla_p^2 + \frac{f_0^2}{\sigma} \frac{\partial^2}{\partial p^2}\right)}_{\text{Term A}} \omega = - \underbrace{\frac{f_0}{\sigma} \frac{\partial}{\partial p} [-\vec{V}_g \cdot \vec{\nabla}_p (\zeta_g + f)]}_{\text{Term B}} - \underbrace{\frac{R}{\sigma p} \nabla_p^2 (-\vec{V}_g \cdot \vec{V}_p T)}_{\text{Term C}} \quad \text{Eq. (1)}$$

This equation states that the forcing for vertical motion (Term A) can be estimated on the basis of the sum of the forcing from differential vorticity advection (Term B) and thickness advection (Term C).

The differential vorticity advection (Eq. (1), Term B) is related to the shape of the flow at upper levels (i.e. troughs and ridges). As parcels of air move through an upper level trough, they must conserve their angular momentum. As the curvature of the flow decreases downstream from a trough axis, divergence must occur to uphold the conservation of angular momentum. Because divergence aloft is associated with upward vertical motion in the mid troposphere and convergence at low levels (via the conservation of mass), surface cyclogenesis often occurs downstream from trough axes. Cyclonic differential vorticity advection will lead to forcing for upward vertical motion while anticyclonic differential vorticity advection will be associated with forcing for downward vertical motion. Generally, winds in the middle and upper troposphere will be significantly stronger than surface winds. Therefore, assuming that the vorticity gradients at the surface and in the middle troposphere are similar, vorticity advection in the mid-levels will be much stronger than it will be at the surface. Therefore, differential vorticity advection will tend to have the same sign as the vorticity advection in the middle troposphere. In other words, the forcing for vertical motion due to differential vorticity advection can be estimated by examining mid-level vorticity advection alone. For this study, maps of geopotential height at 500 mb and 250 mb will be used to qualitatively estimate the forcing due to differential vorticity advection.

The hypsometric equation (Bluestein 1992, p. 58) states that the thickness of a column (Δz) is proportional to the mean virtual temperature of the column (\bar{T}):

$$\Delta z = \frac{R_d}{g} \bar{T} \ln \frac{p_1}{p_2} \quad \text{Eq. (2)}$$

where p_1 and p_2 are the bottom and top pressure levels of the column, R_d is the dry gas constant, and g is the gravitational constant. By substituting this relationship into Term C of Eq. (1), the thickness advection term becomes a measurement of the mean temperature advection within the column. Therefore, if a column of air is warmed, there would be a local increase in thickness. At upper levels in the troposphere, the local increase in thickness would create positive height tendencies, which would be associated with horizontal divergence manifested as isallobaric flow away from the region. Due to the conservation of mass, the horizontal divergence aloft would be associated with vertical motion in the mid troposphere and convergence at low levels. In the QG-omega equation, warm air advection will lead to forcing for upward vertical motion while cold air advection is associated with forcing for downward vertical motion. For the purposes of the qualitative deductions of the QG-forcing, the author assumes that the geostrophic winds at the surface are representative of the mean 1000-500 mb layer winds, and the temperature advection can be estimated by examining sea level pressure maps and 1000-500 mb thickness maps as outlined by Palmen and Newton (1992, p. 322).

b. Qualitative Assessment of QG-Forcing on the Basis of the QG-Omega Equation

Quasigeostrophic theory has been used by many authors (e.g. Sanders and Gyakum 1980, Reed and Albright 1986) to lead qualitative discussions of extratropical cyclogenesis. The QG-omega equation (Eq. (1)) suggests that forcing for synoptic scale vertical motion (which would be associated with low-level convergence and surface cyclogenesis) can be expressed by the sum of differential vorticity advection and thickness (i.e. temperature) advection. The assessment of vertical motion fields will be helpful in assessing the development of the surface cyclone, particularly during the period of rapid deepening when synoptic scale vertical motion would have been strong.

As discussed in Chapter 3, upper level height maps (e.g. 500 mb, 250 mb) can be used to estimate the forcing of differential vorticity advection, such that forcing for upward vertical motion is found in areas of cyclonic vorticity advection at upper levels. Cyclonic vorticity advection is found downstream of troughs axes – an area which has been shown to be climatically favorable for explosive cyclogenesis (Sanders and Gyakum 1980). The presence and development of upper level troughs within the vicinity of the surface low will provide the basis for a qualitative discussion of the contribution to surface cyclogenesis from differential vorticity advection.

Thickness advection is analogous to temperature advection via a substitution of the hypsometric equation (Eq. (2)) into the thickness advection term in Eq. (1). In the mid-latitudes of the northern hemisphere (where temperatures generally decrease from south to north), low-level warm air advection is generally found to the east of closed lows

and pressure trough axes, where southerly winds are able to tap into relatively warm air masses to the south. This would provide forcing for upward vertical motion (and associated surface cyclogenesis) downstream from trough axis and to the east of closed lows.

Conventionally, the 1000-500 mb layer has been used to represent the temperature of the lower troposphere (Palmen and Newton 1969, p. 322). By assuming that the surface geostrophic wind is representative of the average wind in the 1000-500 mb layer, temperature advection can be estimated by conventionally available surface pressure and 1000-500 mb thickness maps.

Estimating forcing for vertical motion using conventional meteorological maps is a simple and effective way to identify areas that are favorable for surface cyclogenesis. However, the magnitude of the forcing for vertical motion for each term cannot be accurately assessed using these maps alone. For example, cyclonic vorticity advection and warm air advection may both be contributing the upward vertical motion associated with the development of a cyclone. However, the qualitative diagnosis outlined above cannot provide insight as to which of the two terms is dominating the forcing for upward vertical motion. Additionally, in the case of the two terms resulting in opposing forcing for vertical motion, the net forcing cannot be estimated qualitatively. Since the present study is concerned with the specific mechanisms that led to the explosive development of the 19 February 1993 storm, a quantitative analysis of processes associated with cyclogenesis must be performed. The results of this assessment would allow the author

to remark on the dominant mechanisms leading to the development of the 19 February 1993 storm.

c. Quantitative Assessment of QG-Forcing on the Basis of the Sutcliffe-Petterssen Development Equation

The Sutcliffe-Petterssen Development Equation (SPDE) (Palmen and Newton 1969, pp. 316-326) is a simple equation rooted in quasigeostrophic theory. Each of the terms in the equation can be estimated by readily available meteorological data. See appendix A for a discussion and derivation of the SPDE.

The SPDE in Cartesian coordinates is as follows:

$$\underbrace{\frac{\partial \zeta_{1000}}{\partial t}}_{\text{Term A}} = \underbrace{-\vec{V}_{500} \cdot \vec{\nabla}_p (\zeta_{500} + f)}_{\text{Term B}} + \underbrace{\left(-\frac{g}{f} \nabla^2 \left[\frac{dz_t}{dt} \right] \right)}_{\text{Term C}} \quad \text{Eq. (3)}$$

The equation states that the local 1000 mb relative geostrophic vorticity tendency (Term A) is equal to the 500 mb absolute geostrophic vorticity advection (Term B) minus the Laplacian of the 1000-500 mb thickness tendency (Term C), which is mathematically equivalent to the relative vorticity tendency of the thermal wind.

The SPDE utilizes gradients along the x, y, and z axes, as well as time derivatives. More complicated derivatives, such as gradients and Laplacians, are imbedded within several terms. Therefore, 21st century computing power may prove to be a valuable resource for computing the terms in the SPDE. Modern software has the potential to calculate the terms of the SPDE equations at several time steps with ease. For this study,

the author used IDV (Integrated Data Viewer) from Unidata (2013) to perform calculations of the SPDE.

Gridded data from the North American Regional Reanalysis (NOAA/ESRL PSD, 2013), also known as the NARR, were used in the calculations of the SPDE. Gridded binary files were loaded into IDV as aggregated grids by time. The gridded data has a resolution of approximately 32 km. Therefore, IDV's built in functions that can calculate horizontal gradients and Laplacians will be doing so within the mesoscale range (Bluestein 1992, p. 4). It should be noted that the SPDE is used to estimate the synoptic scale forcing associated with cyclones, so the horizontal resolution of the files is not ideal. Therefore, I will manually perform calculations of the SPDE using a more traditional synoptic scale grid spacing of 200 km. This will allow me to assess the validity of IDV's calculations using mesoscale gradients. The data files are in 6-hour time steps, beginning at 00 UTC 17 February 1993, prior to explosive cyclogenesis, and ending at 18 UTC 20 February 1993, after landfall. Time derivatives will be calculated by using a finite difference approximation over a 12 hour period, with initial and final times of 6 hours before and 6 hours after the time step in question, respectively.

The motion of the storm, symbolized by a 'c', can be subtracted from the advection terms in the SPDE (Term B in Eq. (3)). This will allow the equation to be applied to the center of the cyclone as it moves, with contributions of vorticity advection relative to the storm's center being analyzed. The storm motion can be calculated by observing the changes in latitude and longitude of the low center over a twelve hour

period, centered at the time step to which the SPDE equation is being applied. It is assumed that the average velocity of the storm during this 12 hour period is representative of the instantaneous storm motion at the time step in question. One degree latitude was estimated to be equal to 111 km while one degree longitude was estimated to be 90 km.

The SPDE equation, modified to remove storm motion from the advection terms, is given in Eq. (4).

$$\underbrace{\frac{\partial \zeta_{1000}}{\partial t}}_{\text{Term A}} = \underbrace{(-\vec{V}_{500} - c) \cdot \vec{\nabla}_p (\zeta_{500} + f)}_{\text{Term B}} + \underbrace{\left(-\frac{g}{f} \nabla^2 \left[\frac{dz_t}{dt}\right]\right)}_{\text{Term C}} \quad \text{Eq. (4)}$$

Term A, which can be described as the 1000 mb (near-surface) geostrophic vorticity tendency, has units of square seconds (s^{-2}). By multiplying the term by the 6-hour time step, the 6-hour change in 1000 mb geostrophic vorticity is calculated. Similarly, each of the other terms will have units of s^{-2} and can be multiplied by the time step, yielding the contribution of each term to the 6-hour change in 1000 mb geostrophic vorticity:

$$\underbrace{\partial \zeta_{1000}}_{\text{Term A}} = \underbrace{(-\vec{V}_{500} - c) \cdot \vec{\nabla}_p (\zeta_{500} + f) \cdot \partial t}_{\text{Term B}} + \underbrace{\left(-\frac{g}{f} \nabla^2 \left[\frac{dz_t}{dt}\right]\right) \cdot \partial t}_{\text{Term C}} \quad \text{Eq. (5)}$$

For the present study, Term B was modified so that it could be calculated in IDV with variables that are readily available in NARR files. By substituting the following equation for absolute geostrophic vorticity into Term B,

$$\eta_g = \frac{g}{f} \nabla^2 [z_{500}] + f \quad \text{Eq. (6)}$$

a form of Term B that can be calculated in IDV was obtained:

$$(-\vec{V}_{500} - c) \cdot \vec{\nabla}_p \left(\frac{g}{f} \nabla^2 [z_{500}] + f \right) \cdot dt \quad \text{Eq. (7)}$$

The Laplacian of the thickness tendency (Eq. (3) Term C) did not need to be modified for this study. By calculating the contribution of Term B and Term C to the computed 1000 mb vorticity tendency (Term A), the magnitudes of the terms can be compared to one another, thereby providing insight as to which of the terms (if either) dominated the forcing for surface cyclogenesis. Additionally, by comparing the computed 1000 mb vorticity tendency (Term A) to the actual 1000 mb vorticity tendency (calculated by difference in the 1000 mb vorticity at the cyclone center between time steps within the NARR files), the ability of the SPDE to accurately reproduce forcing for surface cyclogenesis observed in actual storms can be assessed.

d. Quantitative Assessment of the Expanded Thickness Tendency Term of the SPDE

The form of the SPDE given in Eq. (3) will provide useful insight into the nature of the development of the 19 February 1993 storm (i.e., upper-level energy driven vs. thermally driven). However, some ambiguity remains regarding the source of the heating. Temperature changes can be the result of the movement of cold/warm air masses (temperature advection), adiabatic processes (expansional heating and cooling associated with vertical motion), and diabatic heating via latent heat release and sensible heating of the atmosphere from the Earth's surface. Therefore, by expanding the thickness tendency (which is analogous to temperature tendency) in Eq. (3) Term C into the temperature tendencies associated with each of the aforementioned processes, the

contribution of each of the processes can be compared to one another. Such an analysis may suggest that forcing for surface cyclogenesis was dominated by one specific source of heating.

A form of the SPDE in Cartesian coordinates with expanded thermal terms can be obtained by substituting a form of the temperature tendency equation (Bluestein, 1992, pp. 197) into Eq. (3) (see Appendix A for details):

$$\frac{\partial \zeta_{1000}}{\partial t} = -\vec{V}_{500} \cdot \vec{\nabla}_p (\zeta_{500} + f) - \frac{R}{f_0} \nabla^2 \left[-\vec{V}_{700} \cdot \vec{\nabla}_p T_{700} + \omega \sigma \frac{p}{R} + \frac{1}{c_p} \frac{dQ}{dt} \right] \quad \text{Eq. (8)}$$

The thermal terms can be separated by distributing the Laplacian to each of the terms in the brackets. As previously shown, the storm motion will be removed from advection terms and each term will be multiplied by the 6-hr time step.

$$\begin{aligned} \underbrace{\frac{\partial \zeta_{1000}}{\partial t}}_{\text{Term A}} = & \underbrace{(-\vec{V}_{500} - c) \cdot \vec{\nabla}_p (\zeta_{500} + f) \cdot dt}_{\text{Term B}} + \underbrace{\left(-\frac{R}{f_0} \nabla^2 [(-\vec{V}_{700} - c) \cdot \vec{\nabla}_p T_{700}] \right) \cdot dt}_{\text{Term C}} \\ & + \underbrace{\left(-\frac{R}{f_0} \nabla^2 \left[\omega \sigma \frac{p}{R} \right] \right) \cdot dt}_{\text{Term D}} + \underbrace{\left(-\frac{R}{f_0} \nabla^2 \left[\frac{1}{c_p} \frac{dQ}{dt} \right] \right) \cdot dt}_{\text{Term E}} \end{aligned} \quad \text{Eq. (9)}$$

Term A and Term B remain unchanged, and have been discussed in the previous section. Term C is the horizontal Laplacian of 700 mb temperature advection by the 700 mb geostrophic wind. This term assumes that the 700 mb temperature advection is representative of the net temperature advection within the 1000-500 mb layer. This term can be calculated in IDV without modification.

Term D is the horizontal Laplacian of adiabatic heating and cooling based on 700 mb vertical motion. This term assumes that the 700 mb vertical motion is representative

of the synoptic scale vertical motion within the 1000-500 mb layer. It should be noted that vertical motion due to convection is not represented in this term. The static stability parameter (σ) was expanded into terms that the IDV can calculate, as there is no built-in function that calculates the static stability parameter. Using the equation:

$$\sigma = -\frac{\alpha}{\theta} \frac{d\theta}{dp} \quad \text{Eq. (10)}$$

Where

$$\alpha = \frac{RT}{p} \quad \text{Eq. (11)}$$

Term D can be arranged as follows.

$$-\frac{R}{f_0} \nabla^2 \left[\omega \cdot \left(-\frac{RT}{p} \frac{d\theta}{dp} \right) \cdot \frac{p}{R} \right] \cdot dt \quad \text{Eq. (12)}$$

Constants within the equation can be cancelled, and the negative within the Laplacian cancels the negative at the beginning of the term. Next, a form of Poisson's equation (Eq. (13)) will be substituted into Term D, resulting in Eq. (14).

$$\frac{T}{\theta} = \left(\frac{p}{p_0} \right)^{\frac{R}{c_p}} \quad \text{Eq. (13)}$$

$$\frac{R}{f_0} \nabla^2 \left[\omega \cdot \left(\frac{p}{p_0} \right)^{\frac{R}{c_p}} \cdot \frac{d\theta}{dp} \right] \cdot dt \quad \text{Eq. (14)}$$

Constants were brought out of the Laplacian in Term D, yielding an equation that can be calculated in IDV:

$$\frac{R}{f_0} \left(\frac{p}{p_0} \right)^{\frac{R}{c_p}} \cdot \nabla^2 \left[\omega \frac{d\theta}{dp} \right] \cdot dt \quad \text{Eq. (15)}$$

The static stability parameter was calculated for 700 mb, so the 100 mb layer from 750 mb to 650 mb was used to calculate the vertical potential temperature gradient.

Lastly, due to the difficulty of quantifying the Laplacian of diabatic heating within the storm, Term E was calculated as a residual of a form of the SPDE equation without expanded terms (Eq. (3)). By substituting the thickness tendency term in Eq. (3) into Eq. (8), it can be shown that the thermal terms of Eq. (8) are equal to the thickness tendency term in Eq. (3), as shown in Eq. (16):

$$-\frac{g}{f} \nabla^2 \left[\frac{dz_t}{dt} \right] = \underbrace{\left(-\frac{R}{f_0} \nabla^2 [(-\vec{V}_{700} - c) \cdot \vec{\nabla}_p T_{700}] \right)}_{\text{Term C}} + \underbrace{\left(-\frac{R}{f_0} \nabla^2 \left[\omega \sigma \frac{p}{R} \right] \right)}_{\text{Term D}} + \underbrace{\left(-\frac{R}{f_0} \nabla^2 \left[\frac{1}{c_p} \frac{dQ}{dt} \right] \right)}_{\text{Term E}} \quad \text{Eq. (16)}$$

By rearranging Eq. (16), Term E can be calculated as a residual. It is assumed that the contributions of diabatic heating to the temperature tendency within the column are equivalent to the change in thickness minus the contributions from storm relative temperature advection (Term C) and vertical motion (Term D). Eq. (17) shows a form of Term E that can be calculated in IDV.

$$\underbrace{\left(-\frac{R}{f_0} \nabla^2 \left[\frac{1}{c_p} \frac{dQ}{dt} \right] \right)}_{\text{Term E}} = -\frac{g}{f} \nabla^2 \left[\frac{dz_t}{dt} \right] - \text{Term C} - \text{Term D} \quad \text{Eq. (17)}$$

After developing a formula in IDV for each of the terms, the solutions to the terms were obtained at the surface low center at each time step. It is assumed that these values are representative of the average vorticity tendency during the 6-hour period centered at the time step. Therefore, the average of the vorticity tendency associated with

each term at two adjacent time steps represents the average vorticity tendency during the 6 hour period between time steps. These solutions to the SPDE can be compared to the actual 6-hour 1000 mb vorticity changes.

The results of the quantitative assessments of both forms of the SPDE (Eq. (3) and Eq. (16)) will provide numerical evidence that, in addition to qualitative observations, will allow the author to infer the dominant forcing mechanisms associated with the explosive development of the 19 February 1993 storm. Specifically, the magnitudes of the contributions from both vorticity advection and temperature changes can be compared to one another to reveal their relative dominance. The dominant source of the heating will also be identified via the expanded thermal terms. Lastly, both the qualitative observations and quantitative results will lend credence to the assessment of the 19 February 1993 storm as a polar low, based on the evidence of polar low characteristics as outlined in Table 7.

6. Quasigeostrophic Diagnosis and Polar Low Assessment

In the following section, the development of the 19 February 1993 storm is assessed on the basis of the QG-omega equation, which is used to identify synoptic scale vertical motion associated with surface cyclogenesis. Next, the contribution of the forcing mechanisms (vorticity advection and heating/cooling) is analyzed by quantifying the near-surface vorticity tendencies associated with each term in the SPDE. After the magnitude of the contribution of temperature changes is compared to that of vorticity

advection, the relative contributions from individual processes of heating/cooling are assessed via an expanded form of the thermal term in the SPDE. Ultimately, the results from both the qualitative and quantitative analyses, along with other observations, are used to assess the 19 February 1993 storm's explosive deepening and polar low-like characteristics.

a. Qualitative Assessment of QG-Forcing on the Basis of the QG-omega Equation

The QG-omega equation is used to characterize the nature of the forcing for vertical motion due to differential vorticity advection and thickness (temperature) advection. These two terms can be estimated using conventionally available meteorological maps. The maps used in the QG diagnosis are imbedded in Fig. 8a through 7n. Forcing for vertical motion due to vorticity advection is estimated using 500 mb maps (bottom right of Fig. 8a through 8n). The contributions from temperature advection are estimated using the alignment of the surface winds to the thickness gradient in the surface pressure and 1000-500 mb thickness maps (bottom left of Fig. 8a through 8n). The following discussion is meant to assess the qualitative nature of the QG forcing for synoptic scale vertical motion associated with the 19 February 1993 storm, which is summarized in Table 8. See Chapter 3 for a detailed discussion of the development, deepening, and eventual landfall of the low.

The surface low that went on to impact California is first identifiable within the Reanalysis-2 at 12 UTC 16 February 1993, when a surface pressure trough over the

eastern Pacific became closed (bottom left of Fig. 8f). Prior to the initial development, cyclonic vorticity advection had been occurring downstream from a positively tilted 500 mb trough. Though the trough had a large amplitude, with the axis extending from the Aleutian Islands to the subtropical Pacific Ocean, the trough had a large wavelength, keeping curvature weak and vorticity within the trough minimal. There was also weak warm air advection to the east of the low (bottom left of Fig. 8f). During the following 24 hours, a different, negatively tilted trough over North America deepened, with the axis extending over the surface low. With the low under the influence of a deeper trough with greater curvature, cyclonic vorticity advection increased to a moderate level by 12 UTC 17 February 1993 (bottom right of Fig. 8h). Meanwhile, weak warm air advection continued to the east of the low center (bottom right of Fig. 8h).

By 00 UTC 18 February 1993, warm air advection had increased in strength to the southeast and east of the low center (bottom left of Fig. 8i), enhancing forcing for upward vertical motion. Meanwhile, the 1000-500 mb thickness trough deepened to the north and east of the surface low as cold air advection increased in this area. A strong thickness gradient across the low provides evidence of baroclinicity in the lower troposphere.

Cyclonic vorticity advection continued to provide moderate forcing for upward vertical motion over the low. The Reanalysis-2 indicated that the 500 mb trough had closed by this time (bottom right of Fig. 8i). Generally, closed lows are associated with weak vorticity advection due to the relatively constant curvature around the circular low.

Since vorticity advection is associated with a wind and a vorticity gradient, vorticity advection can be weak (or even neutral) in uniformly curved flow, regardless of the presence of winds and cyclonic vorticity. However, a trough axis was still imbedded in the southern portion of the 500 mb low, allowing for cyclonic vorticity advection to continue over the low.

The 24 hour period from 00 UTC 18 February to 00 UTC 19 February 1993 was marked by more rapid pressure falls, with the NARR data indicating a 11.8 mb pressure fall over the period. The 500 mb maps for 12 UTC 18 February and 00 UTC 19 February 1993 (bottom right of Fig. 8j and 8k, respectively) show that the closed low adapted a more symmetrical curvature, indicating weak (if any) vorticity advection during the period of rapid deepening. At the same time, the 1000-500 mb thickness trough had closed (bottom left of Fig. 8k), suggesting the upper level low had developed a cold core, i.e. a cold low – a feature which has been associated with polar low development (Rasmussen and Zick 1987, Rasmussen and Turner 2003, p. 172). Surface winds east of the low were perpendicular to a strong thickness gradient, indicating the presence of strong warm air advection. This suggests that the strong cyclogenesis observed during this 24 hour period was associated with forcing for strong upward vertical motion due to warm air advection. Meanwhile, cold air advection continued to the west of the low.

By 12 UTC 19 February 1993, the surface low in the Reanalysis-2 (top right of Fig. 8l) was located just offshore of Northern California. The 500 mb closed low (bottom right of Fig. 8l) had moved northward over coastal British Columbia. A deep trough had

developed to the south of the low over the coastal waters of western North America, allowing moderate cyclonic vorticity advection to redevelop over the low. This enhanced forcing for upward vertical motion, which would already have been large due to continued strong warm air advection to the east and northeast of the surface low. Therefore, the net forcing for upward vertical motion appears to have reached a maximum at this time, with moderate forcing from cyclonic differential vorticity advection and strong forcing from strong warm air advection both contributing to synoptic scale ascent. It should be noted that infrared satellite imagery for 12 UTC 19 February 1993 (Fig. 9g) shows what appear to be newly developed cyclones in the cold air mass behind the main frontal bands. While these lows are not analyzed by the Reanalysis-2, buoy data from NOAA recorded an explosive deepening associated with the low along the occlude boundary during the following 12 hour period. It should be noted that this explosive deepening occurred within an area of strong QG forcing for synoptic scale upward vertical motion.

The explosively developing cyclone made landfall in Mendocino County around 00 UTC 20 February 1993. By this time, the trough south of the 500 mb low (bottom left of Fig. 8m) had become more circularly curved again, indicating that cyclonic vorticity advection had weakened. Also, as the low moved inland, warm air advection decreased as the thickness gradient decreased over western North America. The net forcing for upward vertical motion had decreased significantly, and this time marks the apparent end of cyclogenesis. During the following hours, the clouds and precipitation associated with

the cyclone moved across the state of California and into the interior western United States.

b. Quantitative Assessment of the QG-forcing on the Basis of the SPDE

The qualitative assessment above illustrates the presence of both cyclonic vorticity advection and warm air advection as having contributed to the development of the 19 February 1993 storm. While the assessment suggests that warming of the column via temperature advection dominated the forcing for upward vertical motion during explosive cyclogenesis, the quantification of these contributions provides a more compelling argument regarding the dominance of one term over another.

First, the SPDE without an expanded thickness tendency term (Eq. (5)) is used to compare the relative contributions of upper level vorticity advection and the Laplacian of heating/cooling to the development of the surface cyclone. Due to time constraints, only two hand calculations were performed using a synoptic scale grid spacing of 200 km. IDV was not used for this analysis.

Two hand-calculations of the SPDE were performed using a synoptic scale gradient of 200 km – the first at 00 UTC 18 February and the latter at 00 UTC 19 February 1993. The results of the SPDE are displayed in Table 9. At 00 UTC 18 February 1993, which marked the beginning of significant pressure falls within the main surface low, the vorticity advection term (Eq. (5) Term B) resulted in a 6-hr 1000 mb absolute geostrophic vorticity increase of $1.78 \times 10^{-5} \text{ s}^{-1}$, suggesting that cyclonic

vorticity advection was contributing to surface cyclogenesis upon the onset of rapid deepening. However, the contribution to surface cyclogenesis from the Laplacian of the thickness tendency term (Eq. (5) Term C) was nearly double that of upper level vorticity advection, with an increase of $3.09 \times 10^{-5} \text{ s}^{-1}$. The total computed vorticity change (Eq. (5) Term A) was $4.87 \times 10^{-5} \text{ s}^{-1}$, which more than doubled the actual 6-hr vorticity change of $2.13 \times 10^{-5} \text{ s}^{-1}$.

By 00 UTC 19 February 1993, the time at which the explosive cyclogenesis occurred within the newly formed cyclone along the old occlusion, the contributions from the vorticity advection term to the development of the surface low had decreased to $1.09 \times 10^{-5} \text{ s}^{-1}$ per 6-hr time step. This matches the qualitative assessment of the vorticity advection, as the 500 mb low had closed and adapted a somewhat symmetrical curvature, thereby inhibiting vorticity advection. However, the contribution from the Laplacian of thickness changes had increased to $3.83 \times 10^{-5} \text{ s}^{-1}$ per 6-hr time step, more than tripling the contribution of vorticity advection at that time. The net total computed 6-hr vorticity change had increased slightly as well, indicating even stronger forcing for surface cyclogenesis at this time.

c. Quantitative Assessment of the SPDE Expanded Thickness Tendency Term

Next, the thickness tendency term is expanded and calculated by IDV and by hand. By comparing the two methods, the validity of the IDV's solution the SPDE using

mesoscale gradients was assessed. However, due to time constraints, Term E was not calculated using IDV.

Table 10 shows the actual 1000 mb geostrophic vorticity tendency and the solution to the SPDE equation with an expanded thickness tendency term (Eq. (9)) that was calculated using the built in IDV functions. Again, the built in functions in IDV calculated all of these terms using mesoscale gradients within the NARR files.

The actual 1000 mb absolute geostrophic vorticity tendency averaged $31.91 \times 10^{-5} \text{ s}^{-1}$ per 6 hours, while the SPDE returned an average of $52.15 \times 10^{-5} \text{ s}^{-1}$ per 6 hours. Both the actual and computed vorticity tendencies varied greatly between time steps, and often times these two values were of the opposite sign, despite being valid for the same time step.

Fig. 14 shows the results of IDV's SPDE calculations during the period of rapid deepening graphically, beginning at 18 UTC 17 February to 06 UTC 19 February 1993. It appears as though the total computed 1000 mb geostrophic vorticity tendency (Eq. (9) Term A) was dominated by the 500 mb geostrophic vorticity advection (Eq. (9) Term B). Graphical representations of the 500 mb vorticity in the NARR show many sub-synoptic scale perturbations in the vorticity field. See Fig. 15 for a graphical representation of the 500 mb vorticity pattern, as analyzed by the NARR. It is likely that these perturbations returned very large vorticity gradients at certain grid points, yielding unrealistic 500 mb geostrophic vorticity advection values. The contributions of the 700 mb temperature advection term (Eq. (9) Term C) were generally negligible during the period of

deepening, especially when compared to Term B. The effects of heating and cooling due to vertical motion (Eq. (9) Term D) contributed to the strengthening of the storm throughout the period of deepening. The magnitude of the contribution of Term D remained relatively constant during this period of time, while Term B (and subsequently Term A) varied significantly with time.

Again, two hand-calculations of the SPDE with an expanded thickness tendency term (Eq. (9)) were performed at the synoptic scale at 00 UTC 18 February and 00 UTC 19 February 1993. These calculations provided much more realistic results, as shown in Table 11. The actual 1000 mb geostrophic vorticity change was calculated using the 1000 mb geopotential height field over synoptic scale gradients. The total computed vorticity tendency (Term A (Eq. (9))) was just below $5.0 \times 10^{-5} \text{ s}^{-1}$ per 6 hours for both time steps, as was discussed in detail in the previous section. Term A was more than double the actual vorticity tendency at the first time step and slightly less than the actual vorticity tendency during the second time step. Again, Eq. (9) Term B was weakly positive at both times, indicating that cyclonic differential vorticity advection was making a small positive contribution to surface cyclogenesis at both times. Eq. (9) Term C was negative at both times, and had nearly doubled in magnitude between the two time steps. This suggests that cold air advection was making a negative contribution to the development of the storm, and this negative contribution became larger over time. Term D was the largest term by magnitude at both time steps, with a relative minimum in upward vertical motion in an unstable environment making a strong positive contribution

to surface cyclogenesis. Lastly, Term E, which was calculated as a residual, had the second largest magnitude at both time steps. However the contribution of this term was negative at both time steps, indicating that diabatic cooling hindered the development of the storm.

7. Discussion of Results

The results presented in Chapter 6 are used to answer the questions regarding the unusual characteristics of the 19 February 1993 storm. The qualitative diagnosis allowed the author to make conclusions about the dominant forcing mechanisms for vertical motion associated with the development of the surface cyclone that impacted California, as well as the subsequent vortex that developed along the old occlusion. Next, the quantitative diagnosis of the processes contributing to surface cyclone development using the SPDE provides numerical evidence to support the assessment of the dominant processes, including vorticity advection and heating/cooling. In addition, the expanded thickness tendency term within the SPDE alludes to the dominant sources of heating/cooling that contributed to surface cyclogenesis. Lastly, the qualitative observations and quantitative results provide evidence of the explosive nature of the 19 February 1993 storm's development and its resemblance to a polar low.

a. Results of Qualitative Assessment of QG Forcing on the Basis of the QG-omega equation

Table 8 shows the qualitative results regarding the forcing for vertical motion within the 19 February 1993 storm on the basis of the QG-omega equation (Eq. (1)). Firstly, differential vorticity advection associated with an upper level trough consistently provided forcing for upward vertical motion over the surface low throughout the development of the cyclone. Without the presence of short-amplitude troughs with large curvature, the magnitude of the cyclonic vorticity advection remained relatively weak. However, just prior to the explosive deepening of the cyclonic vortex that developed along the occlusion, troughing south of a closed low at 500 mb provided more moderate forcing for upward vertical motion off the coast of Northern California.

Still, the net forcing for upward vertical motion within the storm was dominated by warm air advection the east of the surface low, especially during a period of rapid deepening when strong surface winds and a tight thickness gradient over the storm resulted in strong warm air advection in the coastal waters of California. This, combined with cold air advection to the west of the cyclone, suggests to the author that strong baroclinicity was present in the lower troposphere during the development of the main extratropical cyclone. In summary, despite the lack of significant cyclonic vorticity advection aloft, strong forcing for upward vertical motion due to favorable thickness changes provided a suitable environment for surface cyclogenesis.

b. Results of Quantitative Assessment of the QG Forcing on the Basis of the SPDE

The SPDE without an expanded thickness tendency term was calculated using a synoptic scale gradient at two different times, the results of which are shown in Table 9. These results support the conclusions drawn in the previous section, which are that forcing for upward vertical motion over the developing surface low was dominated by positive thickness tendencies while cyclonic vorticity advection made a more modest contribution. In fact, at the second time step (00 UTC 19 February 1993), the contribution of the thickness changes to the 1000 mb absolute geostrophic vorticity tendency more than tripled the contribution of vorticity advection.

The calculated total 1000 mb vorticity changes (Term A) increased only slightly between the two time steps. This suggests that the net forcing for surface cyclogenesis remained relatively constant over time. However, the actual vorticity tendency more than doubled over time. The increasingly rapid surface cyclone development indicates that other forcing mechanisms for surface cyclogenesis developed as the cyclone matured.

One surprising result from this portion of the study was that the calculated surface vorticity tendency actually exceeded the observed vorticity tendency at the first time step and nearly matched it at the second time step. Conversely, Sanders and Gyakum (1980) found that quantitative analyses of cyclogenesis using QG theory underestimated the deepening rates of storms. Yet, in this study, the SPDE greatly overestimated the rate of surface cyclogenesis at one time and slightly underestimated it later.

c. Results of Quantitative Assessment of the SPDE with Expanded Thickness Tendency Term

The results of the expanded thickness tendency term in the SPDE (Eq. (9)) were calculated both by IDV using a mesoscale grid spacing and by hand using a synoptic scale grid spacing. While both the sets of solutions to the SPDE provided unexpected results, the synoptic scale results were much more sensible given the synoptic and planetary scale pattern in which the storm developed. The IDV's SPDE results provided wildly fluctuating contributions from Term B, with several time steps having negative contributions from anticyclonic differential vorticity advection. Additionally, the magnitude of the contributions from vorticity advection was often one to two orders of magnitude larger than the expanded thickness tendency terms, which contradicts the conclusions drawn from both qualitative observations and synoptic scale hand calculations of the SPDE. This error stems from unrealistic mesoscale gradients in the 500 mb vorticity field within the NARR, as displayed via IDV in Fig. 15. Therefore, I will be using the more realistic synoptic scale calculations to quantify the contribution to cyclogenesis from various sources.

Presently, the contributions from each of the processes in the expanded thickness tendency term, as calculated using the SPDE over a synoptic scale gradient, are discussed in detail. While the net forcing for surface cyclogenesis from these terms exceeded the forcing associated with vorticity advection, the relative contributions from each of the heating/cooling processes varied greatly. Firstly, the effects of temperature advection

were negative at both time steps, suggesting a localized maximum in cold air advection (or minimum in warm air advection) over the low. This would have led to negative thickness tendencies over the low, inhibiting surface cyclogenesis. While this may have been the case, the alignment of the 1000-500 mb thickness gradient and the surface pressure gradient suggests that warm air advection was present to the east and southeast of the low center throughout the life of the surface low, especially during a period of rapid pressure falls. Therefore, the author concludes that warm air advection did play a role in the development of the main extratropical cyclone.

Secondly, the effects of vertical motion on adiabatic heating and cooling of the column were consistently positive and of a large magnitude. These results were unexpected, as enhanced upward vertical motion within the center of a storm would cause a localized temperature decrease within the ascending air due to adiabatic cooling. The largely positive contribution of the term suggests that a local minimum in synoptic scale upward vertical motion in an area of low static stability strongly contributed to increasing thickness tendencies relative to the surrounding environment, driving surface cyclogenesis. Lastly, the contribution of the diabatic heating term was largely negative at both times. Again, this result was unexpected, as both previous work and meteorological data suggest that sensible heating from the warm ocean surface and latent heating from convection would have contributed positively to the development of the storm. This suggests that calculating the contributions of diabatic heating via a residual from the

thickness tendency did not produce realistic results. The effects of upward vertical motion and static stability, as well as diabatic heating, need to be examined more closely.

d. Discussion of Static Stability and Diabatic Terms

The most significant contribution to surface cyclogenesis, as calculated by the SPDE, came from upward vertical motion in a statically stable environment. The positive contribution of the upward vertical motion term is unexpected. However, the apparent sign error can be explained by examining the 700 mb vertical velocity field. Within the SPDE, the inflection (i.e. maxima and minima) of both the vertical motion field and the stability field are calculated as a Laplacian. Therefore, a positive result can be calculated if there is a locally negative inflection in upward vertical motion over the center of the low. In that case, the weak (relative to the surrounding environment) vertical motion over the low center would be collocated with a maximum in the thickness tendency due to adiabatic cooling. Subsequently, upper level divergence associated with isallobaric flow over the low center would coincide with increasing surface cyclogenesis.

A plot of the vertical motion field (Fig. 16) suggests that this is the case. While there is a maximum in upward vertical motion field at the 700 mb, it is not located over the center of the surface cyclone, the location at which the SPDE was calculated. In fact, the Laplacian of the vertical motion field over the surface low revealed that there was a negative inflection in upward vertical motion over the low, resulting in a positive contribution to surface cyclogenesis, as described in the previous paragraph.

It should be noted that the surface analysis in both the NARR and Reanalysis-2 did not match observed meteorological data and satellite imagery. Therefore, the true nature of the vertical motion field over both the main low and the secondary low remains unknown. While the inflection of the vertical motion field cannot be estimated without further analysis, the author concludes that there was strong upward vertical motion within the secondary low, based on the strong convection in and around the center of that low.

Additionally, errors within the static stability parameter embedded in the vertical motion term may have arisen due to errors within the static stability field. Within the SPDE, the static stability parameter was represented by the change in potential temperature between 750 mb and 650 mb. Within the NARR files, this potential temperature difference generally varied on the order of 0.1°C across synoptic scales. Therefore, even a small error in the temperature profile at any particular grid point could significantly alter the shape of the static stability field. In essence, the calculations of the vertical motion term are considered unreliable do not only to the possibly erroneous vertical motion field, but also due to the term's sensitivity to noise within the static stability field.

As previously mentioned, the negative contribution of diabatic heating to the development of the storm is not realistic. This error is attributed to the aforementioned errors within the vertical motion term, as the diabatic heating term was calculated as a residual of the total thickness tendency minus the effects of temperature advection and vertical motion. However, two equations used to calculate the sensible and latent heat

fluxes (Roberts et. al. 2012) demonstrate that both of these processes must have made positive contributions to surface cyclogenesis:

$$\text{Sensible heat flux} = \rho C_h C_p (T_s - T_a)(U_{10}) \quad \text{Eq. (18)}$$

$$\text{Latent heat flux} = \rho C_e L_v (Q_s - Q_a)(U_{10}) \quad \text{Eq. (19)}$$

Eq. (18) states that the sensible heat flux from the sea surface to the overlying air is a product of the air-sea temperature difference multiplied by a set of constants, including density (ρ), heat exchange coefficients (C_h), the specific heat capacity of air (C_p), and the wind speed at 10 m above the surface (U_{10}). If the sea surface is warmer than the overlying air, there must be a flux of heat from the sea surface into the atmosphere. Therefore, the air-sea temperature difference map in Fig. 5 serves as proof of a positive sensible heat flux as sea surface temperatures were as much as 7°C warmer than the overlying air in the vicinity of the developing low. In essence, sensible heating did contribute positively to surface cyclogenesis.

The latent heat flux in Eq. (19) is a product of some constants (density, moisture exchange coefficients (C_e), the latent heat of vaporization (L_v), and the 10 m wind speed) and the difference between the specific humidity at the surface (Q_s) and in the ambient air (Q_a). While there are no direct observations of the difference between the specific humidity at the surface and in the air, the strong convection observed in satellite imagery (e.g. Fig. 2, Fig. 6) indicates the presence of low level moisture, which, upon rising and condensing via convection, heated the lower troposphere via a latent heat flux. It is inferred that latent heating also contributed positively to surface cyclogenesis, resulting in

a strongly positive contribution to the development of the surface low due to the net diabatic heating term.

Additionally, the positive contribution from the diabatic heating term suggests that secondary processes may have contributed to the development of the surface low. The main extratropical cyclone, as well as the vortex that developed along the occlusion, formed in areas where sea surface temperatures exceeded the temperature of the overrunning air (Fig. 5). Sensible heat fluxes from the ocean to the atmosphere caused weakening stability, leading to buoyancy in the lower troposphere, as evidenced by consistently high surface based CAPE values over coastal waters (Fig. 17). At 00 UTC 18 February and 00 UTC 19 February 1993, surface based CAPE values exceeded 1000 J/kg to the east of the surface low, where convective clouds can be seen on infrared satellite imagery. CAPE values of this magnitude suggest that the environment is favorable for strong, deep convection, leading to the development of thunderstorms.

Soundings from stations along the west coast of North America provide in situ observations demonstrating the presence of statically stable conditions. Fig. 18 shows a sounding from KVBG (Vandenberg Air Force Base, Lompoc, CA) for 00Z Feb 19 1993, which shows 1783 J/kg of surface based CAPE. Note the steep lapse rates throughout the troposphere, save what appears to be a frontal inversion near 750 mb. Interestingly, at the time of this sounding, infrared satellite imagery (Fig. 9f) shows that the main comma cloud that developed over the Pacific Ocean ahead of the surface low had already moved inland over the southwestern United States. This suggests that the frontal inversion in the

sounding was likely the cold front that had already passed KVBG at the surface. Typically, the cold air mass behind a cold front is characterized by statically stable conditions, with little to no surface based CAPE. However, as cold air overrunning a warm sea surface produced a strong sensible heating into the lower troposphere, the stability behind the frontal bands decreased. As the increasingly buoyant conditions enhanced upward vertical motion, latent heating from condensation led to further destabilization of the lower troposphere. Thusly, the positive feedback loop between diabatic heating at the surface and destabilization of the lower troposphere (air-sea latent and sensible heat flux) likely made a positive contribution to surface cyclogenesis. Additionally, CISK may have contributed to the development of the storm as well, as strong convection developed in the center of the large surface low, which would have contributed latent heating to the lower troposphere and enhanced the convergence at the center of the surface low.

e. Assessment of Explosive Cyclogenesis and Polar Low Development

The results from both the qualitative and quantitative analyses have, in addition observed meteorological data, are used to assess the 19 February 1993 storm's explosive deepening and polar low-like characteristics. The results of this assessment are summarized in Table 7. Firstly, the characteristics regarding the explosive nature of the storm's deepening are compared to the climatologically favorable features outlined in the literature (i.e. Sanders and Gyakum 1980, Reed and Albright 1986). The main

extratropical cyclone developed over the ocean during the winter, a setting that is climatologically conducive to rapid cyclogenesis. It developed within a strong baroclinic zone, where positive thickness tendencies in the vicinity of the low contributed favorable to upward vertical motion and surface cyclogenesis. Additional forcing from diabatic heating, statically stable conditions, and cyclonic vorticity advection aloft (associated with an upper level trough) further enhanced the development of the surface low. It should be noted that the dominance of the forcing from the thermal terms was reminiscent of a tropical cyclone, as opposed to typical explosively deepening extratropical cyclones which are dominated by strong cyclonic vorticity advection (Roohollah and Sorteberg 2013).

Lastly, a remarkable cyclone developed within the cold air mass behind the main frontal bands associated with the main cyclone, along the remnants of the occlusion that was still over the ocean. Meteorological data reveal that the cyclone exhibited numerous characteristics that are typical of polar lows. In fact, all but two of the criteria for typical polar low development outlined in Table 7 were identified in the 19 February 1993 storm. These observations were supported by the quantitative results discussed above. Therefore, the author has concluded that the cyclone that made landfall in Mendocino County in Northern California on 19 February 1993 was a polar low that developed along the occluded boundary of a mature extratropical cyclone, which impacted California prior to the development of the new low.

The low matched the 'cold low' type of polar low described by Rasmussen and Turner (2003, p. 172). This polar low developed in an environment characterized by weak low level baroclinicity (i.e. the occluded boundary) and a cold low aloft. The cold air at upper levels, combined with warming of the lower troposphere due to diabatic heating, produced statically stable conditions conducive to convection. The polar low went on to explosively deepen prior to landfall, and featured a nearly cloud-free eye surrounded by a wall of cumulonimbus clouds. As discussed in Chapter 2, the polar low produced near-hurricane force winds in Northern California, resulting in one death and extensive property damage.

8. Summary

This study explored the explosive development of the 19 February 1993 storm on the basis of quasigeostrophic theory. Previous studies (Sanders and Gyakum 1980, Reed and Albright 1986) show that explosive cyclogenesis generally occurred over the ocean during the cold season, when baroclinicity is strong and diabatic heating from both the ocean surface and convection provides conditionally instability in the lower troposphere.

The results of both the qualitative and quantitative diagnosis, presented in Chapter 6 and discussed in Chapter 7, show that the 19 February 1993 storm was dominated by positive thickness tendencies within the vicinity of the storm, which is analogous to warming. The effects of vorticity advection associated with the upper level pattern were smaller in magnitude, although cyclonical vorticity advection provided at least neutral to

weak forcing for surface cyclogenesis. In other words, the development of the storm was not inhibited by the planetary and synoptic scale pattern at upper levels. This conclusion was supported by both qualitative observations made from conventional meteorological charts as well as a calculation of the SPDE without an expanded thickness tendency term (Eq. (5)) using a synoptic scale grid spacing.

The results of the quantitative diagnosis of the expanded thickness tendency term within the SPDE (Eq. (9)) were inconclusive, as the calculated contributions from certain terms were not physically reasonable. The unreasonable results were attributed to the inflection of the vertical motion field and possible errors in the calculations of the static stability parameter, two sources of error which produced an unrealistic positive contribution to surface cyclogenesis. Subsequently, the SPDE resulted in a negative contribution from diabatic heating. However, meteorological data proves that both sensible and latent heating of the lower troposphere contributed positively to surface cyclogenesis, and suggest that the processes of CISK and air-sea latent and sensible heat transfer may have enhanced the development of the low.

The cyclone that developed along the old occluded boundary has been identified as a polar low, a conclusion which is supported by qualitative observations and a quantitative assessment of the forcing mechanisms responsible for the development of the low. Specifically, the low most resembled the 'cold low' type of polar lows, as outlined by Rasmussen and Turner (2003, p. 172). The development of the 19 February 1993

polar low was primarily driven by positive thickness tendencies associated with strong diabatic heating and upward vertical motion in a statically stable environment.

This study presents not only the first documentation of a landfalling polar low along the California Coast, but also, to the author's knowledge, the first documented polar low in the vicinity of the west coast of the Continental United States. This finding suggests that future research opportunities exist in the identification and analysis of other polar low-like cyclones over the eastern Pacific Ocean, including the coastal waters of California.

References

Anderson, R. K., J.P. Ashman, F. Bittner, G.R. Farr, W. Ferguson, V.J. Oliver and A. H. Smith, 1969: Application of meteorological satellite data in analysis and forecasting. ESSA Tech. Rep. NESC51, Government Printing Office, Washington D.C. [NTIS AD-697033.]

Bluestein, H, 1992: *Synoptic-Dynamic Meteorology in Midlatitudes*. Vol. 1. Oxford University Press, 431 pp.

Businger, S., 1987: The synoptic climatology of polar-low outbreaks over the Gulf of Alaska and the Bering Sea. *Tellus*, **39A**, 307-25.

Businger, S. and R. J. Reed, 1989a: Cyclogenesis in cold air masses. *Wea. and Forecasting* **2**, 133-56.

Businger, S. and R. J. Reed, 1989b: Polar Lows. In *Polar and Arctic Lows*, ed. P.F. Twitchell, E. Rasmussen and K. L. Davidson. pp. 3-45. A Deepak, Hampton, VA.

Carlson, T. N., 1998: *Mid-Latitude Weather Systems*. American Meteorological Society, 507pp.

Condrón, A., G. R. Bigg, and I. A. Renfrew, 2006: Polar Mesoscale Cyclones in the Northeast Atlantic: Comparing Climatologies from ERA-40 and Satellite Imagery. *Mon. Wea. Rev.*, **134**, 1518-1533.

Charney, J. and A. Eliassen, 1964: On the growth of the hurricane depression. *J. Atmos. Sci.*, **21**, 68-75.

Conway, E. D., 1997: *An Introduction to Satellite Image Interpretation*. The John Hopkins University Press, 242 pp.

Emanuel, Kerry, A., 1986: *A two stage air sea interaction theory for polar lows*. Proc., The Third International Conference on Polar Lows, Norway.

Emanuel, Kerry A. and Richard Rotunno, 1989: Polar lows as arctic hurricanes. *Tellus*, **41A**, 1-17.

Los Angeles Times, 1993a: O.C. Freeways Awash in Storm: Weather: Latest deluge causes far fewer problems elsewhere, but it's small solace for snarling commuters. [Available online at http://articles.latimes.com/1993-02-19/news/mn-292_1_orange-county]

Los Angeles Times, 1993b: Residents Outmatched by Relentless Flooding: Weather: Backhoes and tractors prove unable to protect homes, as rising rivers close Sierra Highway, wash out driveways and isolate homes. [Available online at http://articles.latimes.com/1993-02-20/local/me-153_1_sierra-highway]

Markowski, P., and Y. Richardson, 2010: *Mesoscale Meteorology in Midlatitudes*. Wiley, 407 pp.

Lynott, Robert E., Owen P. Cramer, 1966: Detailed Analysis of the 1962 Columbus Day Windstorm in Oregon and Washington. *Mon. Wea. Rev.*, **94**, 105–117.

Monteverdi, J. P., 1976: The Single Air Mass Disturbance and Precipitation Characteristics at San Francisco. *Mon. Wea. Rev.*, **104**, 1289–1296.

Monteverdi, J. P. 2008: The Sutcliffe-Petterssen Development Equation: Quasigeostrophic Development. San Francisco State University, 5 pp.

Monteverdi, J. P., E. J. Null, K. L. Pagan, and E. Daghir, 1993: Unpublished report to the National Weather Service.

National Weather Service, 1993a: *Northern and Central California Weather Summary*. National Weather Service San Francisco, CA.

National Weather Service, 1993b: *Storm Report for 2/19/93*. National Weather Service Eureka, CA.

NCDC, 1993: Storm Data and Unusual Weather Phenomena with Late Reports and Corrections, Vol. 35 No. 2. ISSN 0039-1972, 74 pp.

NCDC, cited 2014: Surface Data, Hourly Global. [Available online at <http://hurricane.ncdc.noaa.gov/pls/plclimprod/cdomain.abbrev2id>]

NOAA Coastal Ocean Program, 1993: Coastwatch. El Niño Watch, Advisory no. 93-2. 1 pp.

NOAA/ESRL PSD, cited 2013: NCEP North American Regional Reanalysis. [Available online at <http://www.esrl.noaa.gov/psd/data/gridded/data.narr.html>]

NOAA/ESRL PSD, cited 2014: NCEP/DOE AMIP-II Reanalysis (Reanalysis-2). [Available online at http://nomad3.ncep.noaa.gov/ncep_data/]

NOAA/NESDIS, cited 2014: ISCCP Global ISCCP B1 Browse System (GIBBS). [Available online at <http://www.ncdc.noaa.gov/gibbs/>]

Palmen, E., and C. W. Newton, 1969: *Atmospheric circulation systems: their structure and physical interpretation*. Vol. 13. *International Geophysics Series*, Academic Press, 624 pp.

Rasmussen, E. A. and J. Turner, 2003: *Polar Lows: Mesoscale Weather Systems in the Polar Regions*. Cambridge University Press, 628 pp.

Rasmussen, E. and C. Zick, 1987: A subsynoptic vortex over the Mediterranean Sea with some resemblance to polar lows. *Tellus*, **39A**, 408-425.

Reed, R. J., and M. D. Albright, 1986: A Case Study of Explosive Cyclogenesis in the Eastern Pacific. *Mon. Wea. Rev.*, **114**, 2297-2319.

Roberts, J. B., F. R. Robertson, C. A. Clayson, M. G. Bosilovich, 2012: Characterization of Turbulent Latent and Sensible Heat Flux Exchange between the Atmosphere and Ocean in MERRA. *J. Climate*, **25** Issue 3, 821-838.

Roohollah, A. and A. Sorteberg, 2013: *The Vorticity Budgets of North Atlantic Winter Extratropical Cyclones Development*. EGU General Assembly, Austria.

Sanders, F., and J. R. Gyakum, 1980: Synoptic-Dynamic Climatology of the “Bomb”.

Mon. Wea. Rev., **108**, 1589–1606

Sardie, J. M. and T. T. Warner, 1985: A numerical study of the development mechanism of polar lows. *Tellus*, **37**, 460-477.

Unidata, 2013: Integrated Data Viewer version 4.1. University Corporation for Atmospheric Research

Wilhelmsen, K. (1985): Climatological study of gale-producing polar lows near Norway.

Tellus A, **37A**: 451–459.

World Meteorological Organization, 1973: The use of satellite pictures in weather analysis and forecasting. *Issue 124 of Technical note*, World Meteorological Organization
Issue 333 of WMO, World Meteorological Organization

Yanase, W. and H. Niino, 2007: Dependence of Polar Low Development on Baroclinicity and Physical Processes: An Idealized High-Resolution Numerical Experiment. *J. Atmos. Sci.*, **64**, 3044–3067.

Tables

Table 1: Peak sustained winds in mph at selected stations in California during the Feb 19 1993 storm, from AWOS/ASOS stations.

| Station Name | Date and Time (yyyymmddHHMM) | Wind Speed (mph) |
|---------------------|---------------------------------|---------------------|
| POINT ARENA | 199302200000 | 71 |
| SAN CLEMENTE ISLAND | 199302182200 | 63 |
| MOUNT WILSON | 199302190600 | 55 |
| CHICO MUNI | 199302200300 | 47 |
| HUNTINGTON BEACH | 199302182100 | 46 |
| REDDING MUNICIPAL | 199302200400 | 46 |
| POINT ARGUELLO | 199302181600 | 41 |
| SALINAS MUNI | 199302181504 | 40 |
| NEWPORT BEACH | 199302190000 | 40 |
| SAN FRANCISCO INTL | 199302192200 | 39 |
| SANDBURG (AUT) | 199302190508 | 38 |
| TRUCKEE-TAHOE | 199302191600 | 38 |
| CAMP PENDLETON MCAS | 199302190100 | 37 |
| ARCATA | 199302200536 | 37 |
| SAN SIMEON/PT. PIED | 199302181508 | 36 |

Table 2: Wind gusts in mph at selected stations in California during the Feb 19 1993 storm, from AWOS/ASOS stations. * denotes report from NWS statement. † denotes report from NCDC (1993).

| Station Name | Date and Time (yyyymmddHHMM) | Wind Gust (mph) |
|-----------------------------|---------------------------------|--------------------|
| MENDOCINO CO * | | 90-95 |
| VANDENBERG AIR FORCE BASE † | | 94 |
| POINT ARENA * | | 89 |
| MOUNT WILSON | 199302190600 | 87 |
| CHICO MUNI | 199302200300 | 61 |
| REDDING MUNICIPAL | 199302200400 | 60 |
| SANTA MARIA PUBLIC | 199302181400 | 57 |
| ALAMEDA(USN) | 199302200500 | 55 |
| RED BLUFF MUNICIPAL | 199302200300 | 52 |
| SAN FRANCISCO INTL | 199302192300 | 48 |
| TRUCKEE-TAHOE | 199302191600 | 47 |
| NAPA CO | 199302192305 | 47 |
| NEWPORT BEACH | 199302190600 | 46 |
| FAIRFIELD/TRAVIS AF | 199302182100 | 45 |

Table 3: 1-hr precipitation totals.

| Station Name | Date and Time (yyyymmddHHMM) | 1-hr Precip Totals (in) |
|---------------------|---------------------------------|----------------------------|
| LOS ANGELES INTL | 199302181900 | 0.46 |
| LOS ANGELES INTL | 199302181800 | 0.36 |
| SAN DIEGO/LINDBERGH | 199302192300 | 0.35 |
| SAN DIEGO/LINDBERGH | 199302200000 | 0.30 |
| LONG BEACH/LB AIRP. | 199302191400 | 0.29 |
| SANTA MARIA PUBLIC | 199302190100 | 0.29 |
| LONG BEACH/LB AIRP. | 199302200700 | 0.29 |
| LONG BEACH/LB AIRP. | 199302190700 | 0.28 |
| STOCKTON/METROPOLIT | 199302190500 | 0.26 |
| LONG BEACH/LB AIRP. | 199302182000 | 0.26 |
| SAN DIEGO/LINDBERGH | 199302200100 | 0.26 |
| SAN FRANCISCO INTL | 199302191200 | 0.23 |
| LOS ANGELES INTL | 199302201100 | 0.22 |
| SAN DIEGO/LINDBERGH | 199302191900 | 0.21 |
| BLUE CANYON NYACK | 199302180000 | 0.20 |
| MOUNT SHASTA | 199302191900 | 0.20 |
| MOUNT SHASTA | 199302192000 | 0.20 |
| MOUNT SHASTA | 199302192100 | 0.20 |
| MOUNT SHASTA | 199302182300 | 0.20 |
| MOUNT SHASTA | 199302191600 | 0.20 |
| MOUNT SHASTA | 199302200400 | 0.20 |

Table 4: 6-hr precipitation totals.

| Station Name | Date and Time (yyyymmddHHMM) | 6-hr Precip Totals (in) |
|------------------------------|---------------------------------|----------------------------|
| MOUNT WILSON | 199302190600 | 1.77 |
| MOUNT WILSON | 199302190000 | 1.46 |
| SHELTER COVE | 199302191800 | 1.22 |
| EUREKA | 199302200000 | 1.14 |
| JOLON HUNTER LIGGETT MIL RES | 199302181800 | 1.06 |
| SAN DIEGO/LINDBERGH | 199302180800 | 0.98 |
| MONTGOMERY FLD | 199302191400 | 0.98 |
| SANTA BARBARA MUNI | 199302181800 | 0.94 |
| MONTGOMERY FLD | 199302200000 | 0.94 |
| EL TORO MCAS | 199302190000 | 0.91 |
| SAN DIEGO/LINDBERGH | 199302200000 | 0.87 |
| JOLON HUNTER LIGGETT MIL RES | 199302191600 | 0.83 |
| SANTA BARBARA MUNI | 199302190000 | 0.83 |
| PASO ROBLES MUNI | 199302190600 | 0.83 |
| LOS ANGELES INTL | 199302190000 | 0.79 |
| LONG BEACH/LB AIRP. | 199302191800 | 0.79 |
| MOUNT WILSON | 199302191800 | 0.79 |
| JACK MC NAMARA FLD | 199302191800 | 0.79 |
| BARSTOW DAGGETT | 199302201200 | 0.79 |
| NORTH ISLAND NAS | 199302200000 | 0.79 |
| NORTH ISLAND NAS | 199302200600 | 0.75 |
| UKIAH MUNI | 199302180000 | 0.75 |

Table 5: 24-hr precipitation totals.

| Station Name | Date and Time (yyyymmddHHMM) | 24-hr Precip Totals (in) |
|---------------------|---------------------------------|-----------------------------|
| EUREKA | 199302200600 | 1.78 |
| SAN BERNARDINO INTL | 199302201200 | 1.54 |
| BISHOP AIRPORT | 199302191500 | 1.46 |
| SAN DIEGO/LINDBERGH | 199302201200 | 1.44 |
| SAN DIEGO/LINDBERGH | 199302200600 | 1.41 |
| LOS ANGELES INTL | 199302191200 | 1.30 |
| CAMPO | 199302192300 | 1.26 |
| EUREKA | 199302200000 | 1.26 |
| SAN FRANCISCO INTL | 199302200600 | 1.24 |
| SAN DIEGO/LINDBERGH | 199302200000 | 1.11 |
| LOS ANGELES INTL | 199302190000 | 1.09 |
| LOS ANGELES INTL | 199302191800 | 1.03 |
| RIVERSIDE/MARCH AFB | 199302191200 | 1.02 |

Table 6: Classification of polar lows from, adapted from table in Rasmussen and Turner (2003, p. 159).

| Group | Type of Polar Low |
|-------|-------------------------------|
| 1 | Reverse shear-systems |
| 2 | Trough systems |
| 3 | Boundary layer fronts |
| 4 | Cold lows |
| 5 | Comma Clouds |
| 6 | Baroclinic wave-forward shear |
| 7 | Orographic polar lows |

Table 7: Comparison between 19 February 1993 storm with typical explosively developing cyclones (Sanders and Gyakum 1980, Reed and Albright 1986), 'cold low' polar lows (Rasmussen and Turner 2003, p. 172-189, 335-340), and strong polar lows (Rasmussen 1981).

| Characteristic | Present in Explosive Cyclones | Present in Polar Lows | Present in 19 February 1993 Storm |
|---|-------------------------------|---------------------------------------|-----------------------------------|
| Environment conducive to formation | | | |
| Primarily maritime, winter events | Yes | Yes | Yes |
| Large air-sea temperature difference | Not necessary | Yes | Yes |
| Cyclonic curvature upper levels | Yes | Yes | Yes |
| Occluded large scale baroclinic wave | No | Yes | Yes |
| Cold upper level trough | Not necessary | Yes | Yes |
| Formation of low-level vortex (or vortices) | Yes | Yes | Yes |
| Formation of cloud streets | Not necessary | Yes | No |
| Cyclone Formation | | | |
| Rapid pressure falls in low center | Yes | Yes | Yes |
| Strong surface winds | Yes | Yes | Yes |
| Organized convection | Not necessary | Yes | Yes |
| Spiral cloud formation | Not necessary | Yes | Yes |
| Cloud-free eye | Not necessary | Maybe, during mature stage | Yes |
| Development of warm core | Not necessary | Sometimes | Yes |
| Upper level cirrus shield | Not necessary | Sometimes, indicates strong polar low | No |

Table 7 (continued)

| | | | |
|--|-----------|--------------|-------|
| Development of low level instability, high CAPE values | Sometimes | Yes | Yes |
| Formation Relative to 'main' baroclinic zone | Within | North | North |
| Dissipation | | | |
| Short-lived events | -No | Yes, usually | Yes |
| Dissipates after heat source is lost | No | Yes | Yes |

Table 8: A summary of the qualitative nature of forcing for upward vertical motion as assessed by the QG-omega equation (Eq. (1)).

| Date and Time | Pressure at center of low from NARR (mb) | Forcing for vertical motion from differential vorticity advection | Forcing for vertical motion from temperature advection | Net forcing for vertical motion from QG-omega equation |
|-------------------------|--|---|--|--|
| 00 UTC 17 February 1993 | 1006.5 | Upward, weak | Upward, weak | Upward, weak |
| 12 UTC 17 February 1993 | 1005.5 | Upward, moderate | Upward, weak | Upward, moderate |
| 00 UTC 18 February 1993 | 1004.2 | Upward, moderate | Upward, moderate | Upward, strong |
| 12 UTC 18 February 1993 | 998.3 | Upward, weak | Upward, strong | Upward, strong |
| 00 UTC 19 February 1993 | 992.4 | Upward, weak | Upward, strong | Upward, strong |
| 12 UTC 19 February 1993 | 990.8 | Upward, moderate | Upward, strong | Upward, very strong |
| 00 UTC 20 February 1993 | 987.8 | Upward, weak | Upward, weak | Upward, weak |

Table 9: Solution to the SPDE without expanded thickness term (Eq. (5)), calculated by hand, compared to actual 6-hr vorticity changes. Terms B and C contribute to the total computed vorticity tendency (Term A). All values are in units of 10^{-5} s^{-1} per 6 hour time step.

| Time Step (Begin Time) | Actual 6-hr Vorticity Change | Term A (Total) | Term B | Term C |
|-------------------------|------------------------------|----------------|--------|--------|
| 00 UTC 18 February 1993 | 2.13 | 4.87 | 1.78 | 3.09 |
| 00 UTC 19 February 1993 | 5.64 | 4.93 | 1.09 | 3.83 |

Table 10: Solution to the SPDE with expanded thickness term (Eq. (9)) using IDV, compared to actual 6-hr vorticity changes. Terms B, C, and D contribute to the total computed vorticity tendency (term A). All values are in units of 10^{-5} s^{-1} per 6 hour time step.

| Time Step (Begin Time) | Actual 6-hr Vort. Change | Term A (Total) | Term B | Term C | Term D |
|------------------------|--------------------------|----------------|---------|--------|---------|
| Feb 17 00Z | 8.82 | -68.36 | -55.08 | 10.37 | -23.65 |
| Feb 17 06Z | -34.12 | -7.02 | -55.08 | 25.06 | 23.00 |
| Feb 17 12Z | -26.68 | 58.54 | 38.12 | -4.00 | 24.41 |
| Feb 17 18Z | 58.06 | 67.87 | 30.72 | -9.72 | 46.87 |
| Feb 18 00Z | 16.96 | -132.71 | -230.88 | -1.51 | 99.68 |
| Feb 18 06Z | 65.61 | 89.19 | 61.43 | -0.97 | 28.73 |
| Feb 18 12Z | 109.74 | 746.06 | 646.06 | 9.07 | 90.94 |
| Feb 18 18Z | -138.57 | 275.90 | 166.28 | -20.74 | 130.36 |
| Feb 19 00Z | 254.48 | -181.67 | -216.23 | -15.55 | 50.11 |
| Feb 19 06Z | 78.06 | -13.00 | -6.52 | 26.24 | -32.72 |
| Feb 19 12Z | -41.38 | -261.11 | 118.62 | 69.55 | -449.28 |

Table 11: Solution to SPDE with expanded thickness terms (Eq. (9)), calculated by hand, compared to actual 6-hr vorticity changes. Terms B, C, D, and E contribute to the total computed vorticity tendency (term A). All values are in units of 10^{-5} s^{-1} per 6 hour time step.

| Time Step (Begin Time) | Actual 6-hr Vorticity Change | Term A (Total) | Term B | Term C | Term D | Term E |
|------------------------|------------------------------|----------------|--------|--------|--------|--------|
| Feb 18 00Z | 2.13 | 4.87 | 1.78 | -3.60 | 27.71 | -21.02 |
| Feb 19 00Z | 5.64 | 4.93 | 1.09 | -6.79 | 39.95 | -29.32 |

Figures

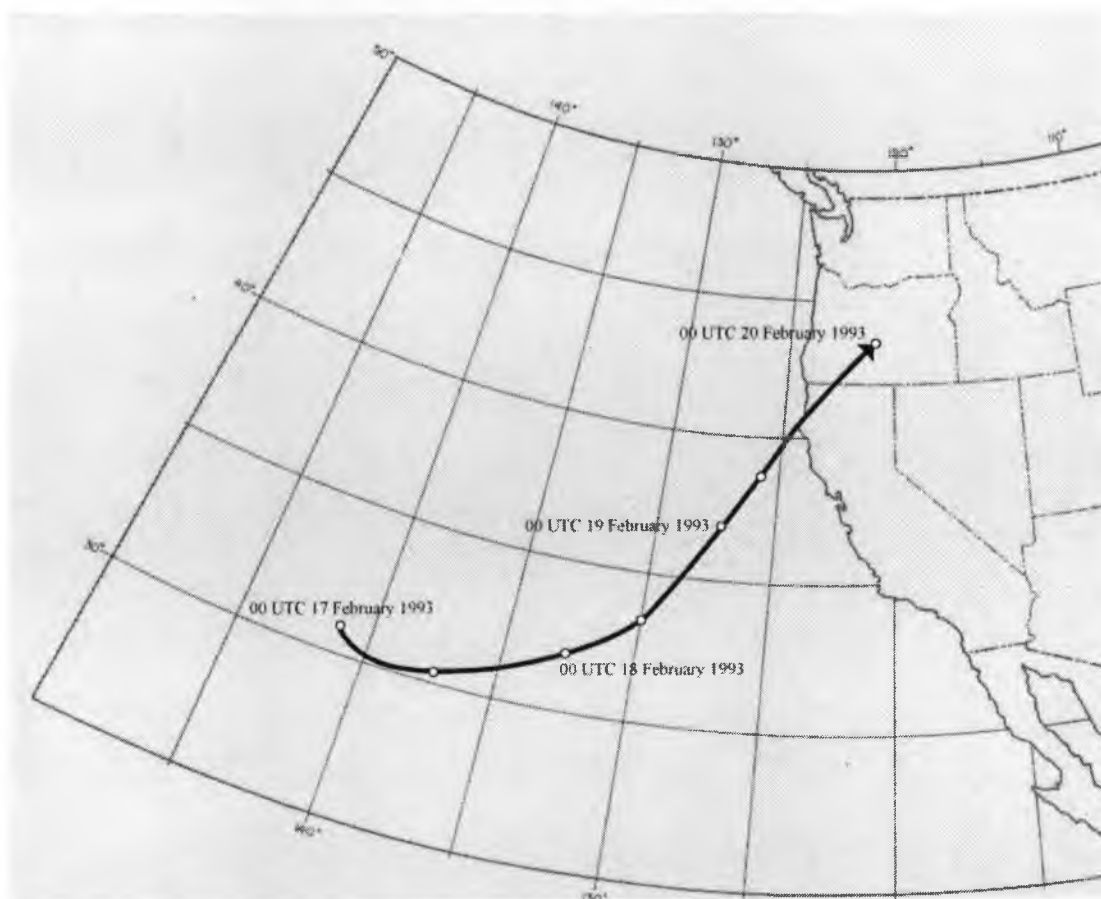


Figure 1: Track of the main low-pressure center based on the NARR surface analysis, from 00 UTC 17 February 1993 to 00 UTC 20 February 1993.

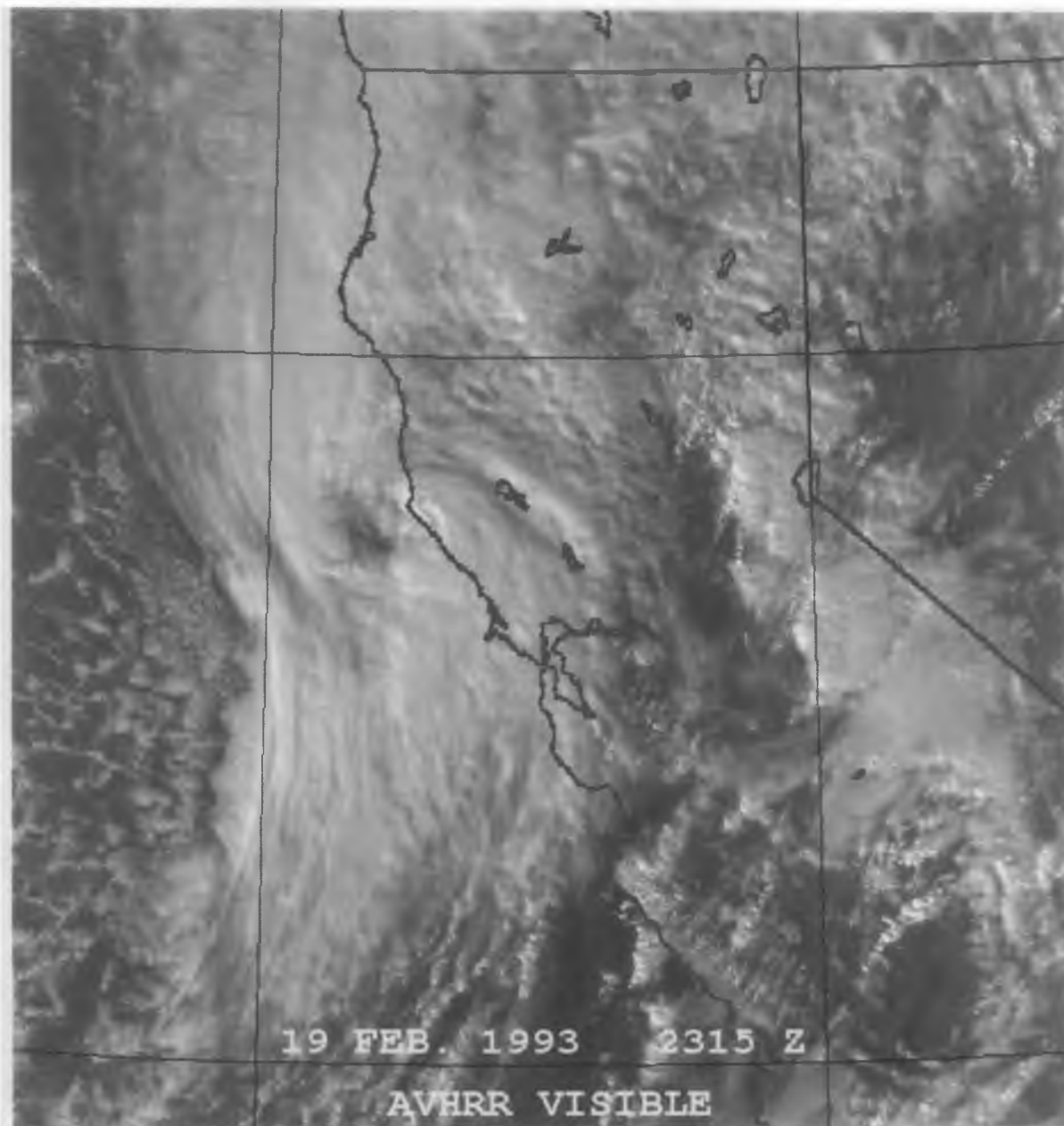


Figure 2: Visible satellite image for 2315 UTC 19 February 1993, showing cyclone with eye-like feature making landfall on Northern California coast. Thunderstorm anvils can be seen in the eastern Central Valley and Sierra Nevada regions.

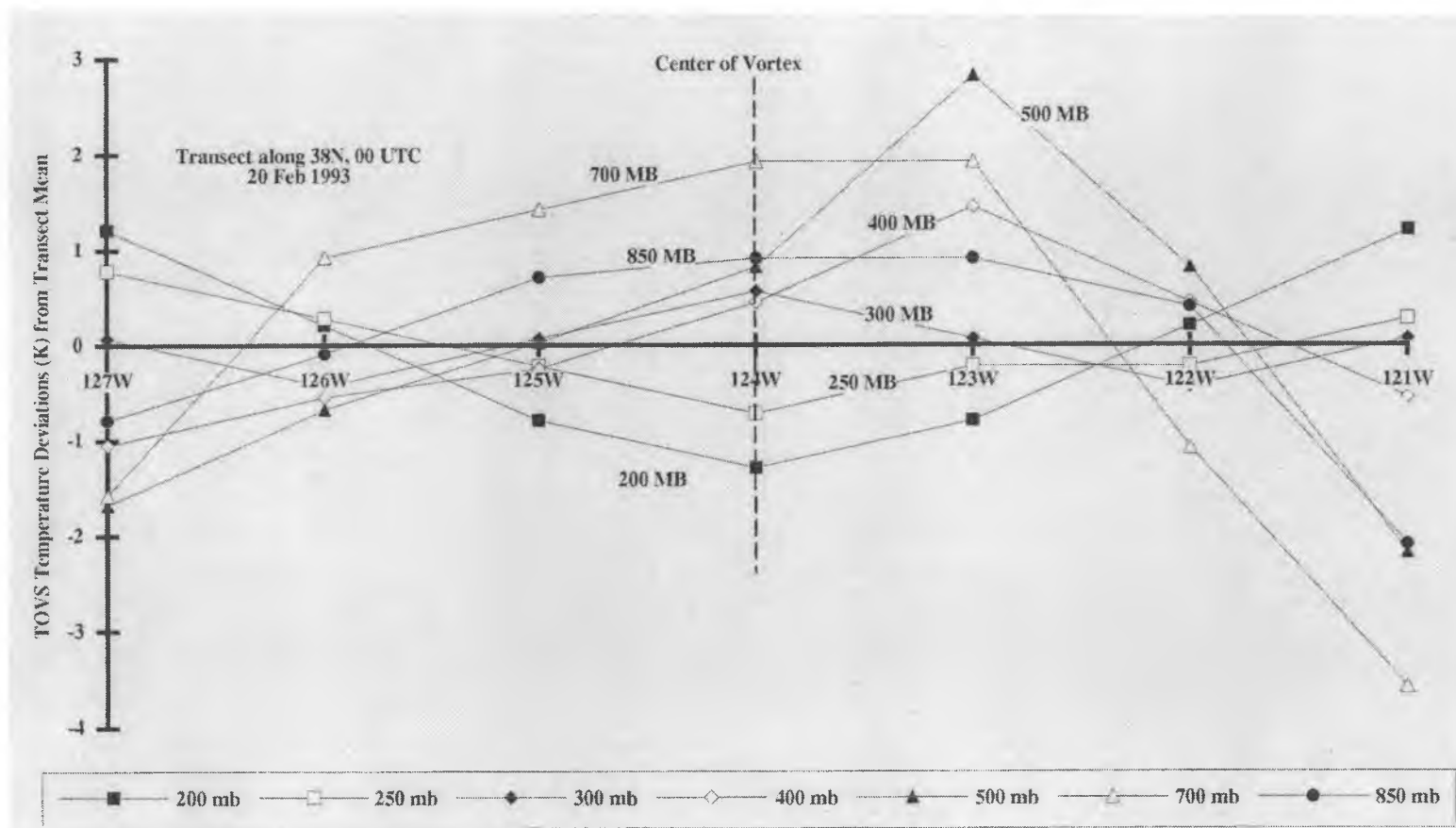


Figure 3a: Transect through the storm along 38°N, from 127°W (left) to 121°W (right), 00 UTC 20 February 1993. The lines show temperature deviations (K) from the transect mean at various pressure levels.

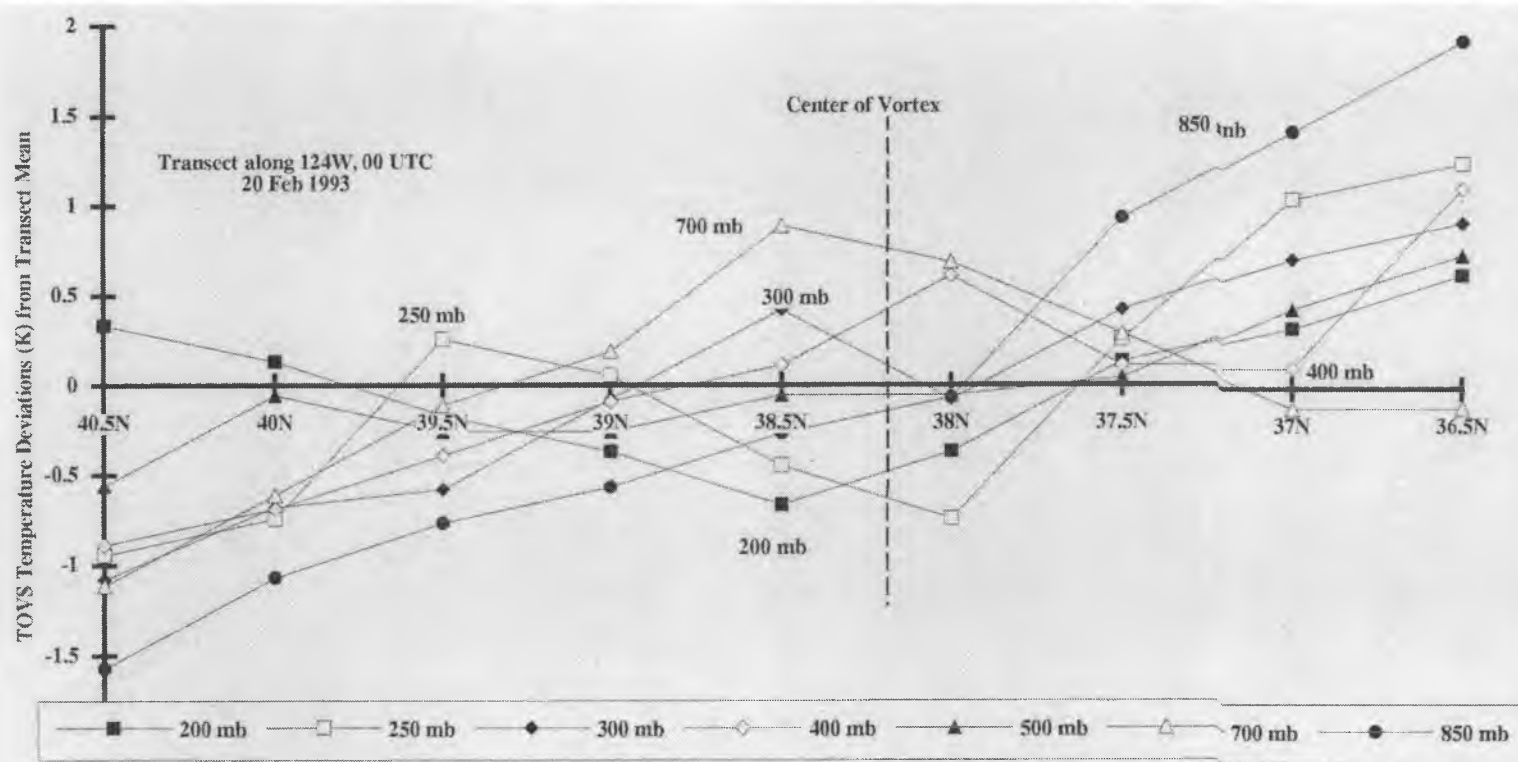


Figure 3b: Transect through the storm along 124°W, from 36.5°N (right) to 40.5°N (left), 00 UTC 20 February 1993. The lines show temperature deviations (K) from the transect mean at various pressure levels.

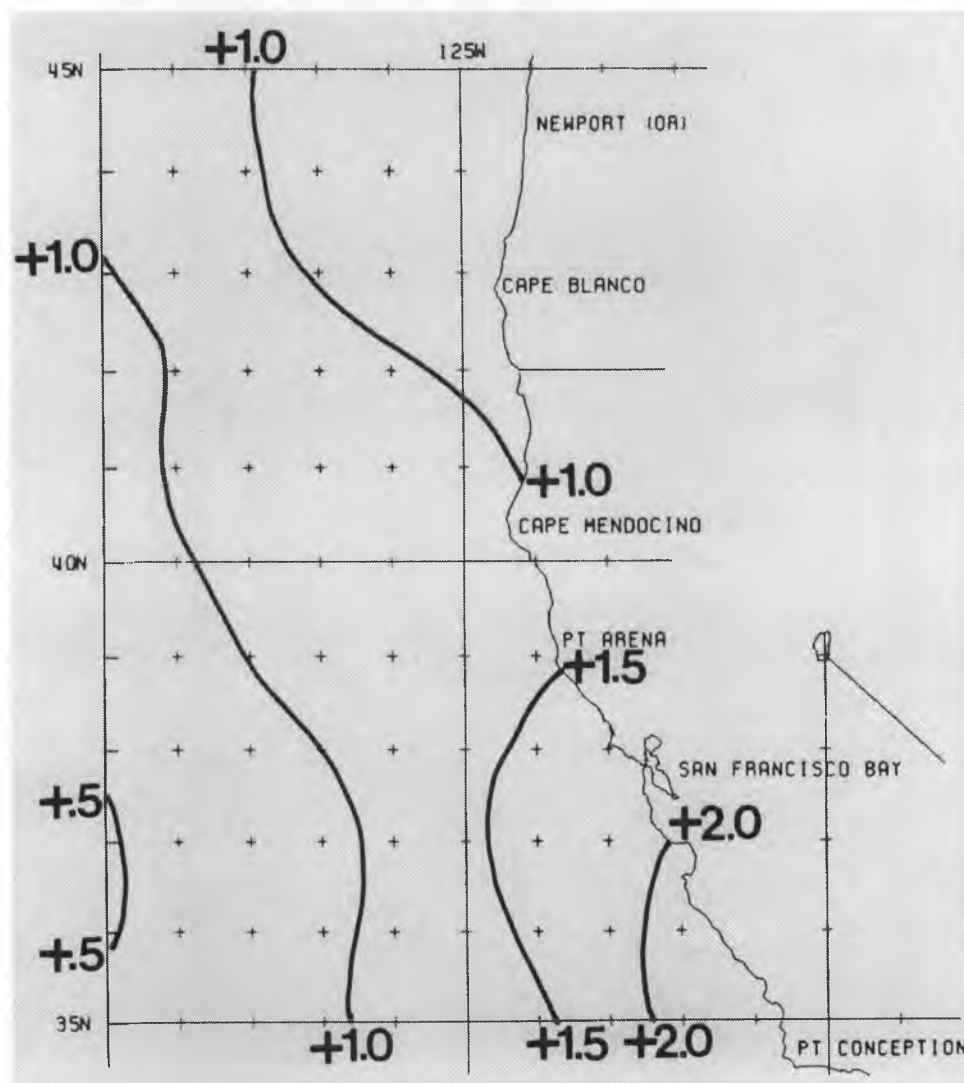


Figure 4: Sea surface temperature anomalies ($^{\circ}\text{C}$) in coastal waters of Northern California and Oregon for 19 February 1993.

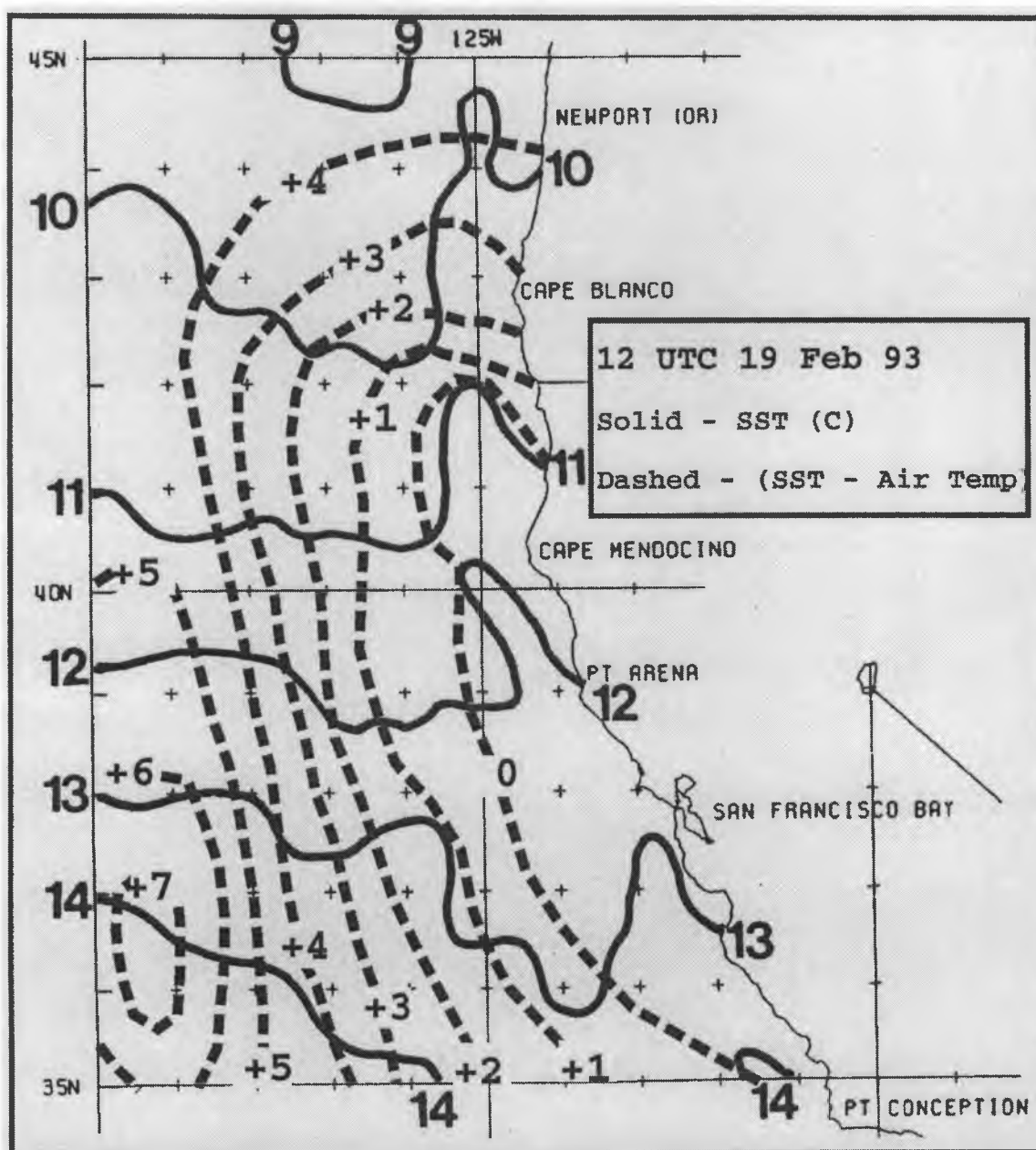


Figure 5: Sea surface temperatures (solid, °C) and sea surface – air temperature difference (dashed, °C) for 12 UTC 19 February 1993. Positive sea surface – air temperature differences indicate sea surface temperature is warmer than air temperature.

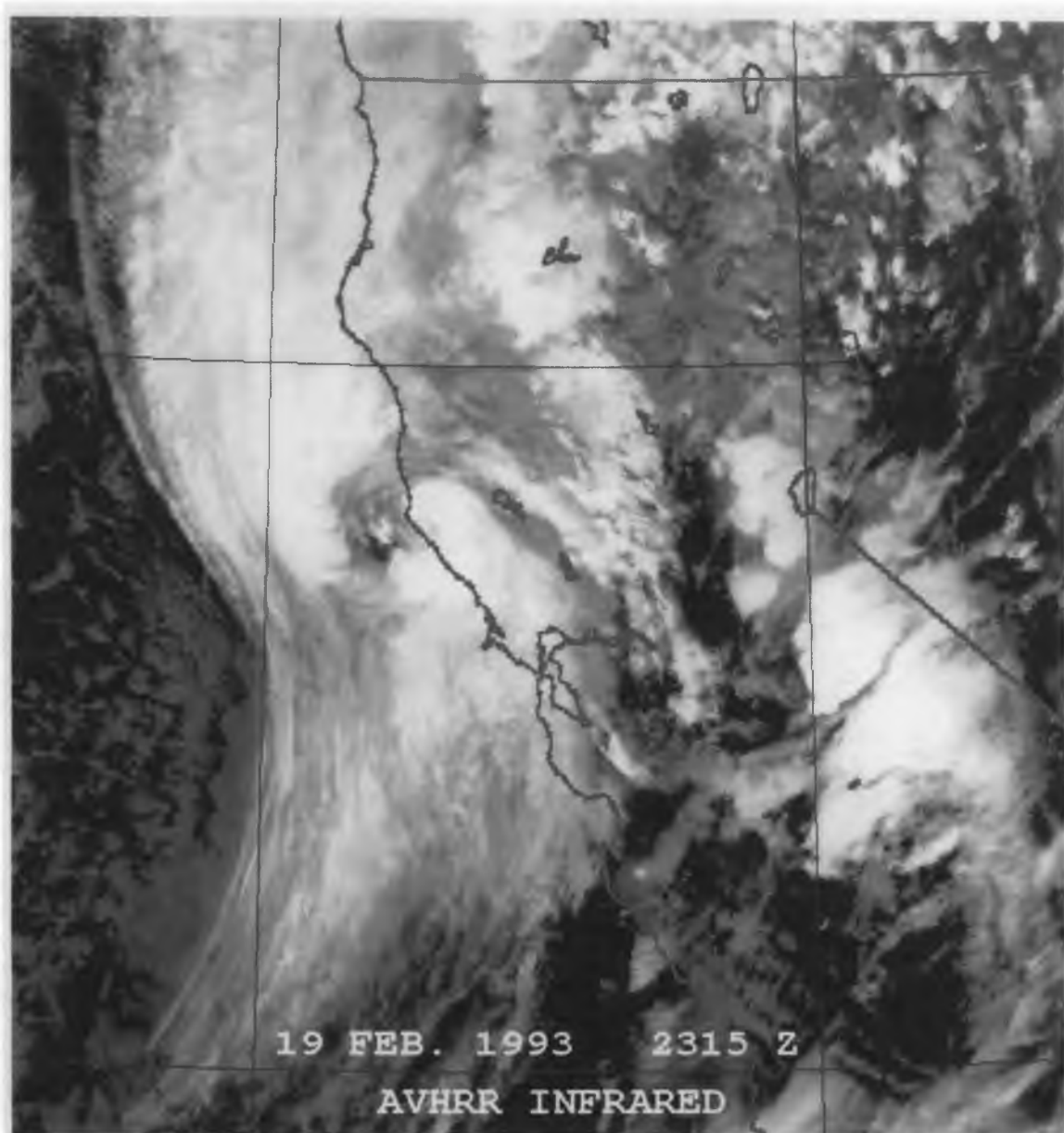


Figure 6: AVHRR infrared satellite image for Northern California for 2315 UTC 19 February 1993.

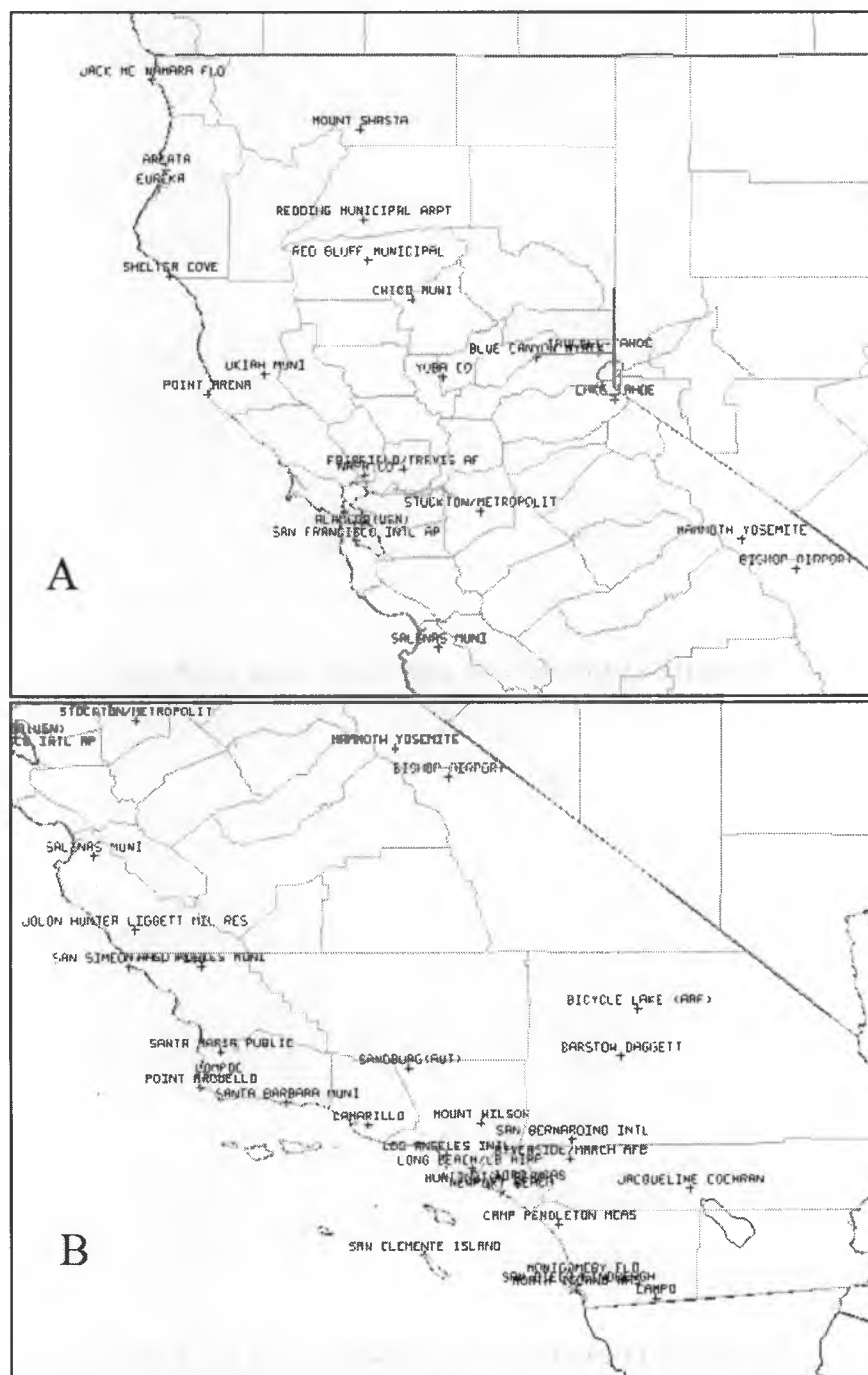


Figure 7: ASOS/AWOS in Northern California (A) and Southern California (B) used for wind and rainfall data in Tables 2 through 5.

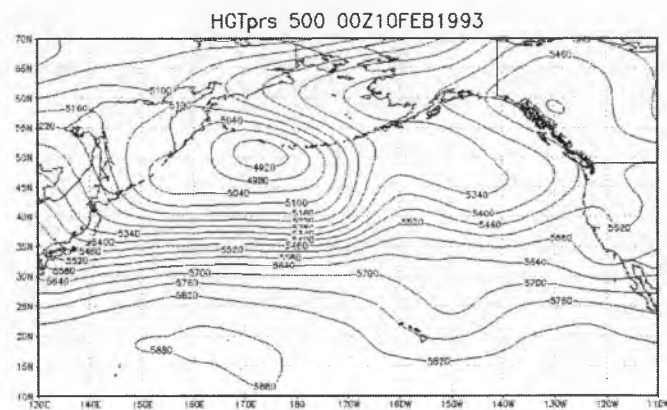
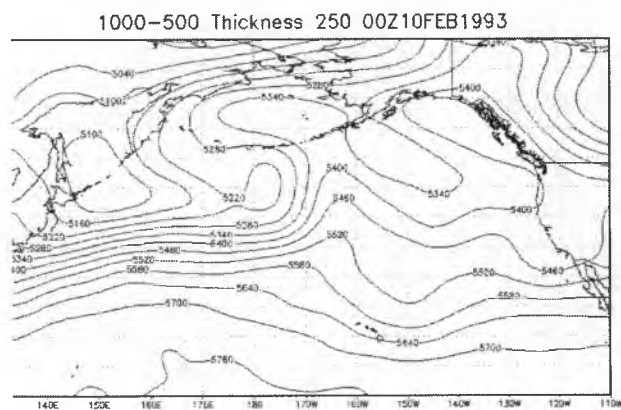
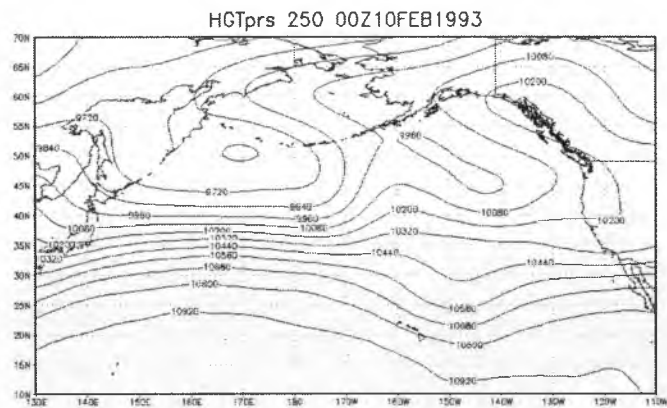
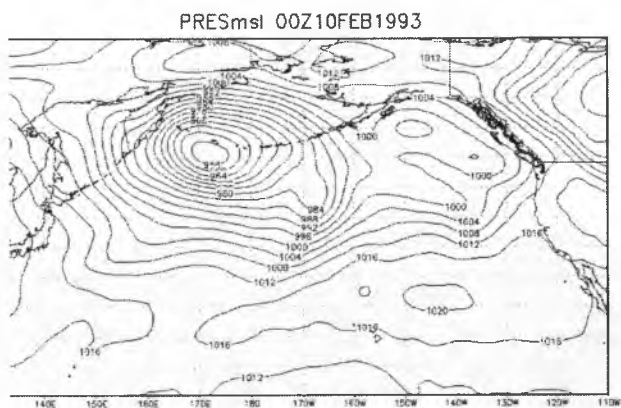


Figure 8a: Pressure at mean sea level (top left), 1000-500 mb thickness (bottom left), 250 mb geopotential heights (top right), and 500 mb geopotential heights (bottom right) for 00 UTC 10 February 1993. From Reanalysis-2 (NOAA/NCEP 2014)

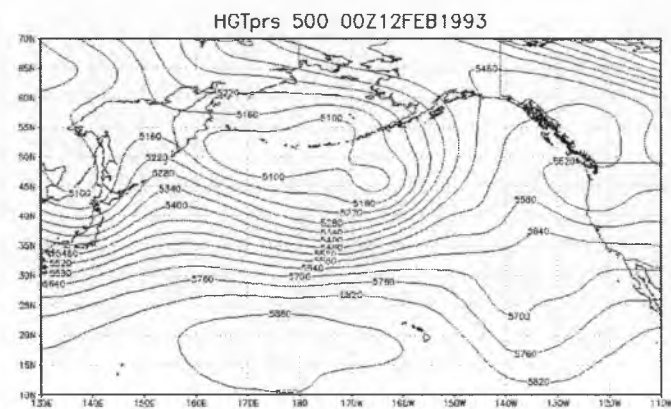
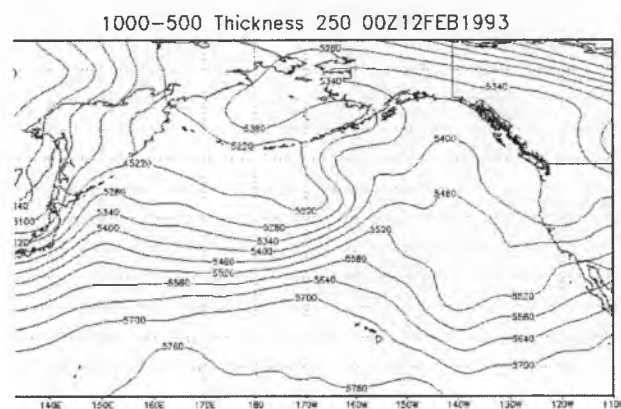
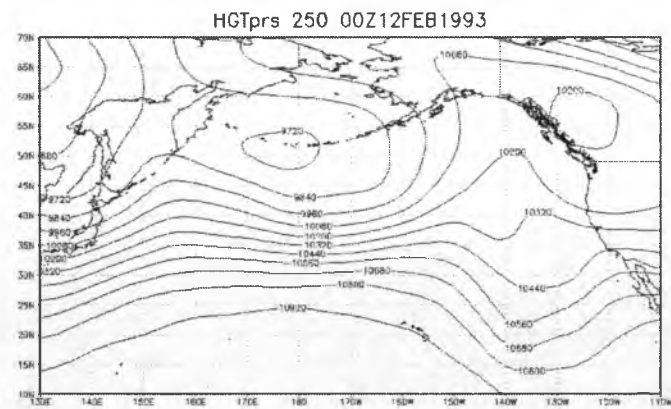
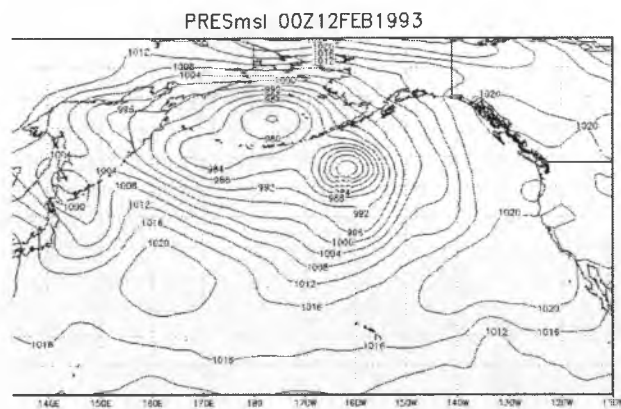


Figure 8b: As in Fig. 8a, but for 00 UTC 12 February 1993.

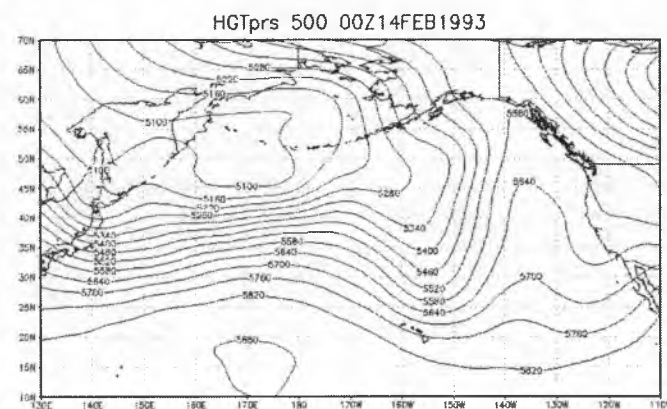
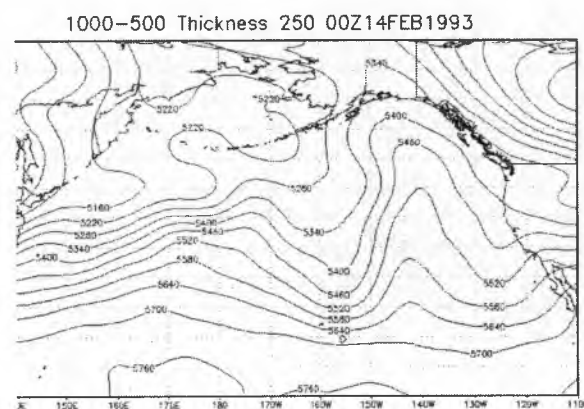
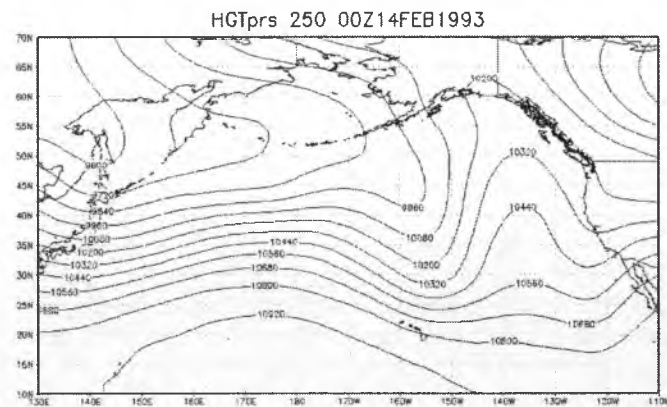
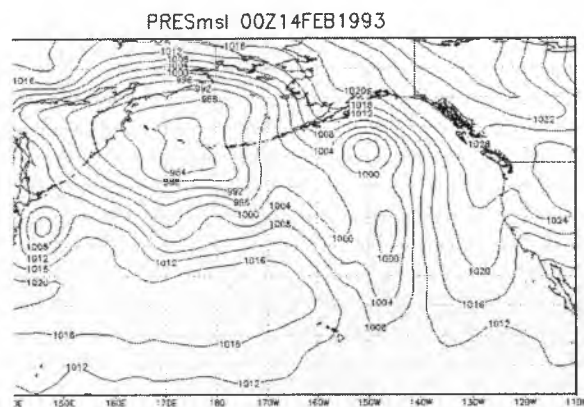


Figure 8c: As in Fig. 8a, but for 00 UTC 14 February 1993.

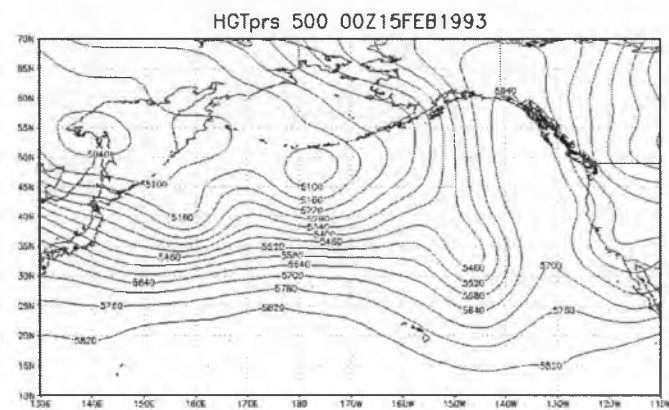
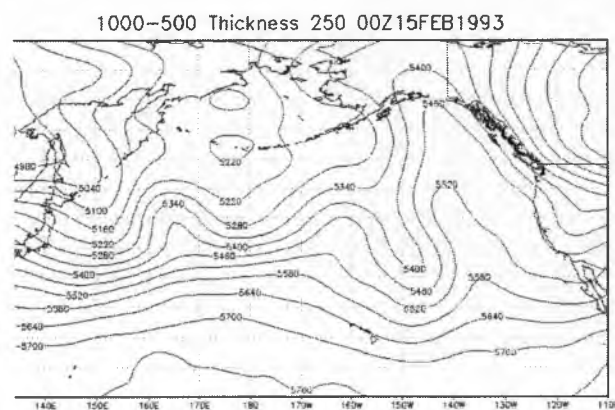
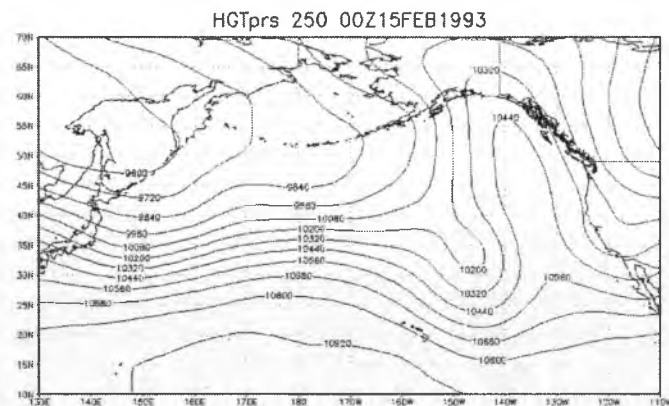
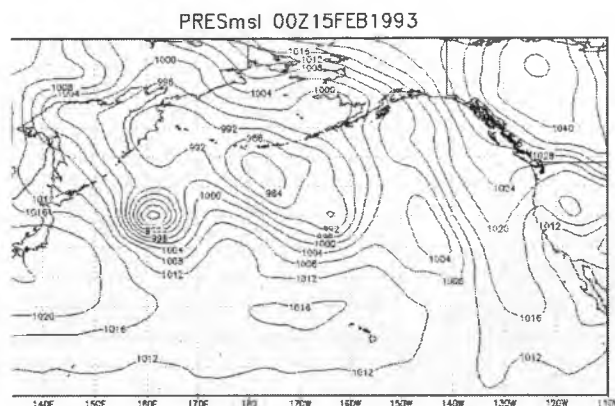


Figure 8d: As in Fig. 8a, but for 00 UTC 15 February 1993.

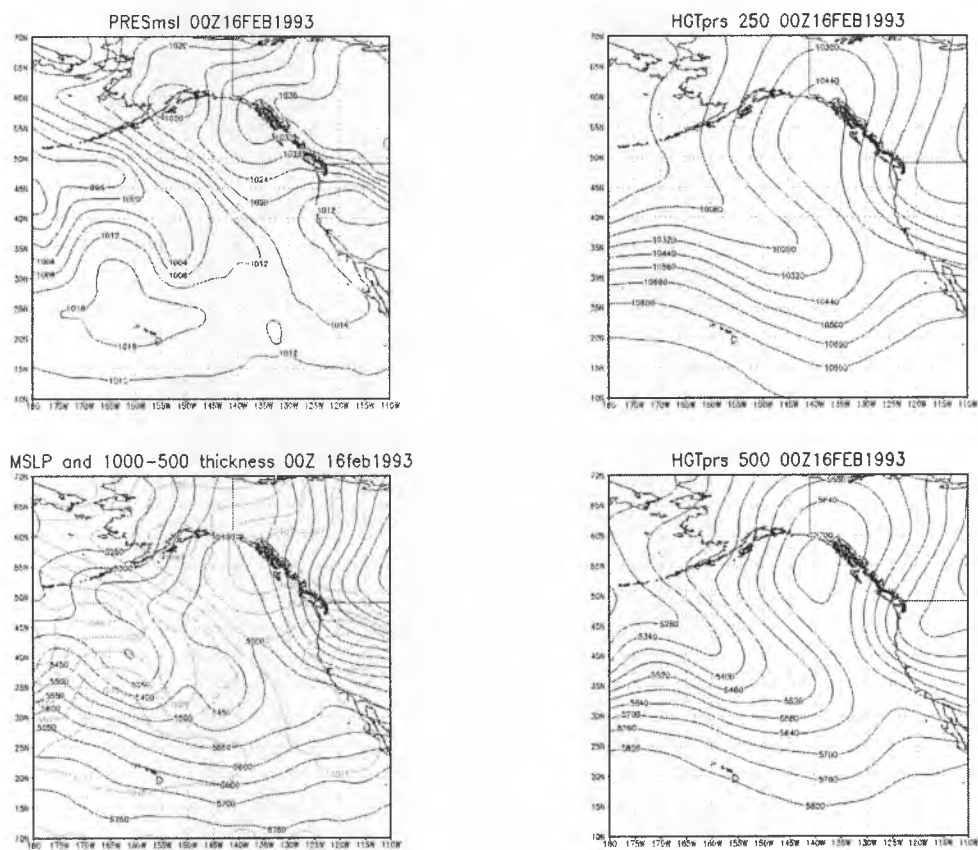


Figure 8e: As in Fig. 8a, but for 00 UTC 16 February 1993.

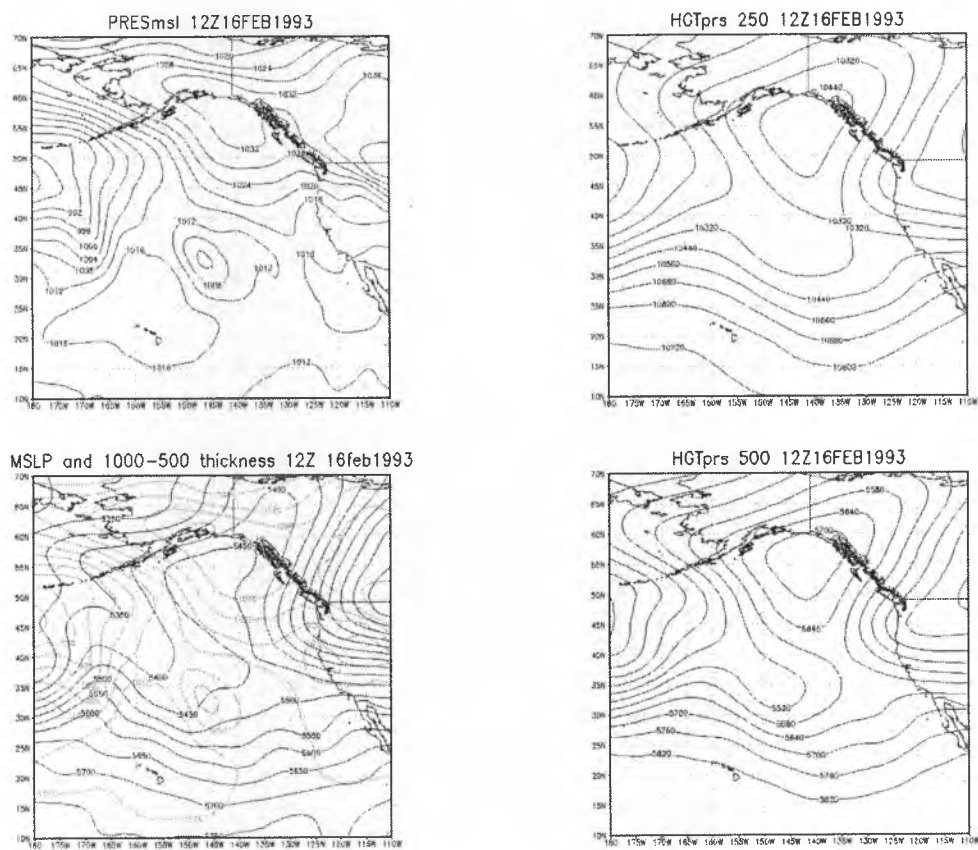


Figure 8f: As in Fig. 8a, but for 12 UTC 16 February 1993.

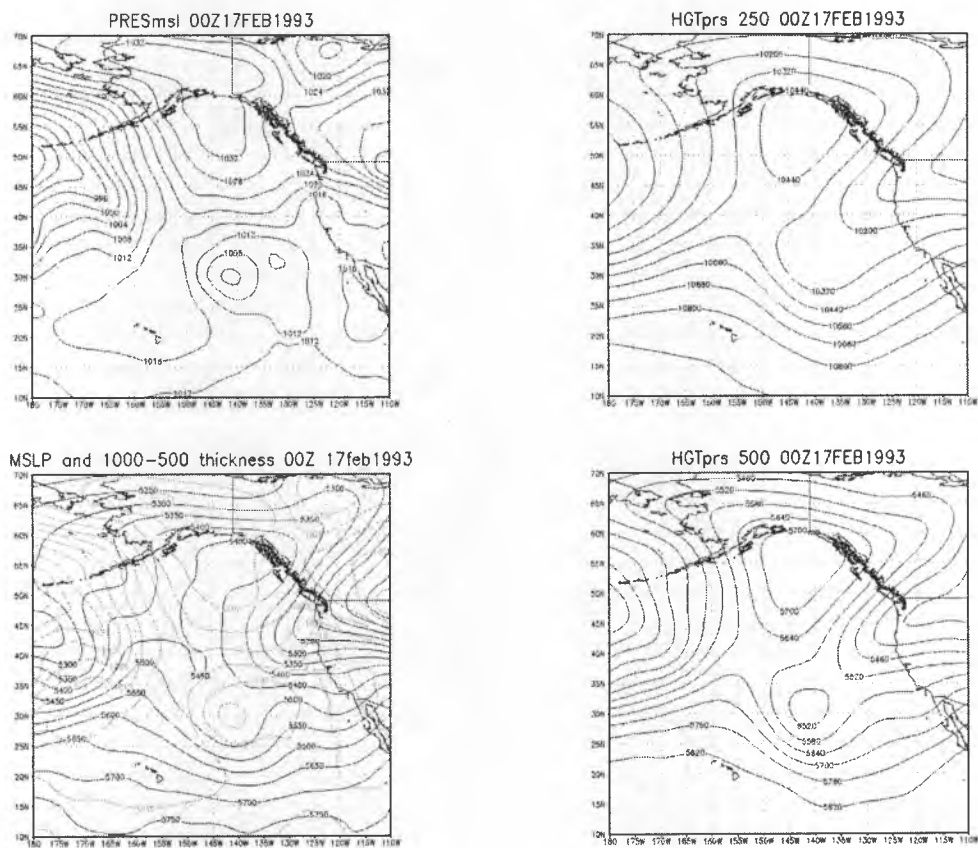
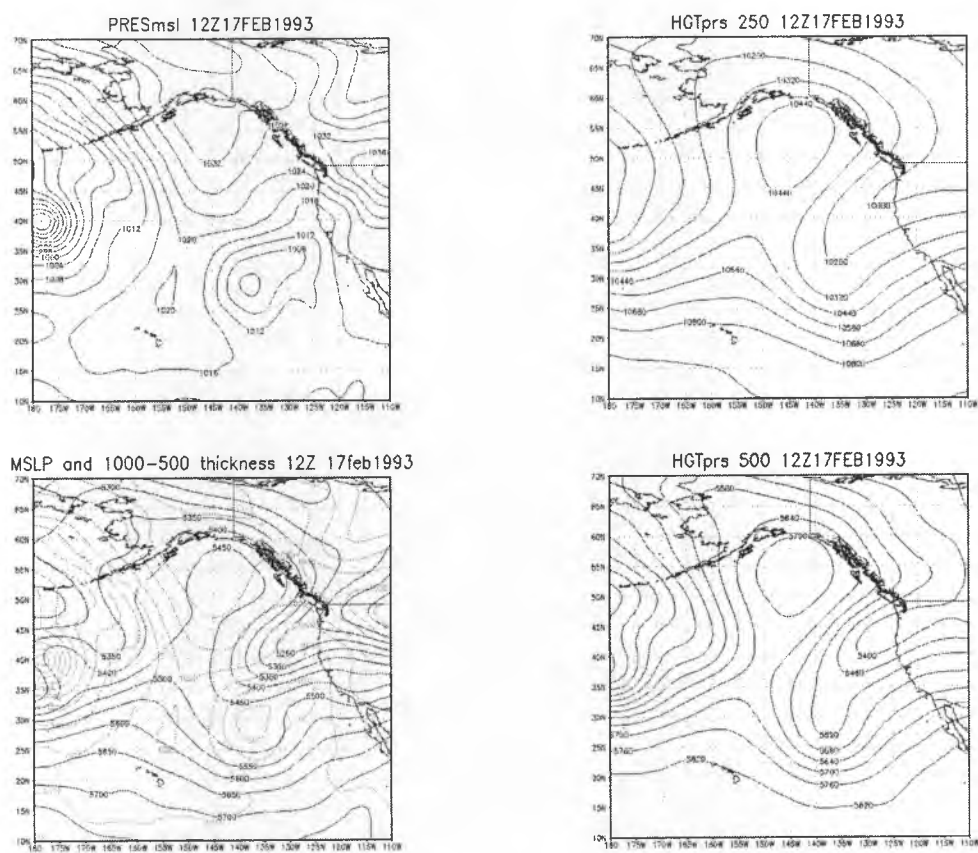


Figure 8g: As in Fig. 8a, but for 00 UTC 17 February 1993.



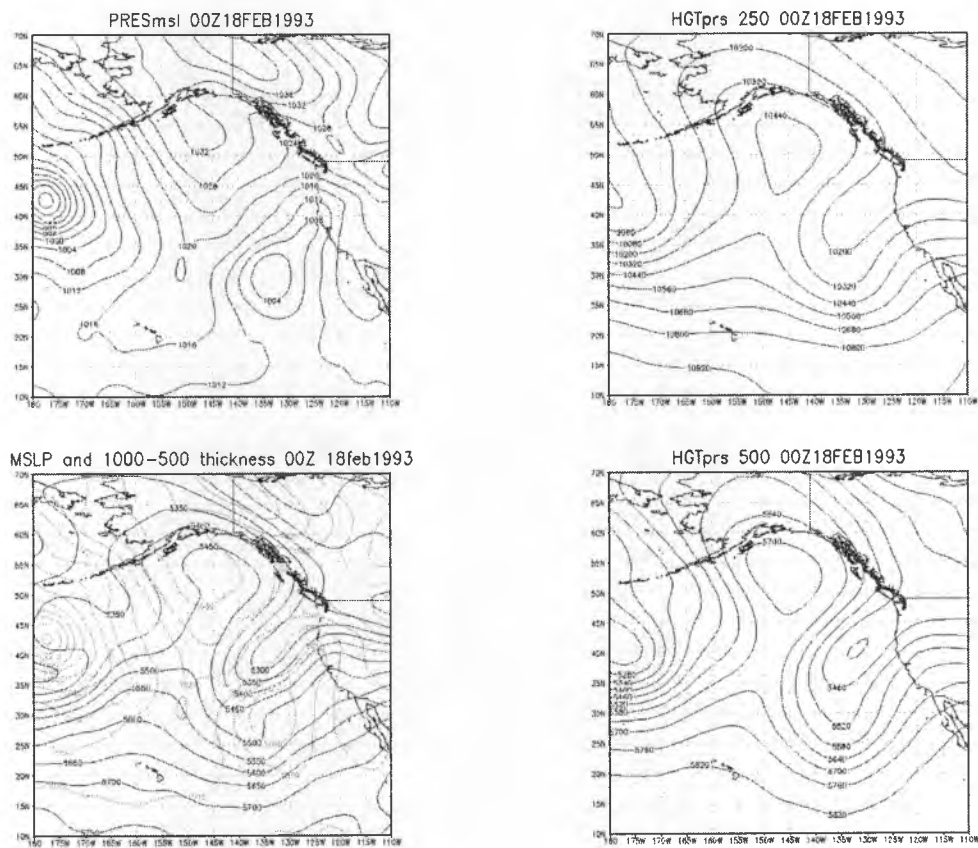


Figure 8i: As in Fig. 8a, but for 00 UTC 18 February 1993.

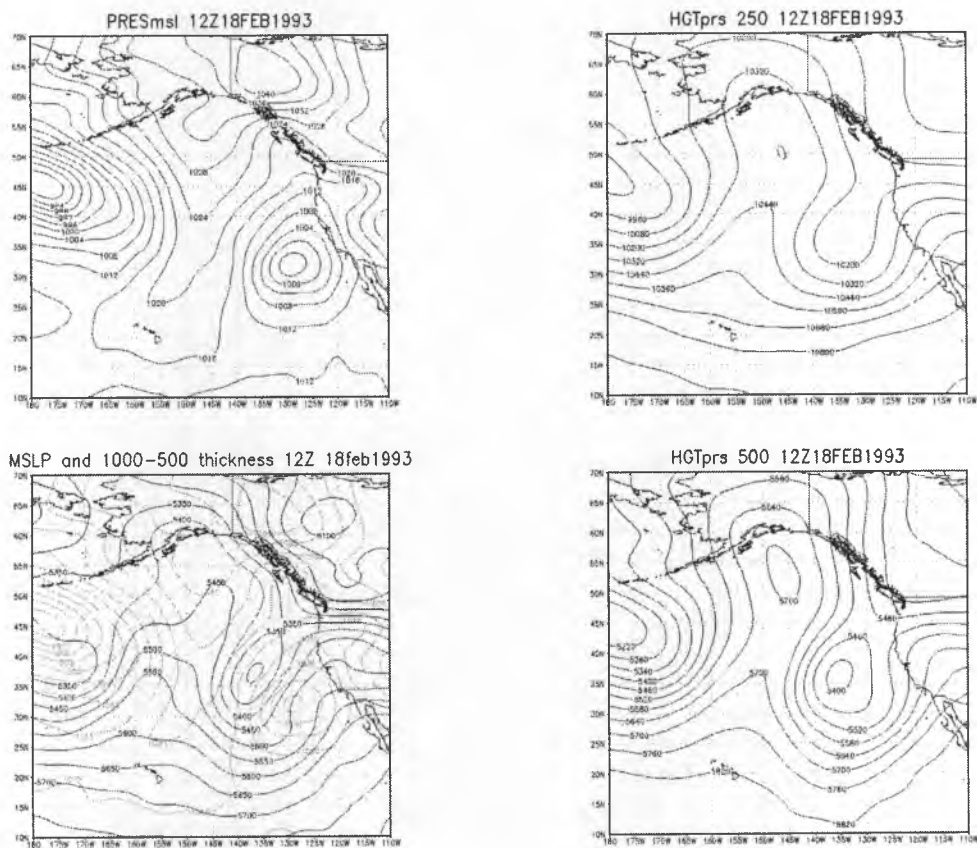


Figure 8j: As in Fig. 8a, but for 12 UTC 18 February 1993.

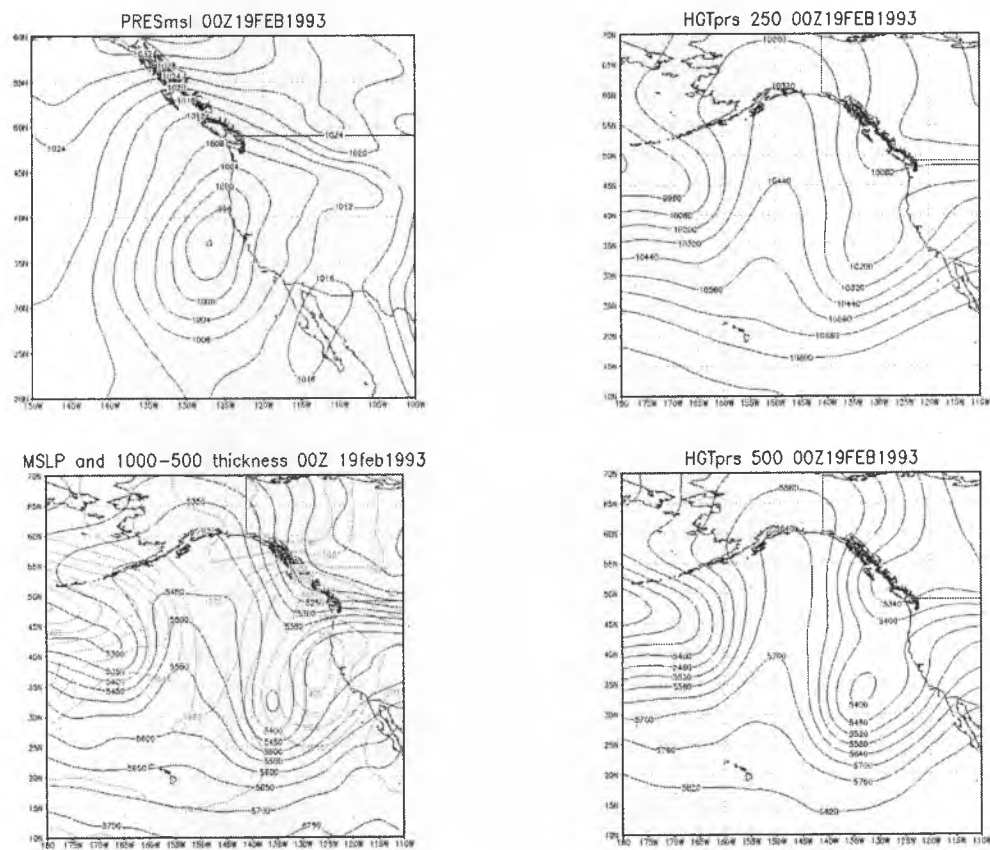
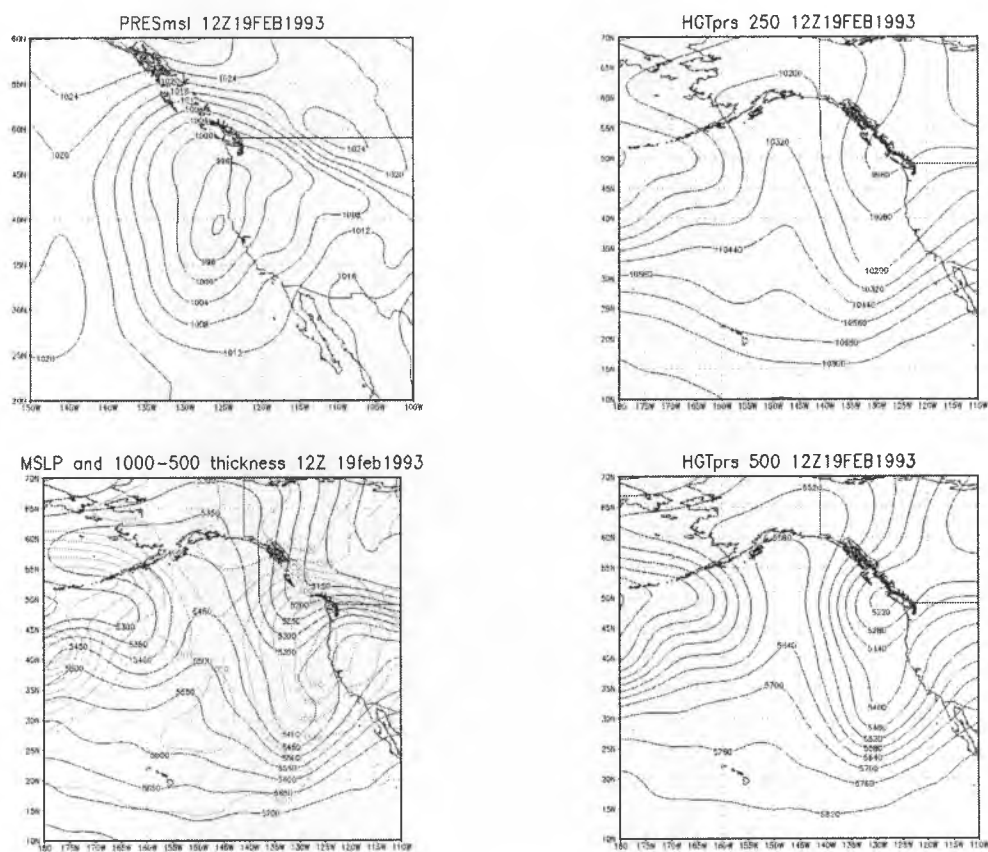


Figure 8k: As in Fig. 8a, but for 00 UTC 19 February 1993.



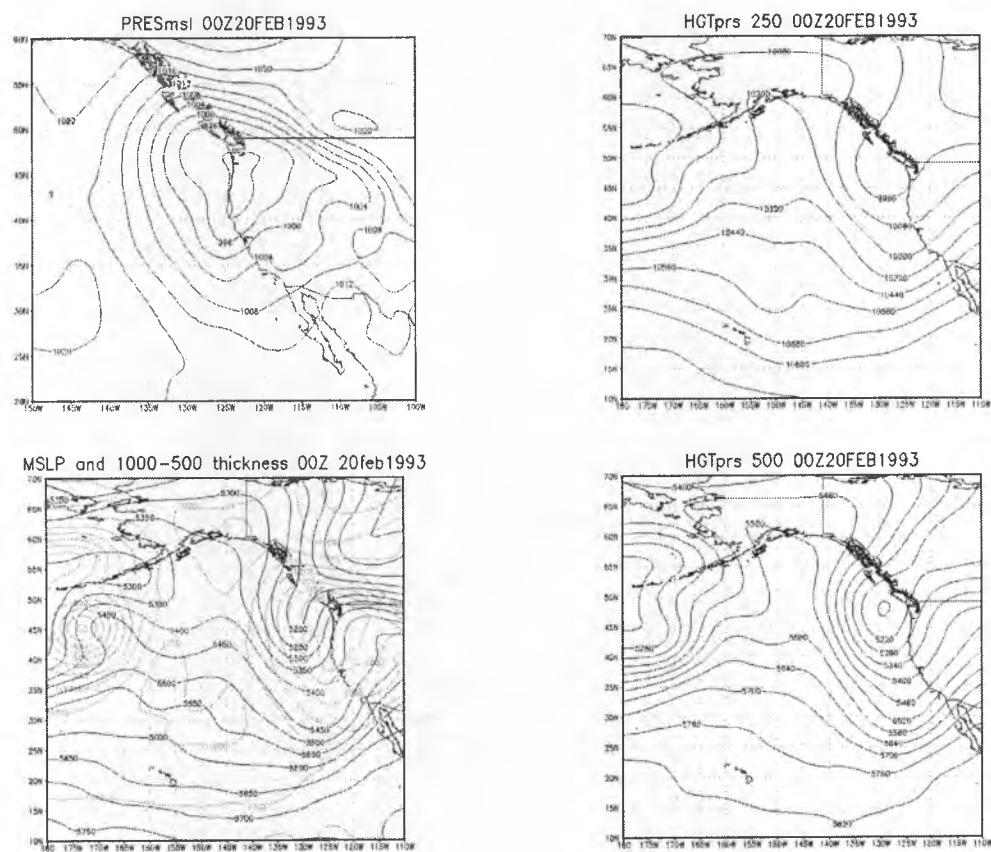
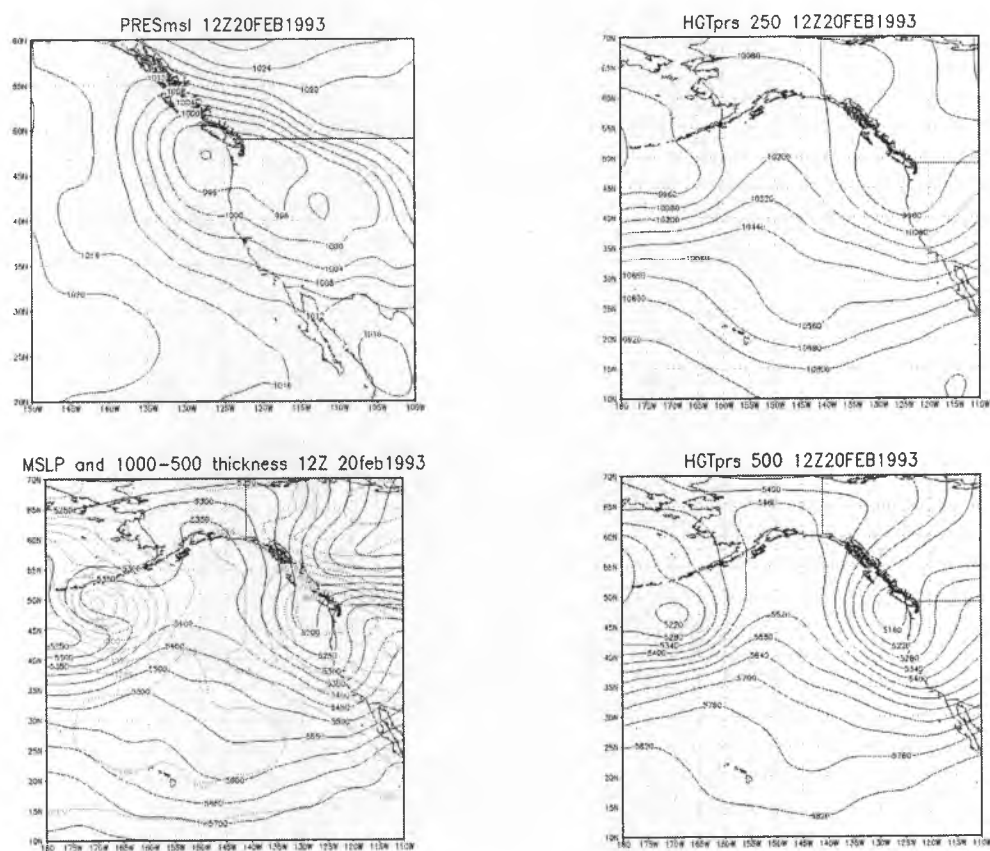


Figure 8m: As in Fig. 8a, but for 00 UTC 20 February 1993.



Feb-16-1993 12:01UTC
1993 047
GOES-7

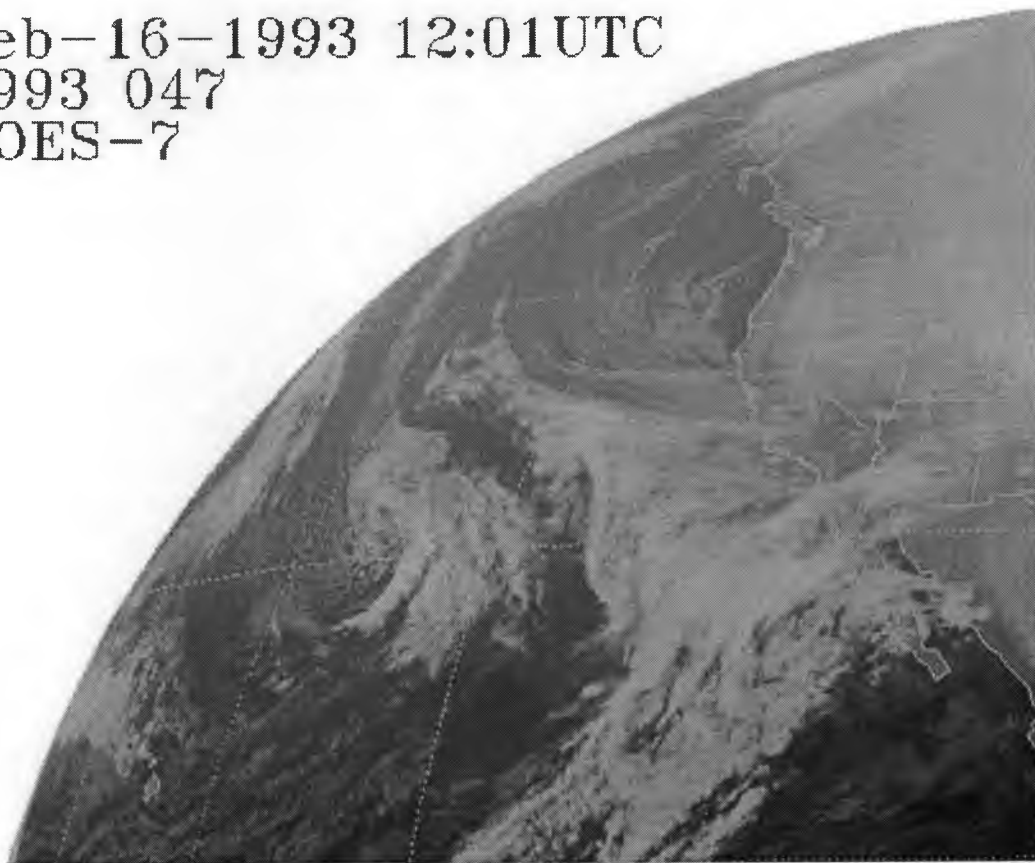


Figure 9a: GOES west imagery for 12 UTC 16 February 1993 (NOAA/NESDIS, 2014).

Feb-17-1993 00:01UTC
1993 048
GOES-7



Figure 9b: As in Fig. 9a, but for 00 UTC 17 February 1993.

Feb-17-1993 12:01UTC
1993 048
GOES-7



Figure 9c: As in Fig. 9a, but for 12 UTC 17 February 1993.

Feb-18-1993 00:01UTC
1993 049
GOES-7



Figure 9d: As in Fig. 9a, but for 00 UTC 18 February 1993.

Feb-18-1993 12:01UTC
1993 049
GOES-7



Figure 9e: As in Fig. 9a, but for 12 UTC 18 February 1993.

Feb-19-1993 00:01UTC
1993 050
GOES-7



Figure 9f: As in Fig. 9a, but for 00 UTC 19 February 1993.

Feb-19-1993 12:03UTC
1993 050
GOES-7



Figure 9g: As in Fig. 9a, but for 12 UTC 19 February 1993.

Feb-19-1993 18:01UTC
1993 050
GOES-7



Figure 9h: As in Fig. 9a, but for 18 UTC 19 February 1993.

Feb-20-1993 00:01UTC
1993 051
GOES-7



Figure 9i: As in Fig. 9a, but for 00 UTC 20 February 1993.

Feb-20-1993 06:01UTC
1993 051
GOES-7



Figure 9j: As in Fig. 9a, but for 06 UTC 20 February 1993.



Figure 10: An infrared satellite image of the eastern Pacific and western North America for 10 UTC 19 February 1993.



Figure 11: An infrared satellite image of the eastern Pacific and western North America for 18 UTC 19 February 1993.

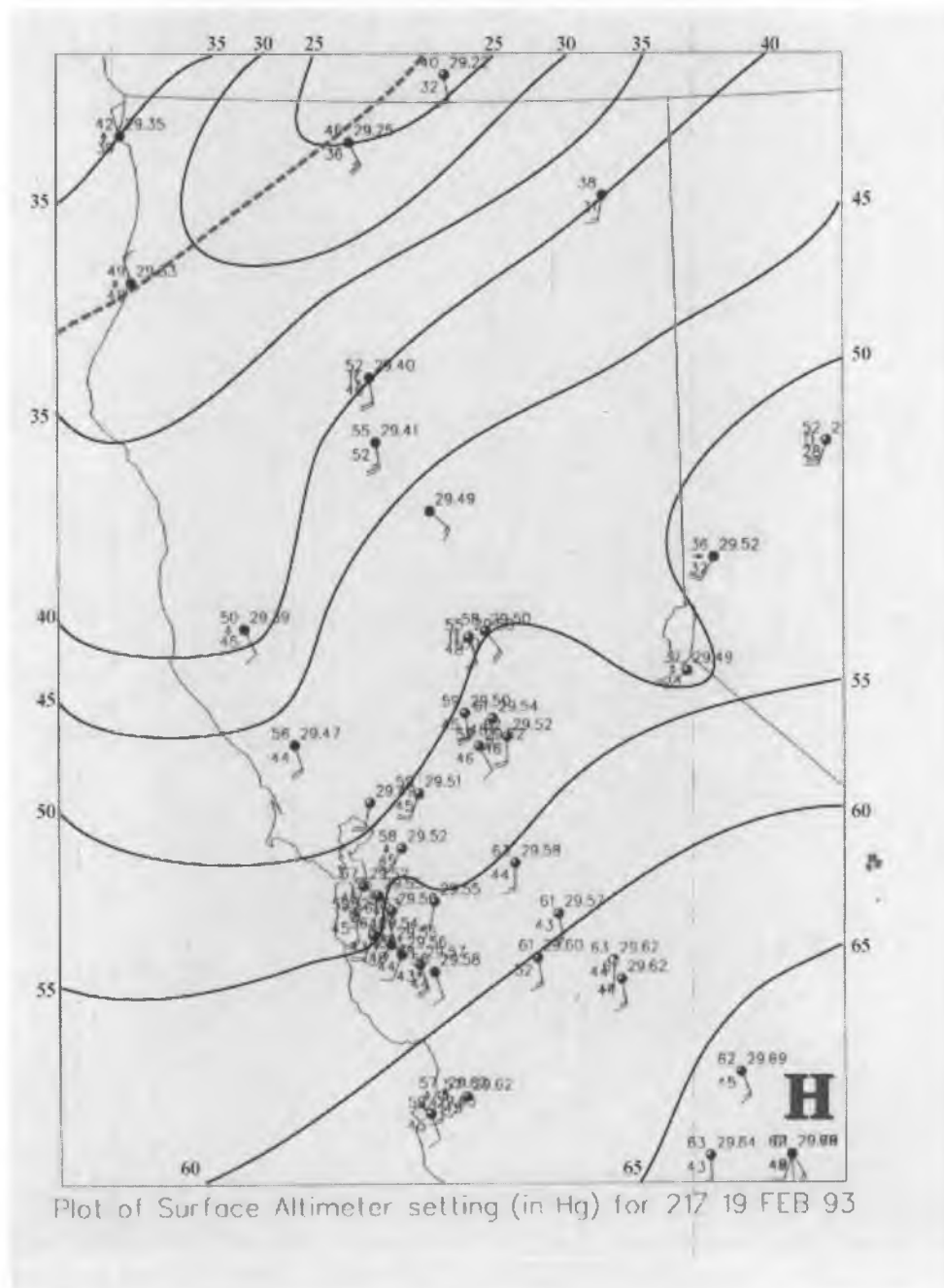


Figure 12b: Analyzed surface analysis for Northern California for 21 UTC 19 February 1993. Due to time constraints, the exact nature of the surface boundary was not analyzed. However, this boundary (represented by a dashed purple line) formed from the remnants of the occlusion of the main cyclone. This pertains to subsequent surface analyses as well.

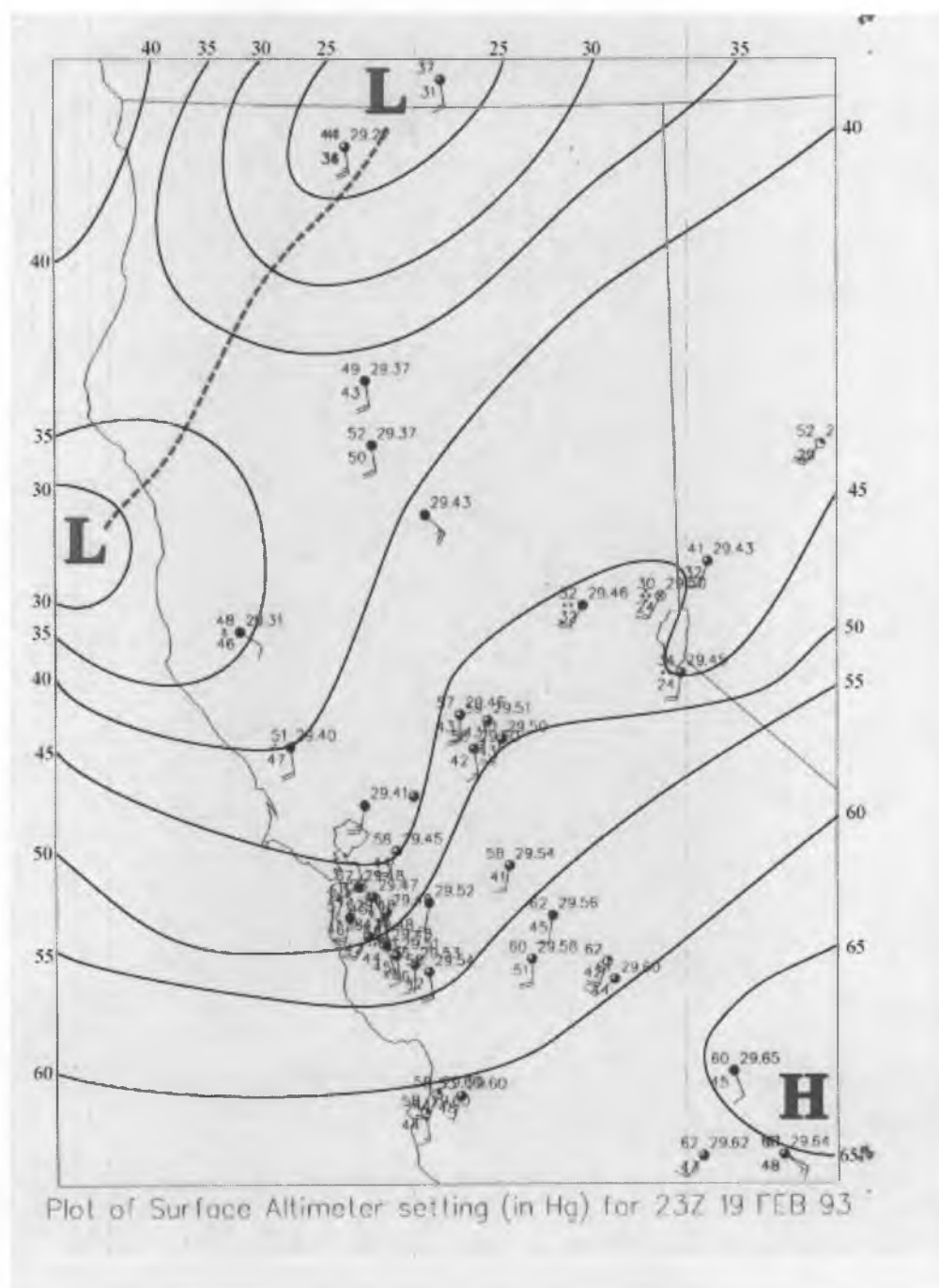


Figure 12c: Analyzed surface analysis for Northern California for 23 UTC 19 February 1993.

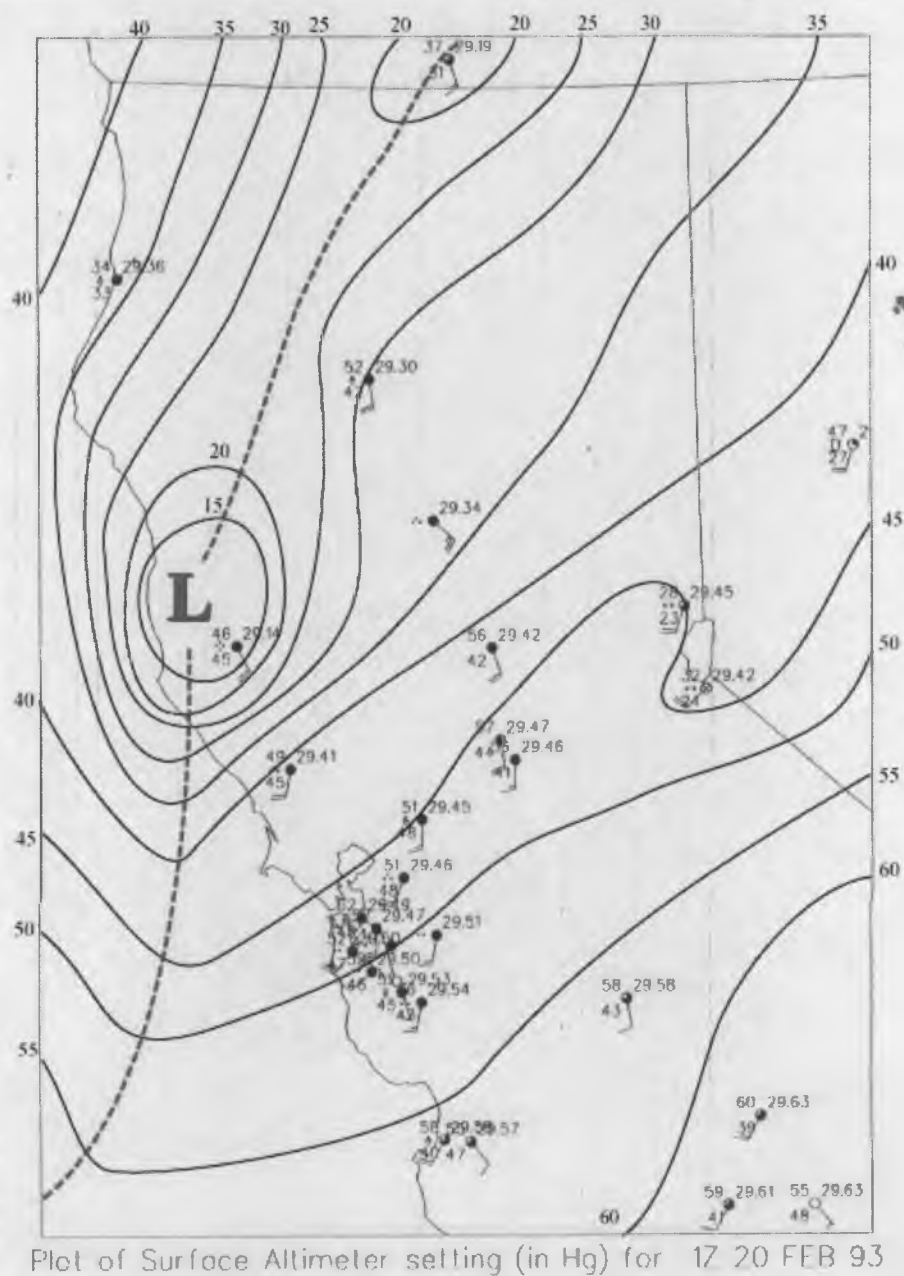


Figure 12d: Analyzed surface analysis for Northern California for 01 UTC 20 February 1993.

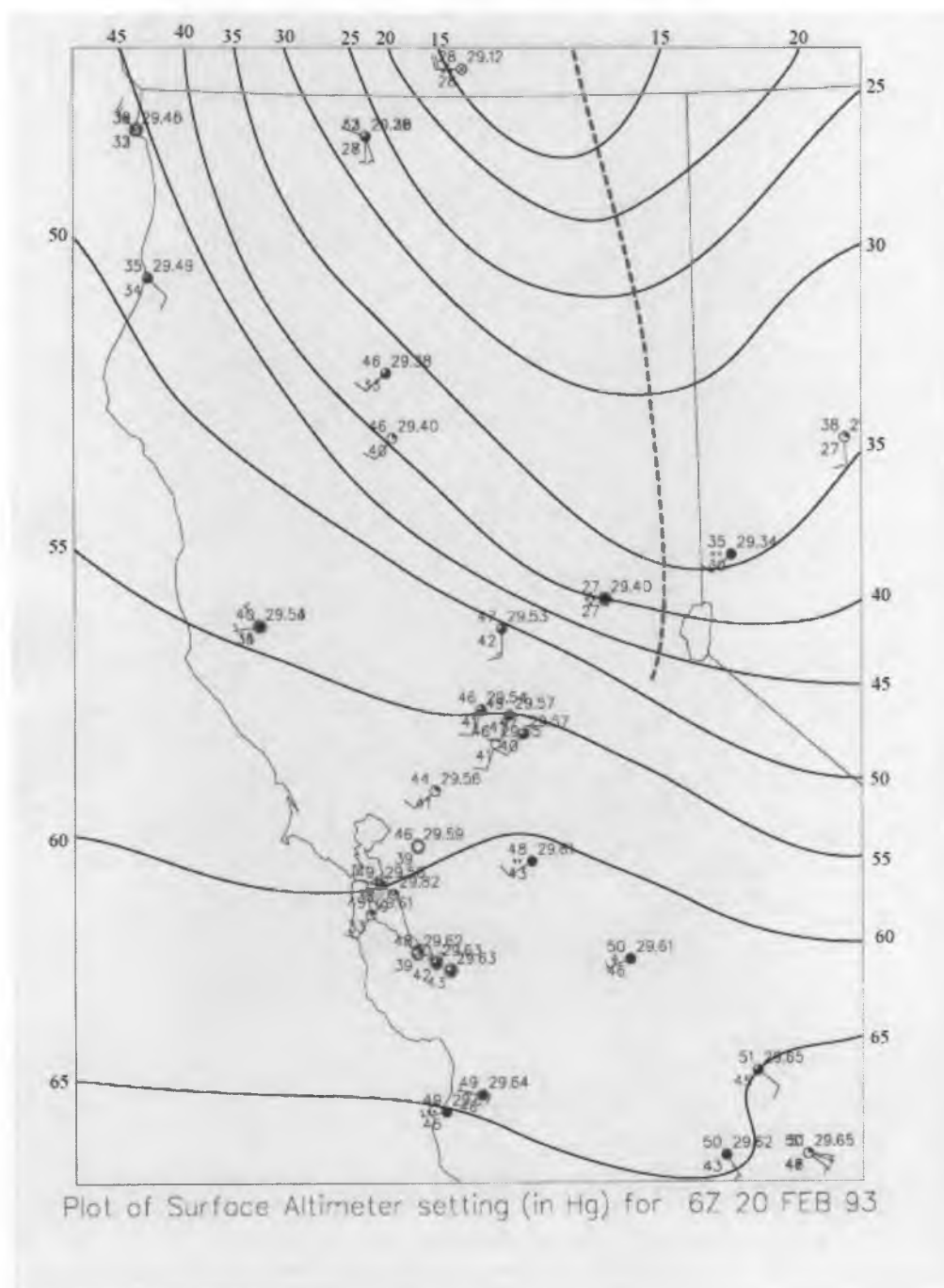


Figure 12c: Analyzed surface analysis for Northern California for 06 UTC 20 February 1993.



Figure 13: Climatology of 'bombs' in the eastern Pacific and western North America developed by Sanders and Gyakum (1980). Numbers represent number of bombs observed in 2.5° latitude by 2.5° grid during three cold seasons. Note the maxima in frequency in the north-central Pacific and the Gulf of Alaska, as well as the lack of bomb observations along the California Coast.

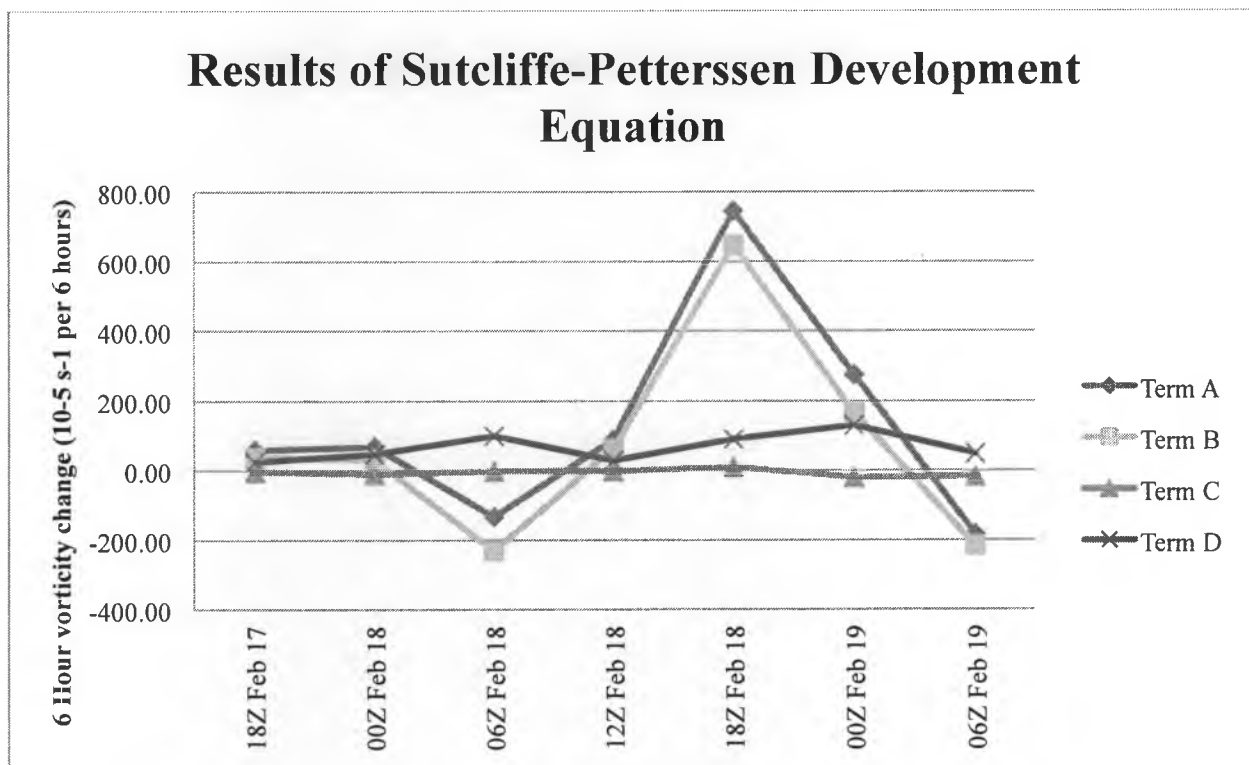


Figure 14: Comparison of terms in the Sutcliffe-Petterssen Development Equation during the period of surface pressure falls.

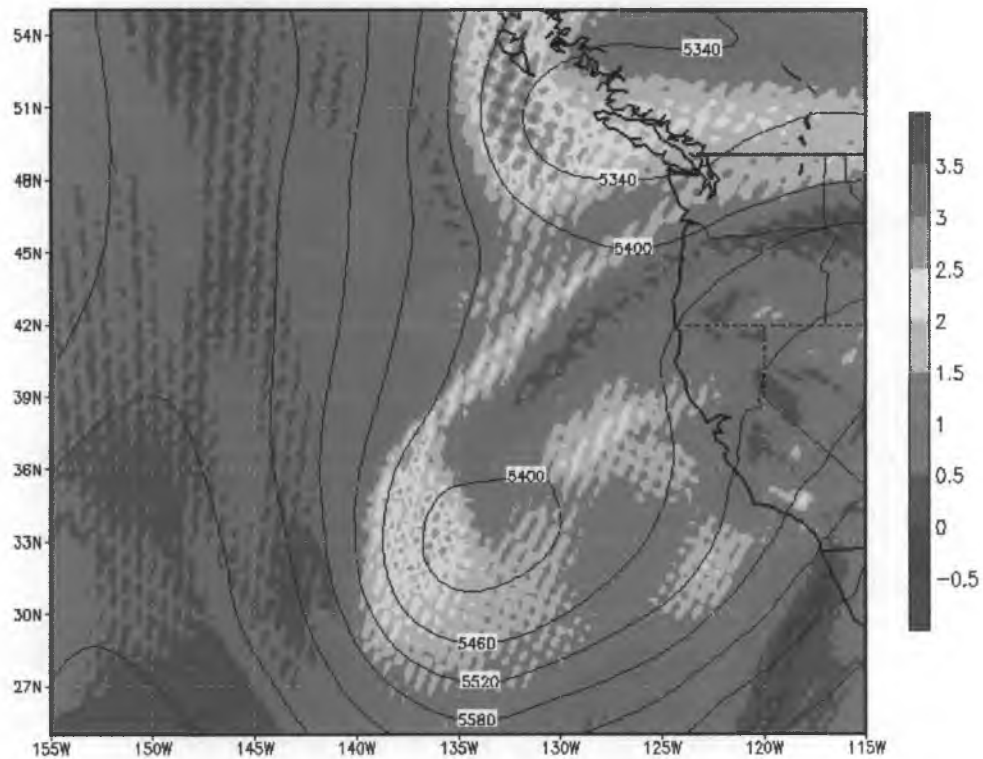


Figure 15: 500 mb vorticity ($\times 10^{-5} \text{ s}^{-1}$), as analyzed by the NARR and displayed with IDV, for 00 UTC February 1993. Note the strong small-scale gradients, which are not representative of synoptic scale gradients

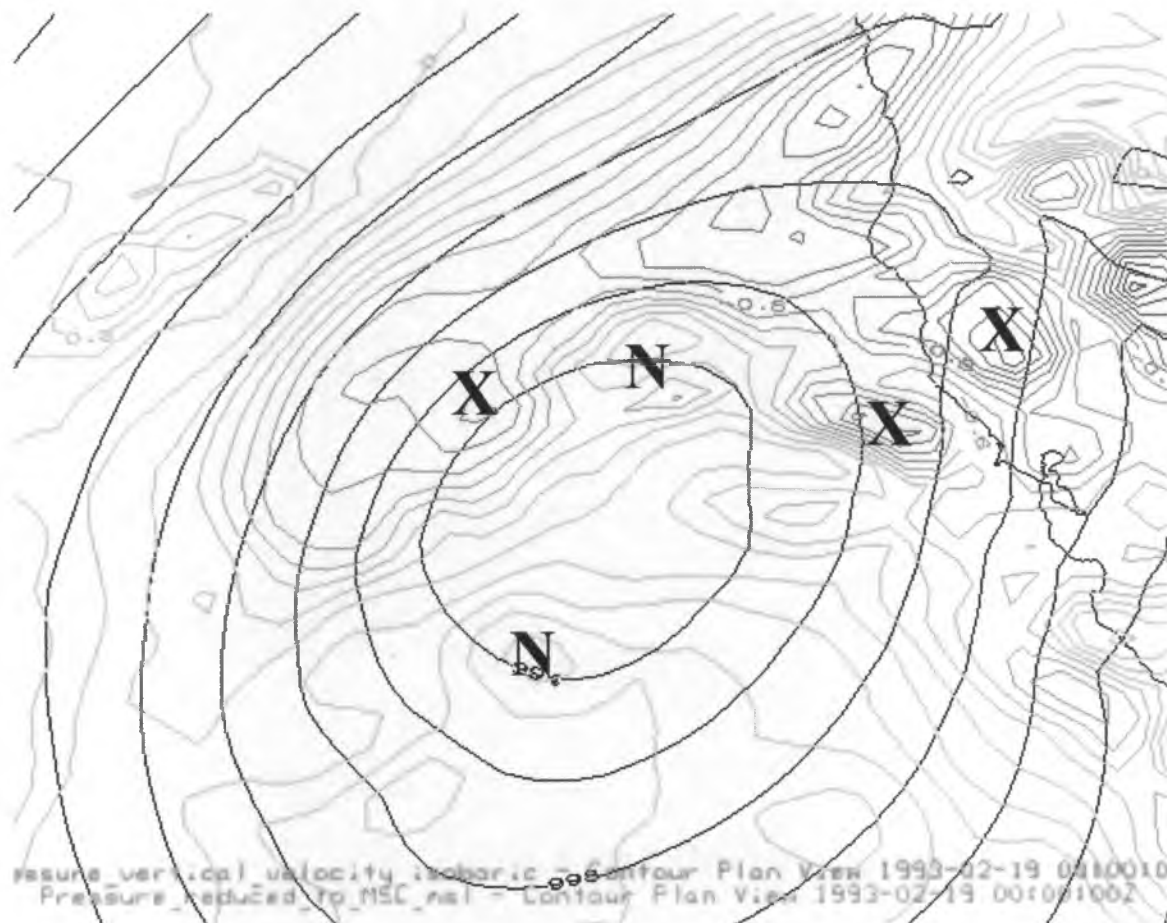


Figure 16: Sea surface pressure (mb, black) and 700 mb vertical velocity (Pa s^{-1} , blue) from the NARR for 00 UTC 19 February 1993. X's mark maxima in upward vertical motion while N's represent minima in upward vertical motion (or maxima in downward vertical motion).

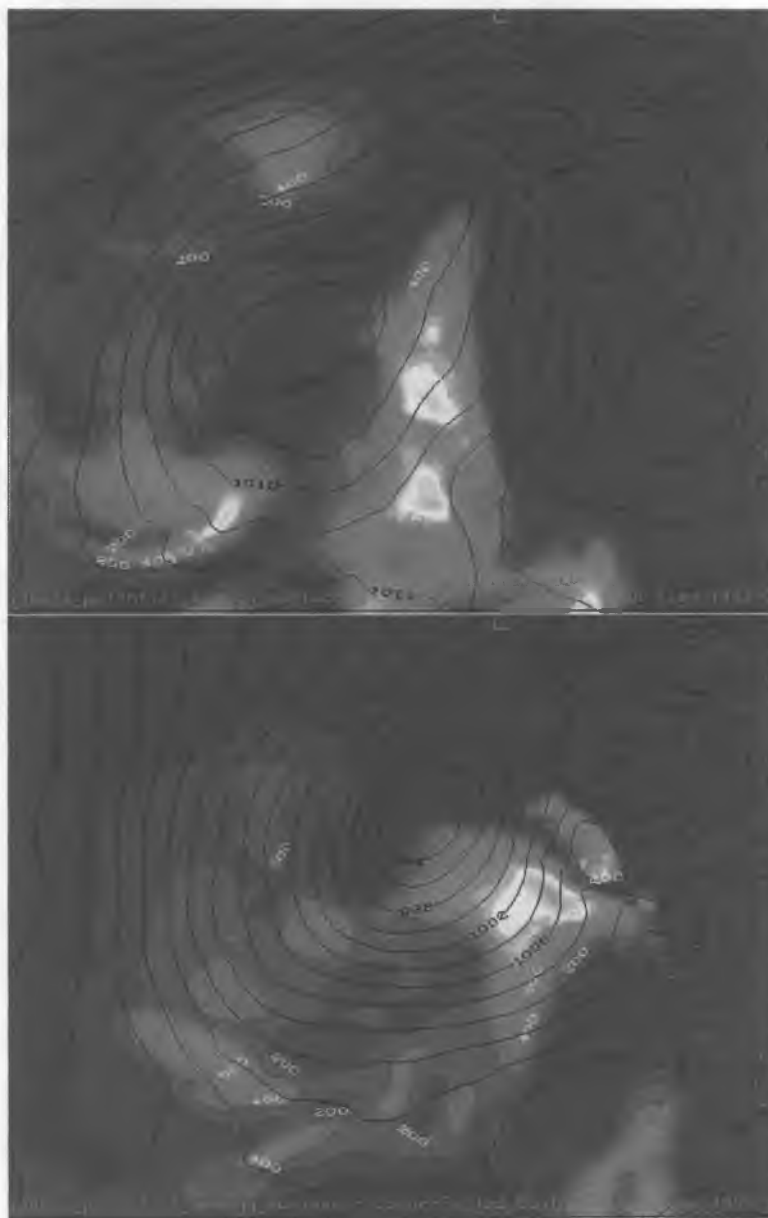


Figure 17: NARR analyzed surface based CAPE (J/kg) over the eastern Pacific and western North America for 00Z February 18 1993 (top) and 00Z February 19 1993 (bottom).

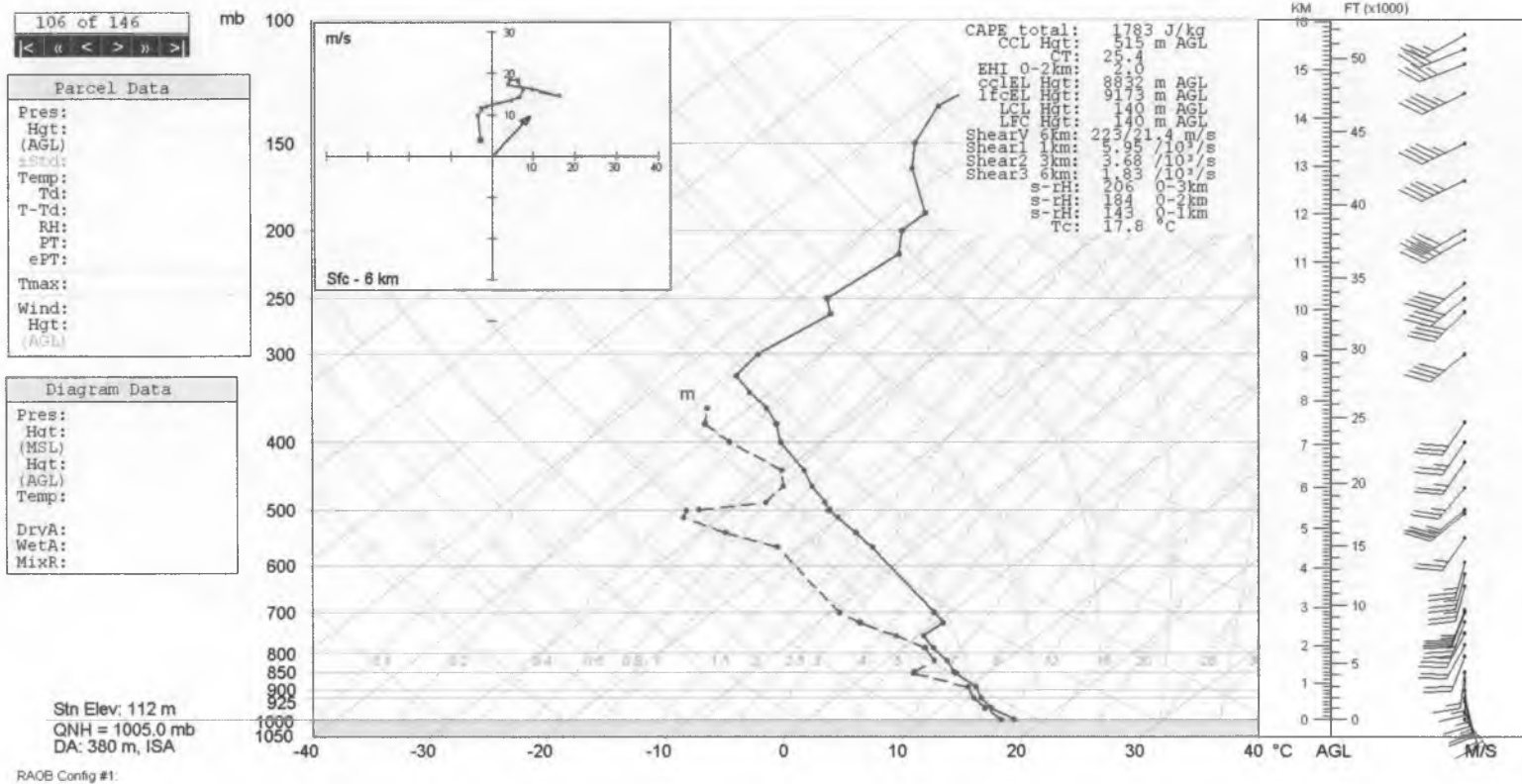


Figure 18: Sounding for KVBG for 00Z Feb 19 1993.

Appendix A

The Sutcliffe-Petterssen Development Equation (SPDE) is based on the relationship between the 1000 mb geostrophic winds and 500 mb geostrophic winds via the thermal wind.

$$\vec{V}_{1000} = \vec{V}_{500} - \vec{V}_T \quad (\text{eq. A1})$$

where \vec{V}_T is the thermal wind. By finding the vertical component of the curl of each term, the following equation is obtained:

$$\vec{\zeta}_{1000} = \vec{\zeta}_{500} - \vec{\zeta}_T \quad (\text{eq. A2})$$

The Coriolis parameter can be added to both sides to obtain the absolute vorticity geostrophic vorticity at 1000 and 500 mb. The ‘thermal vorticity’ (the vorticity of the thermal wind) remains relative. The derivative of each term is taken with respect to time:

$$\frac{d\eta_{1000}}{dt} = \frac{d\eta_{500}}{dt} - \frac{d\zeta_T}{dt} \quad (\text{eq. A3})$$

The next step in the derivation of the SPDE involves the assumption that the level of non-divergence is at 500 mb. This means that the local 500 mb absolute geostrophic vorticity tendency is due entirely to absolute vorticity advection. The absolute vorticity will be expressed as the advection of the relative vorticity plus the Coriolis parameter. Additionally, the local 1000 mb absolute geostrophic vorticity tendency is simplified to the relative geostrophic vorticity tendency, since the Coriolis parameter is constant with respect to time at a fixed location.

$$\frac{d\zeta_{1000}}{dt} = -\vec{V}_{500} \cdot \vec{\nabla}_p (\zeta_{500} + f) - \frac{d\zeta_T}{dt} \quad (\text{eq. A4})$$

Lastly, the relationship between the relative vorticity and the Laplacian of the height field is applied to the thermal vorticity tendency term. The derivatives are then rearranged so that the thermal vorticity tendency term is expressed in terms of the Laplacian of the 1000-500 mb thickness tendency:

$$\frac{d\zeta_{1000}}{dt} = -\vec{V}_{500} \cdot \vec{\nabla}_p (\zeta_{500} + f) - \frac{g}{f} \nabla^2 \left[\frac{dz_t}{dt} \right] \quad (\text{eq. A5})$$

Eq. A5 is a form of the SPDE in Cartesian coordinates. The equation states that the 1000 mb relative geostrophic vorticity tendency is equal to the 500 mb absolute geostrophic vorticity advection minus the change in thermal vorticity associated with the 1000-500 mb thickness pattern.

The change in 1000-500 mb thickness is proportional to the change in the mean virtual temperature of the column through the hypsometric equation. The thickness tendency term can be expanded by substituting in a form of the temperature tendency equation (Bluestein, 1992, pp. 197), as shown in equation A6:

$$\frac{\partial T}{\partial t} = -\vec{V} \cdot \vec{\nabla}_p T + \omega \sigma \frac{p}{R} + \frac{1}{c_p} \frac{dQ}{dt} \quad (\text{eq. A6})$$

It is assumed that temperature advection, adiabatic heating and cooling associated with vertical motion, and diabatic heating and cooling each contribute to the local change in the mean virtual temperature of a column. These assumptions lead to the following form of the SPDE (Carlson, 1998, pp. 185).

$$\frac{\partial \zeta_{1000}}{\partial t} = -\vec{V}_{500} \cdot \vec{\nabla}_p (\zeta_{500} + f) - \frac{R}{f_0} \nabla^2 \left[-\vec{V}_{700} \cdot \vec{\nabla}_p T_{700} + \omega \sigma \frac{p}{R} + \frac{1}{c_p} \frac{dQ}{dt} \right] \quad (\text{eq. A7})$$

(Monteverdi 2008)